EXPLORING THE PHOTOPHYSICS AND PHOTOCATALYTIC PROPERTIES OF PLATINUM AND PALLADIUM NANOPARTICLES

by

Kevin John Major

A dissertation submitted to the faculty of
The University of North Carolina at Charlotte
in partial fulfillment of the requirements
for the degree of Doctor of Philosophy in
Nanoscale Science

Charlotte

2012

Approved by:

_____
Dr. Marcus Jones

_____
Dr. Patrick Moyer

_____
Dr. Edward Stokes

_____
Dr. Ana Jofre

_____
Dr. Amy Ringwood

ABSTRACT

KEVIN JOHN MAJOR. Exploring the photophysics and photocatalytic properties of platinum and palladium nanoparticles. (Under the direction of DR. MARCUS JONES)

Platinum and Palladium nanoparticles are important nanoscale materials for a variety of materials science and industrial applications. The presented research covers a broad spectrum of these unique nanoparticles, from their synthesis and characterization to their use in systems that examine their photophysical properties and as catalysts and photocatalysts.

We developed a new synthetic method for producing well-defined platinum and palladium nanoparticles of less than 5 nm diameter. The nanoparticles are stabilized by long chain thioethers, which allow them to retain their stability in a variety of solvent environments. Stability and size control are critical to the application of these particles to experimental research in a variety of systems.

After demonstrating the catalytic activity of these nanoparticles, we developed a method for linking them to magnetic cobalt ferrite nanoparticles. These linked particles were found to be highly recoverable when placed in a magnetic field, allowing for their reuse. In addition to traditional catalytic systems, platinum and palladium nanoparticles hold great potential as photocatalysts. We chose to study their use in two such systems.

The first system explored involved utilizing platinum nanoparticles as charge transfer catalysts from titanium dioxide nanoparticles. We demonstrated the ability of this system for the degradation of an organic dye as well as for hydrogen production via water splitting, both under dark conditions.

The final system explored involved studying the interaction between cadmium selenide quantum dots and palladium nanoparticles in solution. As a prelude to this research, we conducted an extensive study on the effects of stabilizing ligands on quantum dot fluorescence dynamics. We developed a model to define the dynamics of the dots based on changes in native ligand coverage upon sample dilution.

These studies allowed us to take these effects into account before studying the interaction of the dots with palladium nanoparticles. Palladium nanoparticles were found to exhibit two distinct effects on quantum dot fluorescence in solution. At higher palladium concentrations, we observed a quenching of the quantum dot fluorescence and shortening of the lifetime, which was attributed to Förster energy transfer from the quantum dots to the nanoparticles. Low palladium concentrations exhibited opposite effects, which were attributed to enhanced absorption, similar to previously studied quantum dot – gold nanoparticle systems.

By fully studying these nanoparticles, from their synthesis and characterization to their use in various systems, we in turn developed a thorough understanding of their unique photophysical properties.

DEDICATION

I dedicate this dissertation to the memory of my grandfathers, Edward Kazar and Glenn Major who were two of the hardest working and most dedicated family men I have ever known. The work ethic and focus, which they instilled in me allowed this dissertation to become reality.

ACKNOWLEDGEMENTS

For me to properly be able to acknowledge and thank all of the people who made this dissertation possible, this section would need to be longer than the rest of the paper combined. Therefore I will try to be as concise as possible.

I first need to acknowledge the guidance of both of my advisors, Dr. Marcus Jones and Dr. Sherine Obare. Dr. Jones has been a source of knowledge and support throughout this process after being willing to take me on as a mentee. I have learned countless skills from working under his guidance and expertise. Dr. Obare was an inspiring presence who allowed me to begin to realize my potential by believing in my ability to accomplish any task she could come up with. I sincerely appreciate both of their support and encouragement throughout my career. I would also like to recognize the members of my dissertation committee for taking time out of their busy schedules to serve in this capacity.

I would like to thank all of the members of my research groups throughout my time at Charlotte. From the Obare lab, MyCia, Ruel, Wen, Ming-Hong, Kausik, and Kaitlyn were supportive in training and assisting me as I gained experience working in a chemistry lab. The entire Jones group has also been extremely helpful, especially Drew who has been both a great friend and quantum dot synthesis wizard, Scott for his enthusiasm and willingness to help in his lime green shoes and José for his willingness to spend hours in a pitch-black windowless room collecting blinking traces. Danielle, Guarav and Mike have also been helpful through informative discussions and their willingness to listen. I also need to acknowledge the Moyer group, specifically Sharonda

and Ryan for their time and discussions. Special thanks also to Dr. Patrick Moyer whose challenging and thoughtful questions in group meetings generated countless experiment ideas.

The support staff in the UNCC chemistry department have been an invaluable resource. Dr. Merkert was always willing to lend a hand in training me on any piece of instrumentation I needed to use. Robin Burns has been a constant source of help in the front office. I also need to specially acknowledge Caroline Kennedy for her tireless efforts to ensure that I was able to make it through this Ph.D. program. Additionally I need to thank the UNC Charlotte chemistry department as a whole for the use the majority of the equipment used for this dissertation as well as the UNC Charlotte Optics Center for use of specialty equipment.

Throughout my years in Charlotte, I have made many valuable friends who have assisted in this journey. I need to specially acknowledge Natalie, Mikey, Jeff, Jon, and Stacy who have gone through the ups and downs of graduate school with me and were able to lend their empathy and support whenever I needed.

In addition to my support network in Charlotte, this degree would not have been possible without my amazing friends and family back home in Pennsylvania. I have truly been blessed with the greatest group of friends who spent the last 5 years constantly asking me when I would be done so that I could move back home to hang out with them. Putting their names in this section is not enough to truly thank them for all of their love and encouragement throughout the years, but here goes anyway. So thank you to Lance, Spencer, Quinton, Lunger, Pete, Josh, Kenny, Chad, Jason, Ashley, Sara, Kristin,

Amanda, Jenny, Carina, and Becky, you guys truly helped me keep my sanity throughout this process, which is ironic because you are all crazy.

Finally, I have endless thanks and appreciation for my amazing family. My grandparents have consistently been models of hard work and determination to live by every day of my life. Thanks to my brother Stephen who initially got me down the path to a science career as well as my sister-in-law Vanessa who somehow manages to keep him in line. Most importantly I need to thank my wonderful, supportive, loving parents Brian and Mary Major. As cliché as it may sounds, words simply cannot describe the debt of gratitude I have for their presence in my life. None of this would have been possible without them.

TABLE OF CONTENTS

LIST OF TABLES

LIST OF FIGURES

LIST OF ABBREVIATIONS

acac	acetylacetonate
DMSO	dimethyl sulfoxide
FRET	Förster resonance energy transfer
GC	gas chromatography
HDA	hexadecylamine
HOMO	highest occupied molecular orbital
IR	infrared
LUMO	lowest unoccupied molecular orbital
MPC	monolayer protected cluster
MUDA	mercaptoundecanoic acid
OAc	acetate
PL	photoluminescence
PMMA	poly(methyl methacrylate)
NP	nanoparticle
QD	quantum dot
SEM	scanning electron microscopy
TCSPC	time-correlated single photon counting
TEM	transmission electron microscopy
TGA	thermogravimetric analysis

TOP	trioctylphosphine
TOPO	trioctylphosphine oxide
TTTR	time tagged time-resolved
UV	ultraviolet
W	watt
XRD	x-ray diffraction

CHAPTER 1: INTRODUCTION

Palladium and Platinum are two of the most widely used metals in the modern industrial world. Both are vital components in a variety of chemical processes, especially for their catalytic properties.[1-15] With the advent of nanotechnology, metal nanoparticles have become one of the most widely studied new particles in the materials science community. The research detailed in this dissertation combines these two important fields, through the development and study of well-defined Pt and Pd nanoparticles, from their synthesis and characterization to their use in a variety of photophysical systems.

Metal nanocrystals in their basic form have been utilized for hundreds of years. From the Lycurgus chalice from Rome, through stained glass in medieval cathedrals, through the early days of colloidal chemistry, the basis for exploiting the unique properties of nanosized metallic crystals has been developed.[16-19] In all of these applications however, a full understanding of the particles was never achieved, often due to the lack of control in the production of the particles. With the explosion of modern synthetic techniques and characterization equipment, metal nanocrystals have become a leading area of study across a multitude of disciplines including biology, chemistry, physics, optics, and materials science.[20-28] By all accounts, gold nanocrystals have been the most widely studied. In 1951, pioneering work by Turkevich showed the controlled production of spherical gold nanoparticles of 10-20 nm diameter through the reduction of $HAuCl_4$ in a sodium citrate solution.[29] Since this first report, a variety of synthetic

methods have been explored to further refine the control over particle morphology. After gold, silver nanoparticles have been the second most synthesized metal nanoparticles. Many of the synthetic methods developed for gold were used as starting points for the synthesis of silver nanoparticles.[30]

With the development and refinement of these synthetic methods, a variety of applications have been explored utilizing these particles. The unique plasmonic properties of Au and Ag nanoparticles lend to their use in sensors and optical devices such as solar cells.[22, 31-38]

Light scattering from metal nanoparticles can be used as a means to direct and trap light in a high-index substrate. Catchpole and Polman investigated the effect of particle shape on this scattering.[33] Their results showed that particle morphology is extremely important to the overall efficiency of these devices due to the differences in near-field coupling effects.

Yu *et. al* examined amorphous silicon solar cells with Au nanoparticles deposited at a density of 3.7×10^8 cm^{-2} showing an increase in short-circuit current density and an 8.3% increase in energy conversion efficiency.[39] Likewise an improvement was shown in InP/InGaAsP quantum-well waveguide solar cells due to scattering by Au and silica nanoparticles using a similar technique.[40]

Nanoparticle plasmons have been exploited to increase the efficiency of both traditional amorphous silicon solar cells[32] as well as newer dye-sensitized[31] and organic cells.[34-35, 41]

In addition to photonic devices, metal nanoparticles have been heavily explored for their use as traditional catalysts and photocatalysts. While in the bulk state Au is

chemically inert, it has been shown that catalytic properties arise on the nanoscale. This fact is illuminated by the dramatic effect of nanoparticle size on catalytic efficiency. One example of this is the conversion of CO to CO_2 using nano-Au catalysts, which depends heavily on cluster size, where maximum activity is found around 3 nm and activity drastically decreases with both larger and smaller diameter clusters.[3]

Platinum and palladium have been important metal elements throughout the history of chemistry, especially in the field of catalysis.[1, 6, 8-13, 15, 42-50] Organometallic compounds of Pd are widely used catalysts for many organic syntheses such as Suzuki and Heck cross-coupling reactions. Suzuki coupling was first reported in 1985 by Akira Suzuki and since that time has developed into a widely-used method for carbon-carbon bond formation.[51]

In 1972 pioneering work by Fujishima and Honda demonstrated a new use for Pt black as an electrode in the electrochemical photolysis of water for hydrogen production.[52]

The driving force behind this research was the development of well-defined Pd and Pt nanoparticles for use in a variety of catalytic, electron-transfer and energy-transfer applications. As such the research was divided into distinct subsections, which fully encompass the design and use of these nanoparticles. The specific projects were chosen to as to fully understand the photophysics and photocatalytic properties of Pd and Pt nanoparticles. These subsections of research are laid out in the subsequent chapters including:

1. Synthesis and characterization of well-defined Pd and Pt nanoparticles
2. Investigation of the catalytic properties of Pd and Pt nanoparticles

3. Examination of the electron transfer properties of Pd and Pt nanoparticles

4. Spectroscopic studies of interactions between semiconductor and metal nanoparticles.

By systematically studying Pt and Pd nanoparticles through the entire process from synthesis, to characterization, and finally studying their use in potential systems, we gained a broad understanding of the photophysical and photocatalytic properties of these unique materials.

CHAPTER 2: SYNTHESIS AND CHARACTERIZATION OF Pd & Pt NANOPARTICLES

2.1 Introduction

Certain metal nanoparticles, especially Au and Ag have been extensively studied for their plasmonic properties. Though top-down methods of nanoparticle fabrication such as lithography[21] have been employed, current thought is that for production of small (< 10 nm) particles, wet chemical and other bottom up methods provide the best options. Vast arrays of synthetic methods have been developed for these metal nanoparticles, and reviews are available in the literature covering the bulk of this work.[53-57]

The most established methods for Au and Ag nanoparticle synthesis involve the reduction of metal salts in the presence of citrate stabilizers.[29] Adsorption of ions on the nanoparticle surface electrostatically stabilizes the particles during growth. Two phase reduction methods have also been developed for Au and Ag particles. This general procedure involves mixing aqueous metal salts (such as $HAuCl_4$ or $AgNO_3$) in a toluene solution with long-chain alkylammonium surfactants. After vigorous stirring for over an hour the metal salt is transferred into the organic phase, which can then be separated. Finally a long chain thiol is added as a stabilizing ligand, after which a reducing agent (such as $NaBH_4$) is also added, producing Au or Ag nanoparticles.[58-59]

Though less studied, Pt and Pd nanoparticle synthetic methods have also been developed. Principally, similar synthetic methods to Au and Ag are known. Precursors such as H_2PdCl_4 and H_2PtCl_6 are reduced with trisodium citrate. This leads to brown-

colored particles, which tend to be stabilized by long chain organic molecules such as sodium sulfanilate (H_2N-$C_6H_4SO_3Na$).[57] More recent synthetic work, especially with relation to Pt, focuses on methods that allow for highly faceted particle formation.[60] Typically, hydrogenation techniques have been employed for these particles, which allows for the formation of particles at a slow rate. Due to the hydrogen pressure, the slow growth rate facilitates the formation of anisotropic and faceted nanoparticles. In one example of this synthetic method by Ren and Tilley,[61] platinum acetlyacetonate ($Pt(C_5H_7O_2)_2$ or $Pt(acac)_2$) was dissolved in toluene along with oleylamine, which acts as the ligand stabilizer. The $Pt(acac)_2$ was decomposed under 3 bar hydrogen pressure in a Fisher-Porter bottle. After purification this method produces relatively disperse nanoparticles (of around 10-20 nm) with various highly faceted shapes depending on reaction time and temperature.

The basic challenge to any nanoparticle synthesis is the development of methods that allow for control of both the size and shape of the particles. Additionally, a need arises that allows for particles of different sizes to be synthesized through the modification of a single variable (ideally reaction time or temperature).

Any nanoparticle synthesis can be related back to classical studies by La Mer and Dinegar,[62] The process involves a temporarily discrete nucleation event, which is followed by a slower controlled growth on these nuclei. In the case that no new precursors are added throughout the reaction, no new nuclei will form. As the growth of all nuclei are similar in this case, particle monodispersity is determined by the time the nuclei are formed and growth begins. Particles can also exhibit a second growth phase, referred to as Oswald ripening. This process refers to the dissolution of small

nanoparticles due to their high surface energy allowing their material to be re-deposited on the larger particles. This general theory can be referred to as the "rich getting richer," basically meaning that large particles grow larger at the expense of the small particles. Oswald ripening can simplify the preparation of a size series of nanoparticles.[62-63] Due to these factors, one-pot synthetic methods are preferred as they often provide the best chance for monodisperse particle formation in a facile manner.

2.2 Synthesis of Pd Nanoparticles

To meet the challenge of producing sub 5 nm monodisperse Pd NPs, a one-pot reduction method was developed.[7] In a typical synthesis an oil bath was heated to 90-95 °C. Palladium acetate [$Pd(OAc)_2$] (0.20 g, 0.30 mM) and n-dodecyl sulfide (1.65 g, 4.45 mM) were added to a 250 mL round bottom flask and dissolved in 50 mL toluene. This flask was placed in the bath under constant stirring and refluxed for one hour. After refluxing, the flask was removed from silicon oil and cooled to room temperature.

This synthesis has a few unique benefits. First, it is a one pot method, which, as mentioned tends to allow for relatively monodisperse particles in a fairly straightforward manner. Additionally, the n-dodecyl sulfide acts as both a reducing agent and the stabilizing ligand on the NPs. The thiol binds to the surface of the Pd NPs, and the long carbon chains prevent agglomeration between particles. A drawing of the Pd NPs with stabilizing ligands is provided in Figure 2.1.

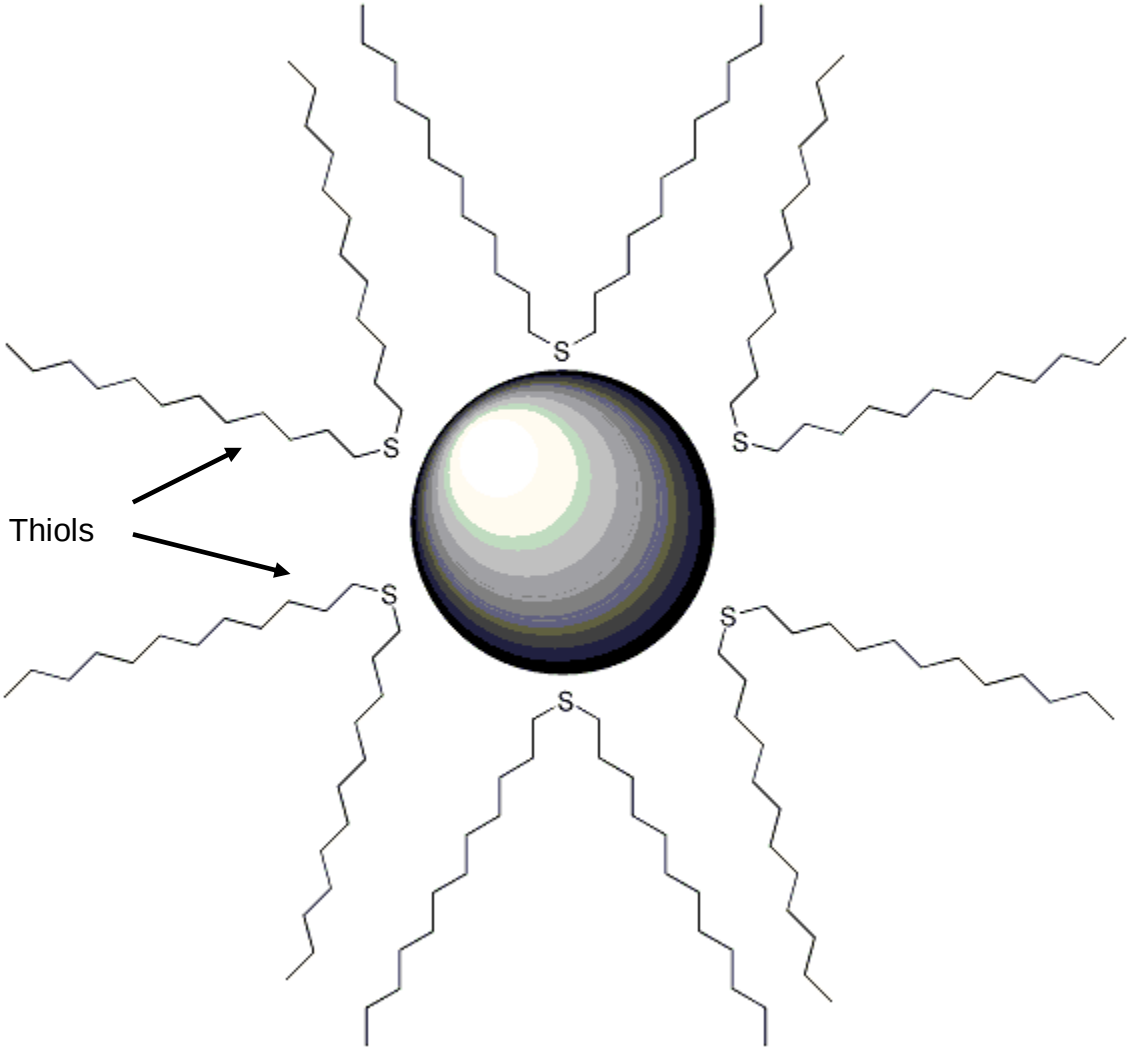

Figure 2.1: Illustration of a n-dodecyl sulfide stabilized Pd or Pt NP. Illustrates the thiols bound to the surface of the NP with the bulkiness of the carbon chains providing stability in solution. Note the figure is drawn with an emphasis on showing the full structure of the molecules and is not drawn to scale.

2.3 Differentiating Factors For Pt Synthesis

The synthetic method for Pd NPs was then used as a jumping off point for the development of a Pt NP synthesis with a few modifications. Because n-dodecyl sulfide proved to be an effective and efficient stabilizing ligand and reducing agent, it was chosen to develop a synthesis that would allow its continued use. Platinum acetylacetonate [$Pt(acac)_2$] was selected as the Pt precursor. Due to the higher difficulty in dissociating the Pt-acac bond (as compared to Pd-OAc), a higher temperature for the reaction was found to be necessary as no particle growth was observed even after 24 hours at 100 °C . This precluded the use of toluene as a solvent due to its boiling point of 110 °C. Dimethyl sulfoxide (DMSO, boiling point = 189 °C) was first chosen as an alternate solvent, which did allow for particle formation. However to achieve reduction of the $Pt(acac)_2$, as observed by UV-visible absorption, the temperature was needed to be increased above 200 °C, at which point the DMSO was itself boiling. To allow for heating temperatures in excess of 200 °C, phenyl ether (boiling point = 259 °C) was finally chosen as the reaction solvent.

2.4 Synthesis of Pt Nanoparticles

In a typical synthesis of Pt NPs an oil bath was heated to 210 °C, to allow for fast reduction of the $Pt(acac)_2$. An approximately 1:5 ratio of $Pt(acac)_2$ (0.20 g, 0.51 mM) and n-dodecyl sulfide (0.95 g, 2.54 mM) were added to a 250 mL round bottom flask and dissolved in 50 mL phenyl ether. This flask was placed in the bath under constant stirring and refluxed for 45 minutes. After approximately 30 minutes of heating, the solution changed from yellow to dark brown indicating formation of the Pt NPs. After a total of

45 minutes of refluxing, the flask was removed from silicon oil and cooled to room temperature.

Other $Pt(acac)_2$ to n-dodecyl sulfide ratios (1:10, 1:3, 1:2) were also examined. The 1:3 and 1:2 solutions demonstrated no noticeable particle growth indicating that there was not enough reducing agent present in the solution. The 1:10 ratio did demonstrate particle formation, however it did not appear that there was any benefit in the form of particle quality or stability to the higher ligand ratio.

Two other synthetic methods were examined for Pt NPs using different reducing agents. First, as another attempt to produce Pt NPs in toluene at a lower temperature, hydrogen gas was introduced as a secondary reducing agent. This experiment was carried out as described above, replacing the phenyl ether with toluene and heating the oil bath to 95 °C. The flask was then connected to a Schlenk line and placed under vacuum for 30 seconds. Hydrogen gas (95%) was then flushed through the system. This was repeated 3 times. The flask was then left under a hydrogen atmosphere for the duration of the reaction. After 3 hours of heating no color change relating to NP formation was observed in solution, thus the reaction was deemed unsuccessful and halted.

Photoreduction was also explored as an alternative method for Pt NP synthesis. To determine the viability of this method, we first prepared a dilute solution of $Pt(acac)_2$ (0.01 g, 0.025 mmol) and n-dodecyl sulfide (0.0471 g, 0.13mmol) in 50 mL of acetone was prepared. This solution was then further diluted using three consecutive 1:1 dilutions to bring the absorbance of the solution below 1 AU. This solution was placed in front of a solar simulator at 400 W. After 30 minutes of irradiation the $Pt(acac)_2$ peak at 350 nm appeared to vanish indicating the reduction of the Pt salt.

Since the above solution was too dilute to observe any color changes (and thus NP formation), we then prepared another solution to observe if we could actually produce Pt NPs using photoreduction. A solution of $Pt(acac)_2$ (0.05 g 0.13mmol) and n-dodecyl sulfide (0.236 g, 0.64mmol) in 50 mL of acetone was prepared and placed in front of a 400 W solar simulator under light stirring. After 75 minutes of irradiation no noticeable color change was observed, and thus the experiment was halted. This led us to conclude that although photoreduction may be a means to assist in the reduction of the $Pt(acac)_2$ salt, it appears as though heat is necessary for Pt NP formation under these conditions. Because of this, we decided to stick to the original reduction method using heating in phenyl ether for all subsequent Pt NP syntheses.

2.5 Characterization

2.5.1 UV-Visible Absorption Spectroscopy

Though Pt and Pd do not have visible plasmonic peaks, as Au and Ag do, UV-Visible absorption spectroscopy can still be used during particle growth to observe the reduction of the metal salts. This allows us to see when particle formation begins and when all of the metal salt has been reduced. As mentioned in section 2.3, this technique was used to determine that temperatures in excess of 200 °C needed to be obtained for the reduction of $Pt(acac)_2$. This is a straightforward process, which involves the removal of aliquots of solution from the reaction mixture at various temperature intervals and observing the absorption peak of the metal salt. The disappearance of the absorption peak is attributed to the reduction of the salt, which corresponds to a resulting color change of the solution from yellow to dark brown.

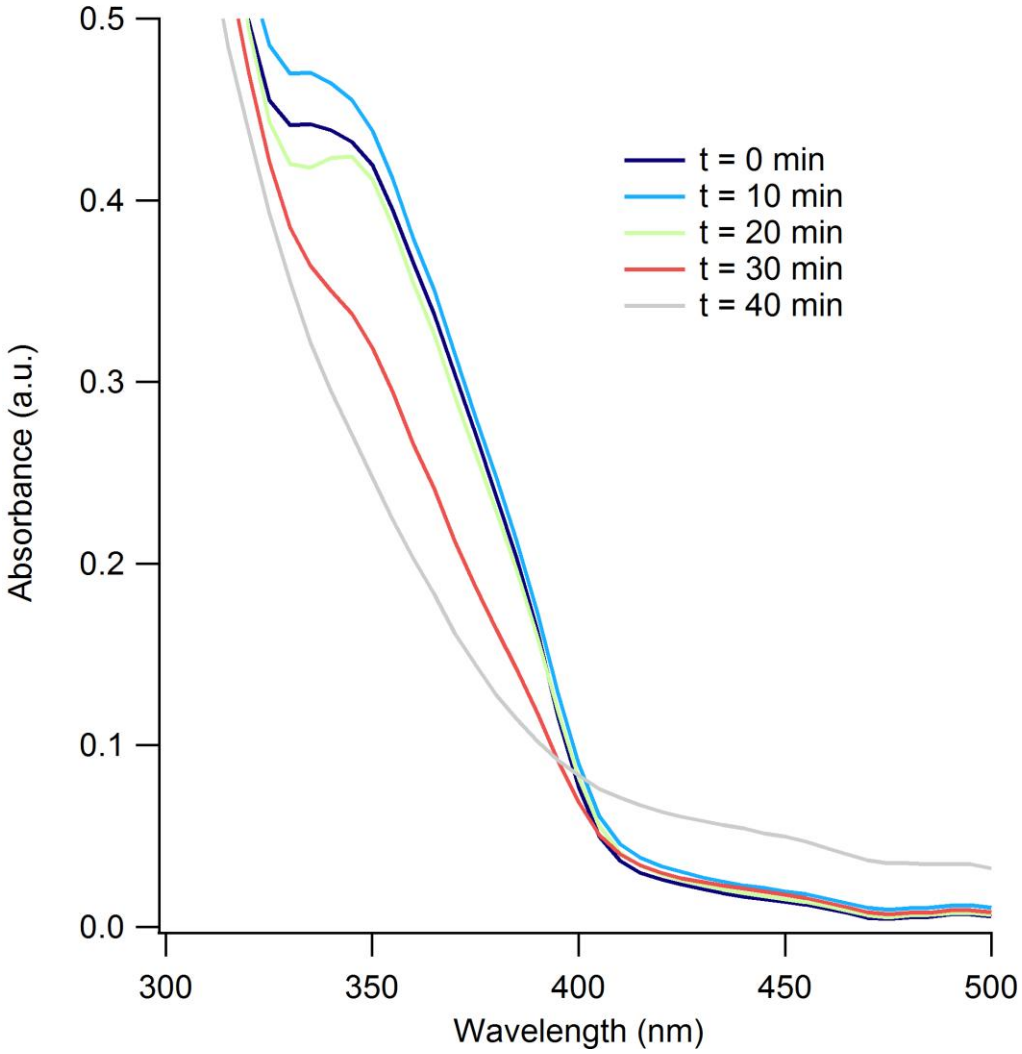

Figure 2.2: UV-visible absorption spectra for aliquots of a Pd NP synthesis taken at 10 minute intervals from the beginning of the reaction.

Figure 2.2 shows a typical particle growth absorption experiment conducted in DMSO. After the NP precursor solution was prepared, a 5 mL aliquot was removed and placed in a quartz cuvette. The sample was placed in a Cary-50 spectrometer and spectra were acquired from 500 to 300 nm using a fast collection time of 0.01 s at 1 nm intervals. The spectra were collected quickly so as obtain the most accurate timing of particle growth. The aliquot was added back to the flask, and the reaction was started. At 10 minute intervals, a 5 mL aliquot was again removed from the reaction vessel and spectra were recorded similarly.

It becomes apparent by examining Figure 2.2, that by 30 minutes of heating the $Pt(acac)_2$ peak at 350 nm begins to disappear and by 40 minutes of heating the peak is completely gone. This indicates that the entire Pt precursor has been reduced. Additionally, the 40 minute spectrum shows an overall increased absorption (readily apparent between 400-500 nm) relating to the presence of Pt NPs in solution.

2.5.2 Transmission Electron Microscopy

Transmission electron microscopy (TEM) is the most powerful tool for examining the shape and structure of synthesized nanoparticles, as well as determining their monodispersity in a sample. This is because the NPs can be viewed directly one at a time. However this comes at the expense of time consuming sample preparation and a complex instrument to operate. Samples were prepared by centrifuging the particles out of solution and redispersing in acetone. A dilute solution of these particles was then drop cast on a carbon coated copper grid and placed in a vacuum oven overnight to remove any organic solvent. High-resolution TEM (HR-TEM) images were acquired with a field emission gun operated at 200kV. Images were collected with a Gatan Multiscan camera.

TEM images showed the synthesis of fairly monodisperse, spherical Pt and Pd nanoparticles with an average diameter of 2.5 nm. HR-TEM images showed well defined lattice fringes. Additionally no noticeable large aggregates were found indicating that the n-dodecyl sulfide acts as an effective stabilizing ligand.

2.5.3 X-Ray Diffraction

X-Ray diffraction measurements of nanoparticles are an important way to determine their crystal structure. Being able to identify the facets of the Pd and Pt NPs is especially important in their use as catalysts as certain facets have been found to be more catalytically active. Samples were prepared by thoroughly washing the nanoparticles with acetone and drying them down overnight in a vacuum oven. These particles were then transferred to a 0.3 mm diameter X-ray capillary tube. The samples were placed in a PANalytical X'Pert Pro Materials Research Diffractometer in the Bragg-Bentano geometry and calibrated with a standard pattern of LaB6 powder. Collected spectra were compared to known literature results to determine the facets relating to each peak.

Both the Pt and Pd NPs were found to have well-defined facets. The XRD of the Pt NPs had strong peaks correlating to the (111), (200), (220), and (311) facets, as well as a weak peak correlating to the (222) facet. The Pd NPs had one well defined peak relating to the (111) facet as well as a weaker peak relating to the (220) facet. The (111) facet is especially important for catalytic work, as single crystalline bulk Pd(111) is often used in catalysis. Additionally it has been observed that for some small Pd NPs it is hard to obtain well defined facets.[14]

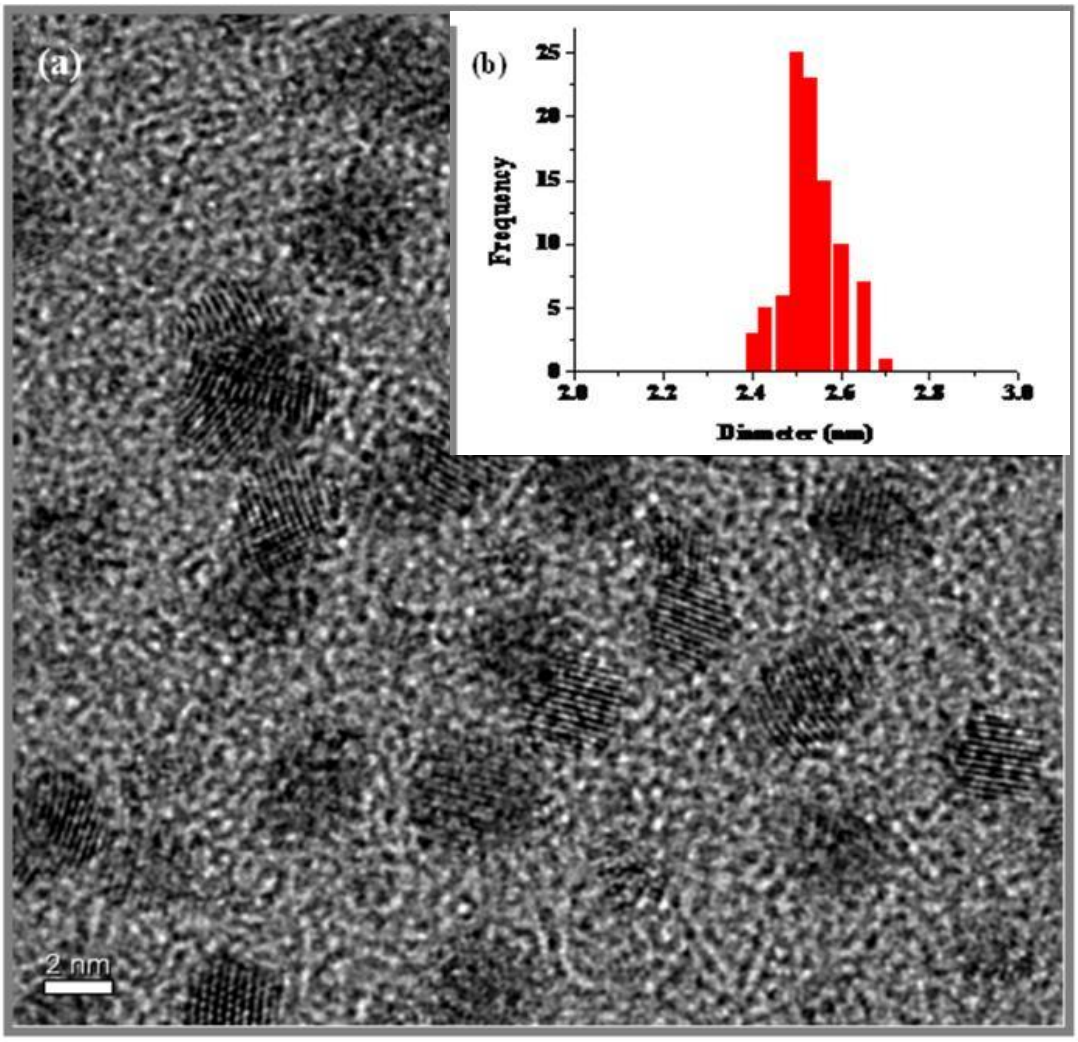

Figure 2.3: Representative TEM image of synthesized Pt NPs with a histogram (inset) showing the relative size distribution

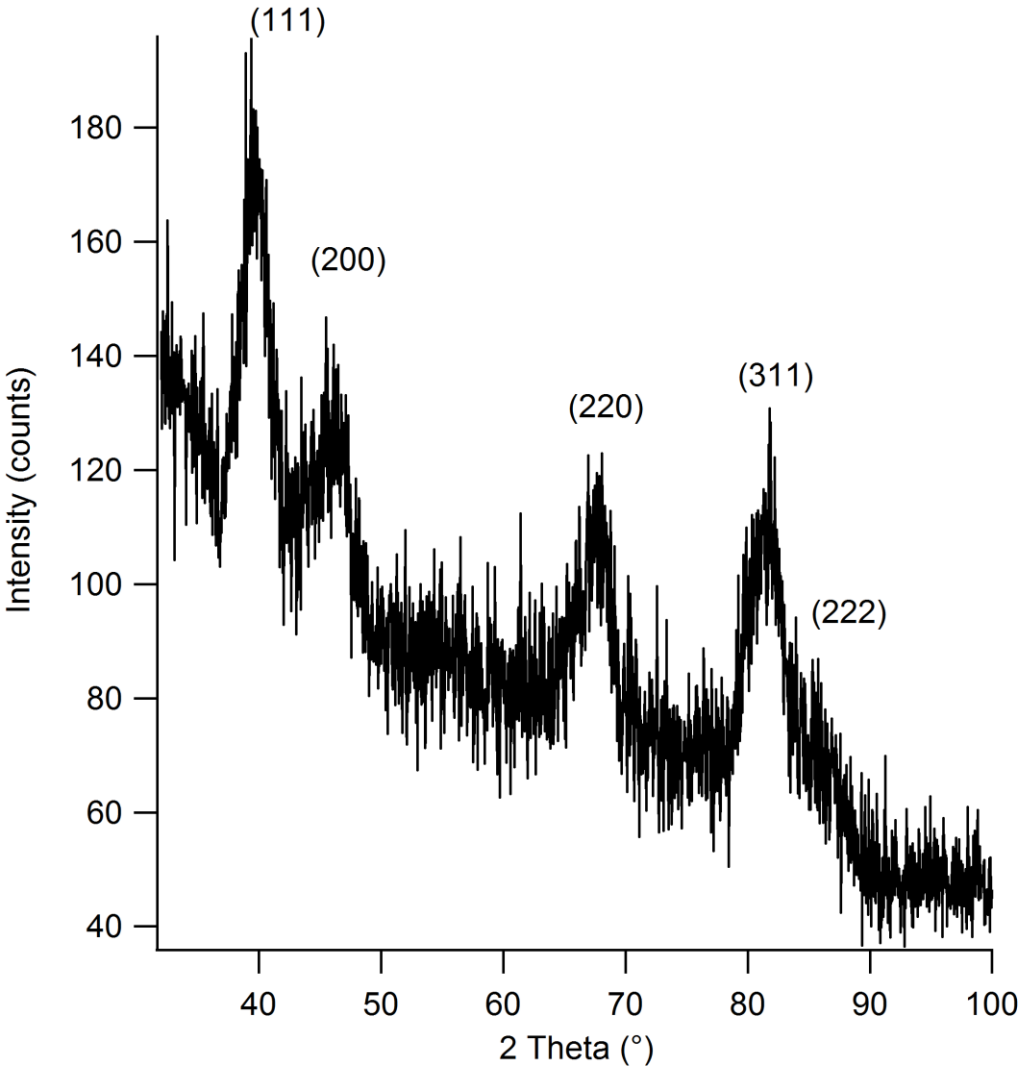

Figure 2.4: XRD spectrum for 2.5 nm Pt NPs

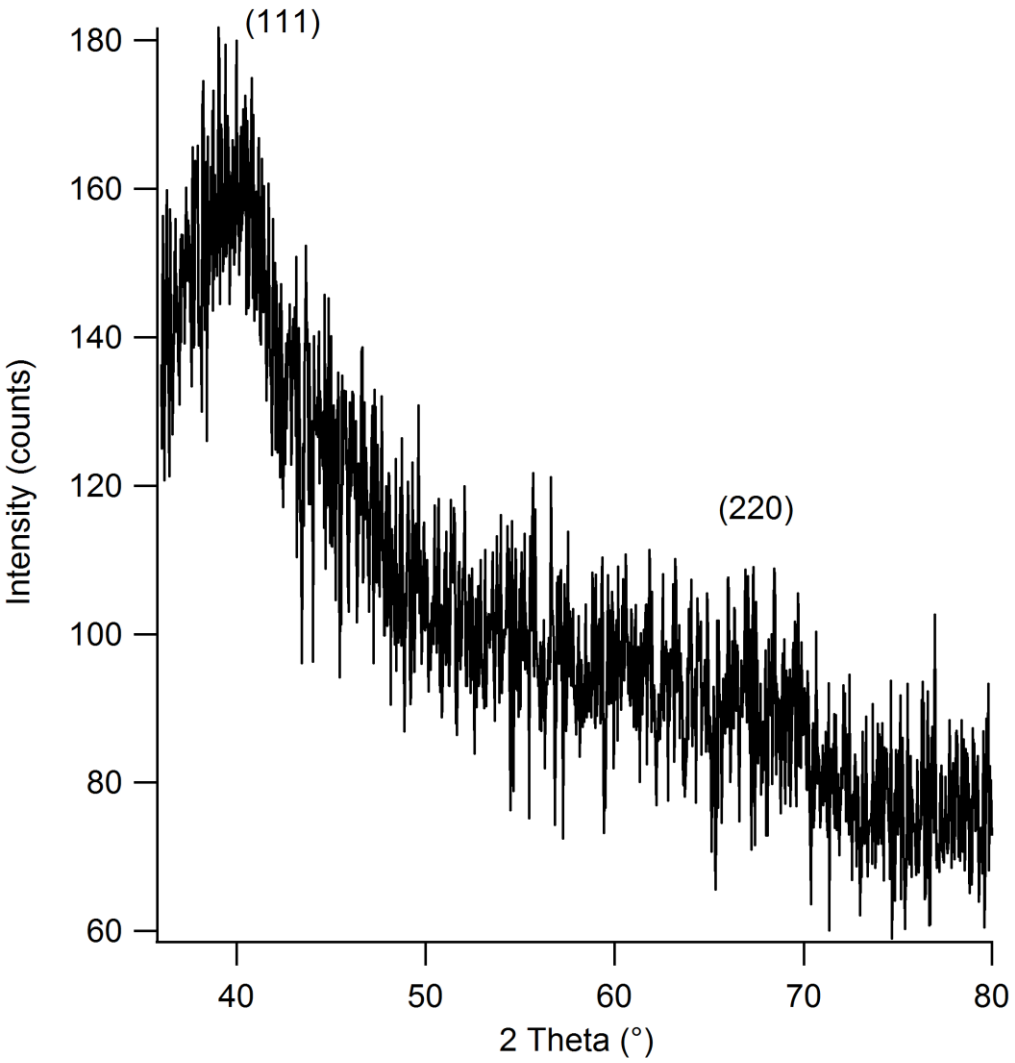

Figure 2.5: XRD spectrum for 2.5 nm Pd NPs

2.6 Solubility of Pt nanoparticles

The solubility of the synthesized Pt nanoparticles was examined to determine their viability in various experimental environments. Pt nanoparticles were synthesized and purified as before. These particles were then placed in 1.5 mL Eppendorf tubes and centrifuged at 15,000 RPM for 10 minutes, and the phenyl ether was removed. These particles were then placed in 10 different common experimental solvents and quickly sonicated for about 10 seconds to disperse. After sitting for 24 hours, the solutions were examined to determine solubility based on the observing the amount of particles that fell out of solution. Since Pd NPs are stabilized by the same n-dodecyl sulfide ligands, their solubilities were found to be similar.

Table 2.1: Solubility of n-dodecyl sulfide stabilized Pt NPs in various experimental solvents.

Solvent	**Solubility**
Toluene	Completely soluble
Hexanes	Completely soluble
Dimethyl formamyde (DMF)	Mostly soluble
Methanol	Weakly soluble
Ethanol	Weakly soluble
Ethyl ether	Mostly soluble
Dichloromethane	Completely soluble
Acetonitrile	Insoluble
Dimethylsulfoxide (DMSO)	Weakly soluble
Acetone	Weakly soluble
Water	Insoluble

2.7 Conclusion

The synthetic methods, which produce well-defined, and stabilized Pt and Pd NPs described in this chapter form the foundation for the rest of the work in this dissertation. The ability to use a one-pot method to synthesize monodisperse Pt and Pd NPs with diameters of less than 5 nm provide a unique opportunity to study their catalytic and photocatalytic properties.

CHAPTER 3: MAGNETICALLY RECOVERABLE $CoFe_2O_4$-Pd LINKED NANOPARTICLE CATALYSTS

3.1 Introduction

Catalysis is a major economic investment in the chemical and petrochemical industries. Catalysts are broken into two distinct types, heterogeneous and homogeneous catalysts. Heterogeneous catalysts are those in different phase than the substrate, most often solid catalysts with a liquid or gas substrate. Heterogeneous catalysts have a distinct advantage in that they are easy to recover leading to greater reusability. Homogeneous catalysts are of the same phase as the substrate. Because they reside in the same phase, these catalysts usually have significantly higher activity than their heterogeneous counterparts. The main issue with homogeneous catalysts however is that because they are in the same phase as the substrate they are extremely hard to recover after their use. So it becomes obvious that both types of catalysts have their own distinct advantages and disadvantages.

These distinct pros and cons of the various catalysts have led to a research push for new types of catalysts. Recent advances in synthetic methods for nanoscale particles have led to their development and use in catalysis. Due to their high surface area to volume ratio and exposed multi-facets, nanoscale catalysts have been shown to benefit from increased activity over bulk materials. In fact, recent studies have even demonstrated that nanoparticle features are responsible for the catalytic activity of an everyday device. Automobile catalytic converters, though not developed to contain

nanoparticles, actually consist of a variety of nanoparticle features, which aid in their efficiency.[3]

A large issue with nanoscale catalysts is their recovery. Previous work in our group has sought to remedy this issue by immobilizing Pd nanoparticles on an SiO_2 substrate.[7] Via this method significant activity of the Pd catalysts (over 80% conversion) was observed for up to 8 cycles of the particles. With normal recovery methods, the catalytic efficiency dropped to almost zero by the third cycle since a majority of the catalysts were lost.

Though this method allowed for reusability of the Pd NP catalysts, some of the surface area of the particles was lost as it was bound to the SiO_2 substrate. We chose to further the use of these Pd NP catalysts by developing magnetically recoverable particles. To ensure that the maximum amount of surface area of the Pd NPs would still be available for catalysis, we decided to synthetically link the Pd NPs to magnetic $CoFe_2O_4$ NPs via long-chain carbon molecules.

3.2 Synthesis of $CoFe_2O_4$

A synthetic method developed by Song and Zhang was followed to produce 5 nm cobalt ferrite ($CoFe_2O_4$) nanoparticles.[64] In a typical synthesis, cobalt acetylacetonate [$Co(acac)_2$] (0.51 g, 2 mmol) and 1,2-hexadecanediol (5.2 g, 20 mmol) were added to a 250 mL round bottom flask and dissolved in 40 mL phenyl ether, 10 mL oleic acid, and 10 mL of oleylamine. The resulting solution was then heated to 140 °C under moderate stirring. Meanwhile, a solution of iron(III) acetylacetonate [$Fe(acac)_3$] (1.4 g, 4 mmol) in 20 mL phenyl ether was prepared and sonicated for 5 minutes to fully dissolve the iron salt. This solution was then added dropwise using a pipette to the cobalt precursor

solution, after which the temperature was increased to 250 °C and heated under reflux for 30 minutes. This dropwise addition of solution was very important to the production of well-defined particles, as too fast of an addition was found to form large polydisperse particles. The flask was then cooled to room temperature, after which the particles were centrifuged out of solution. The particles were then rinsed with acetone and centrifuged three times to remove any un-reacted materials. The particles were finally re-dispersed in toluene for storage or dried under vacuum overnight for ligand exchange.

3.3 Ligand Exchange and Linking of $CoFe_2O_4$ to Pd Nanoparticles

The surface of the as-synthesized $CoFe_2O_4$ NPs were stabilized with oleic acid and 1,2-hexadecanediol. Both of these molecules have hydroxide groups at one end of the carbon chain, which coordinate to the surface of the NPs while they terminate in methyl groups at the other end of the carbon chain. To allow for linking between the $CoFe_2O_4$ NPs and the Pd NPs these ligands were replaced with mercaptoundecanoic acid (MUDA). The terminating thiol on the end of the carbon chain allows for cross linking to the Pd surface.

Various different ligand exchange methods were examined to determine the most efficient means to attach the MUDA to the $CoFe_2O_4$ NPs. We began by centrifuging 29 mL of $CoFe_2O_4$ particles out of solution and redispersing in 35 mL toluene. 1.0 g of MUDA was added to this solution and stirred for 2.5 hours to allow for binding to the $CoFe_2O_4$ NPs. 25 mL of synthesized Pd NPs dispersed in toluene were added to this solution and stirred overnight.

After centrifuging and rinsing with acetone, these particles were used in basic hydrogenation experiments. Though more reusability was found with these particles than

with Pd alone, it was significantly less than we hypothesized. We determined that the problem was most likely that the $CoFe_2O_4$-Pd linking was not occurring for the majority of the particles. We attempted to fix this problem by varying the amount of MUDA added to solution as well as the amount of time, which we allowed the binding between the two particles to occur. For one experiment, 3 days were allowed for both the binding of the MUDA to the $CoFe_2O_4$ as well as the linking between the particles.

While increasing the linking time and ligand concentration both seemed to increase the amount of linking between the NPs, the recoverability of the catalyst still was quite low. After re-examining literature examples of similar ligand exchanges a procedure by Bagaria *et. al.* was found, which we modified for this work.[65]

In a typical exchange, a solution of MUDA (2.5g) in 5 mL cyclohexane was prepared in a 15 mL centrifuge tube. A 50 mg sample of dried $CoFe_2O_4$ NPs was added to this centrifuge tube along with enough cyclohexane to bring the total volume of the solution to 13 mL. The resulting solution was thoroughly shaken for 5 – 10 minutes, and allowed to rest for at least 30 minutes. After resting, the solution was centrifuged at 6500 RPM for 5 minutes and discarded. The remaining particles were redispersed in cyclohexane, centrifuged and solution discarded. This process was repeated two more times before a wash with ethanol and a final wash with acetone to thoroughly remove any excess ligands. After a final centrifugation, the particles were redispersed in 5 mL toluene. This solution was placed in a 25 mL round bottom flask along with 20 mL of synthesized Pd NPs and stirred slowly for 12 hours.

We found that the highly concentrated, nearly super-saturated, MUDA solution was vital for this ligand to replace the original surface coverage consisting of oleic acid

and 1,2-hexadecanediol. The multiple washes allowed for the removal of the majority of the native ligands from solution so that the $CoFe_2O_4$ NPs in solution would be MUDA terminated. The 12 hour stir time after adding the Pd NPs allowed for sufficient time for full linking between the two particles. The ligand exchange process is illustrated in Figure 3.1. The as synthesized $CoFe_2O_4$ particles are surface stabilized via the hydroxyl groups on the oleic acid and 1,2-hexadecandiol. After ligand exchange, the $CoFe_2O_4$ particles become stabilized by MUDA, which is also coordinated to the surface of the NPs via hydroxyl groups. The similar structure of the binding ligands illustrates why such an excess of MUDA must be added for ligand exchange to occur.

The MUDA stabilized $CoFe_2O_4$ NPs then link to the surface of the Pd NPs via the thiol group as illustrated in Figure 3.2. Though an idealized illustration, it helps to illuminate the proposed linking, as well as some potential problems. We know that the thiols will bind to the Pd NPs, however this requires an open site on the surface of the Pd. Steric interference from the n-dodecyl sulfide carbon chains could also pose a potential problem for this linking. Finally there is the potential using this method for $CoFe_2O_4$ NPs to become cross linked to each other or for large clusters of linked $CoFe_2O_4$-Pd NPs to form.

To gain an understanding as to the nature of the linking between the NPs, we conducted a full characterization of the NPs before and after linking.

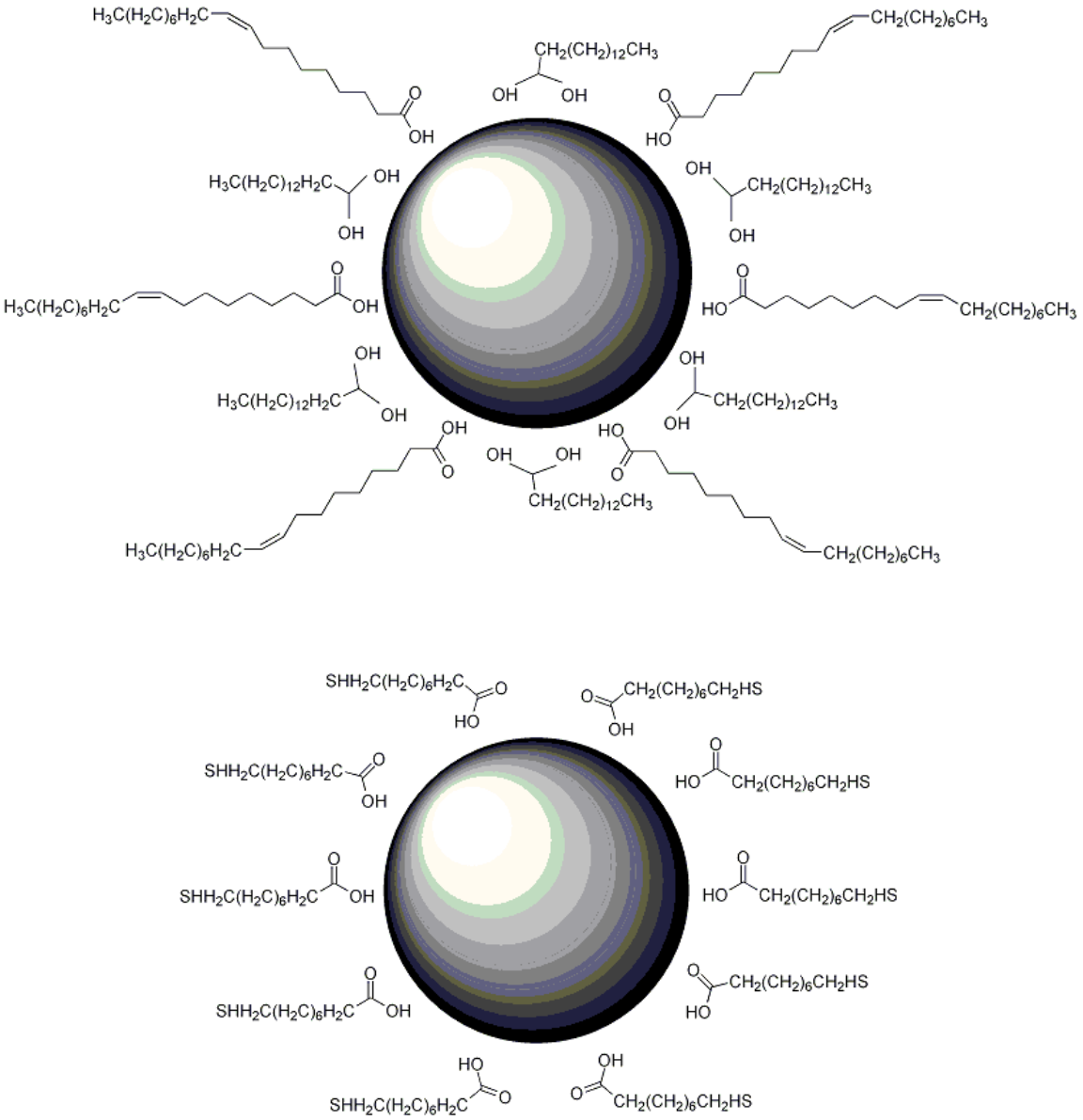

Figure 3.1: Illustrations of a $CoFe_2O_4$ synthesized nanoparticle before and after ligand exchange. Note the figure is drawn as a guide for understanding the surface of the NPs, and is not drawn to scale.

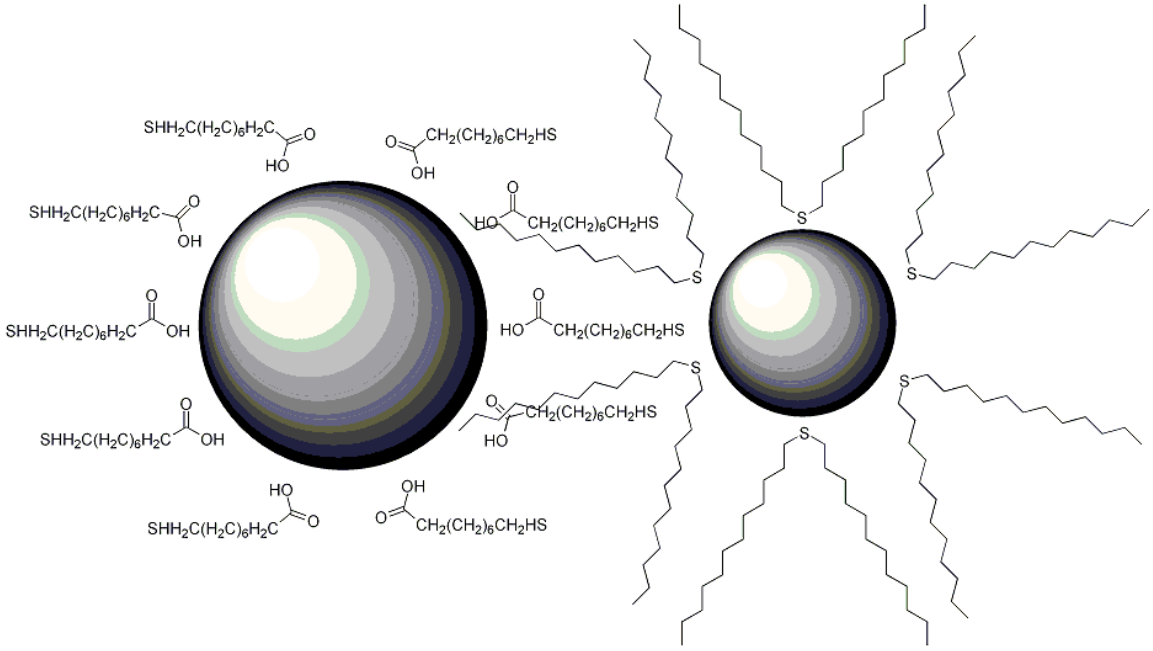

Figure 3.2: Illustration of a $CoFe_2O_4$-Pd linked nanoparticle. Note the figure is drawn as a guide for understanding the interaction between the two particles, and is not drawn to scale, nor suggests an actual proposed geometry.

3.4 Characterization of $CoFe_2O_4$-Pd nanoparticles

Characterization of the $CoFe_2O_4$ NPs, Pd NPs and $CoFe_2O_4$-Pd linked NPs was carried out in largely the same fashion as described in Chapter 2 of this dissertation. A few additional techniques were explored to obtain a better understanding of the linked $CoFe_2O_4$-Pd NPs.

3.4.1 Transmission Electron Microscopy

TEM was again the first characterization technique examined. Samples of Pd, $CoFe_2O_4$, and $CoFe_2O_4$-Pd NPs were prepared, drop cast on copper grids, and analyzed as noted in Chapter 2. It should be noted that for the solution of $CoFe_2O_4$-Pd NPs, before drop-casting the particles were magnetically separated so that only magnetic particles (i.e. $CoFe_2O_4$-Pd linked NPs, or $CoFe_2O_4$ NPs) were present.

TEM images showed that synthesized $CoFe_2O_4$ NPs were well stabilized via the oleic acid and 1,2-hexadecandiol ligands. No noticeable aggregation was found. The particles were fairly monodisperse with an average diameter of 4.7 ± 0.4 nm as shown by the histogram in Figure 3.4.

Images of the $CoFe_2O_4$-Pd linked particles were less defined. Images were collected on multiple occasions however it was difficult to ascertain any concrete structural information about the particles. Most particles appeared to be aggregate "clumps" without very-well defined edges. Because of this it was not possible to obtain a size distribution. One of the best collected images is shown in Figure 3.5.

Figure 3.3.: Demonstration of magnetic properties of $CoFe_2O_4$-Pd linked NPs. The image on the left shows a concentrated solution of the NPs. The image on the right shows the same solution immediately after placing it in a magnetic field.

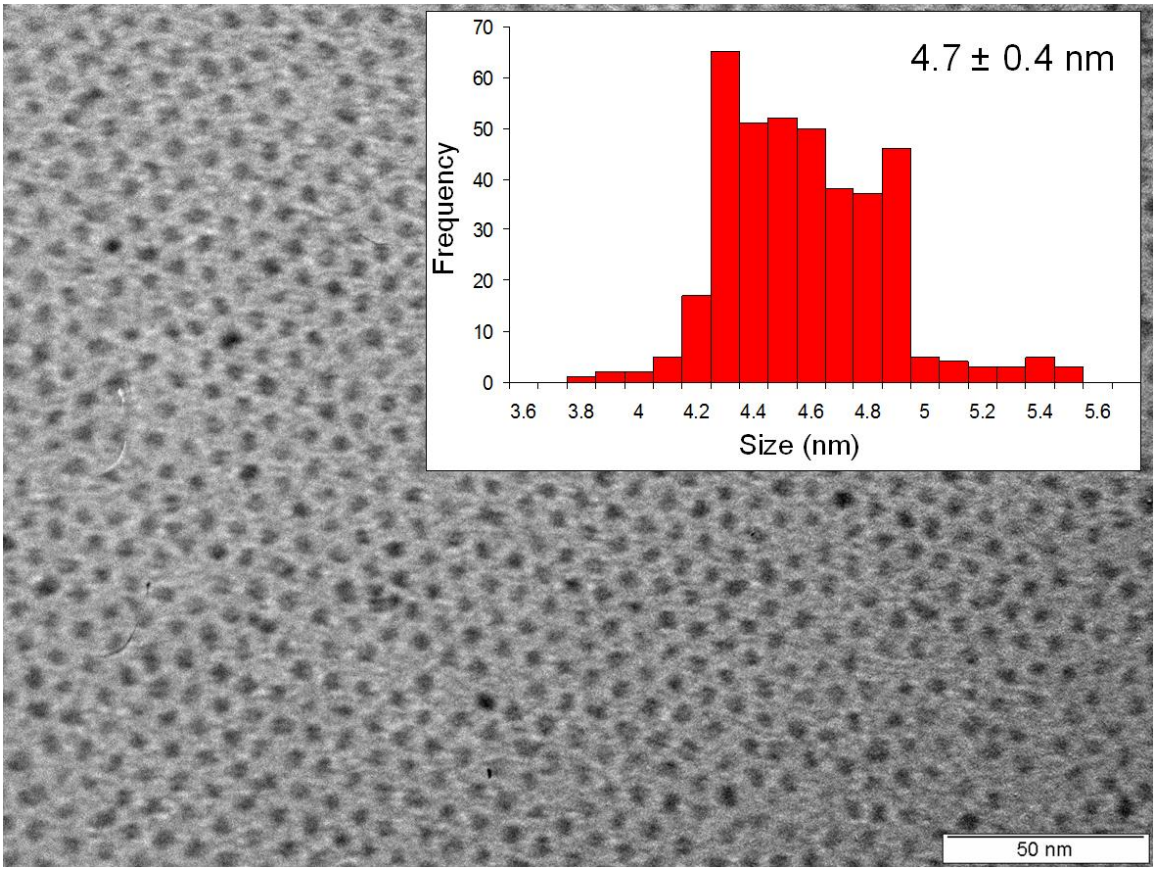

Figure 3.4: TEM image of synthesized $CoFe_2O_4$ NPs. Inset gives a histogram of the relative particle size distribution

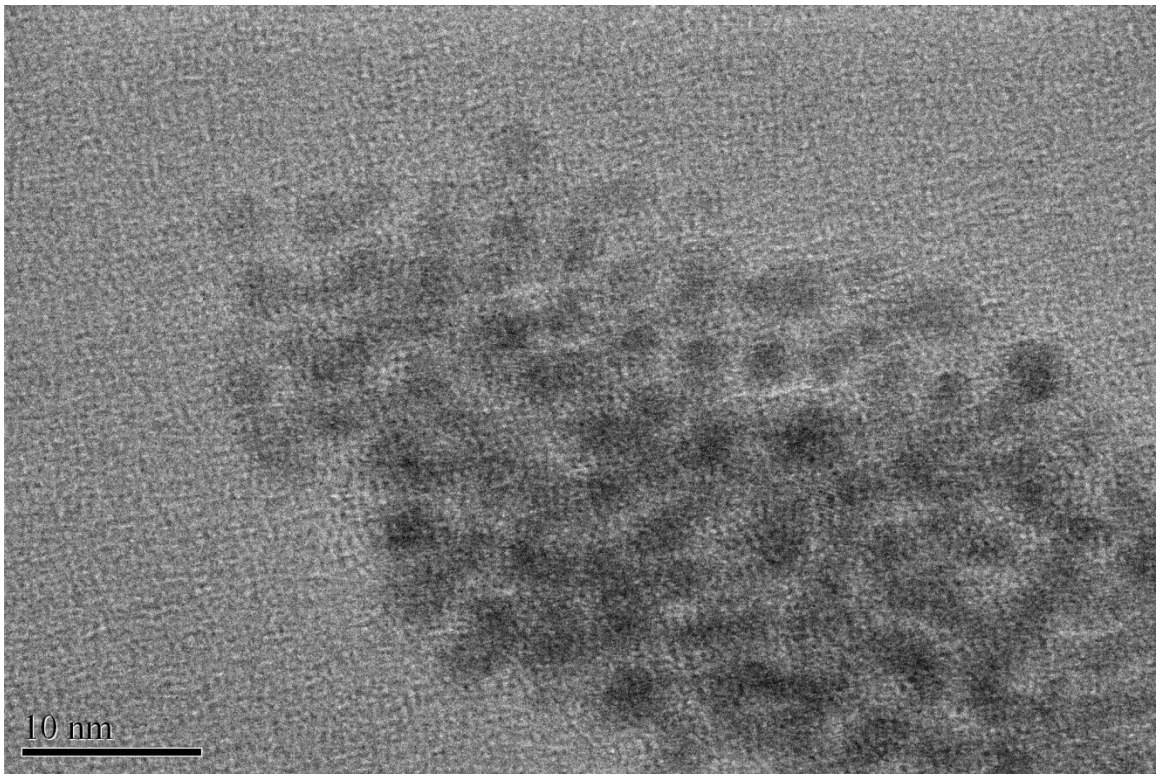

Figure 3.5: TEM image of linked $CoFe_2O_4$-Pd NPs.

3.4.2 Energy-dispersive X-ray spectroscopy

After imaging the NPs we utilized Energy-dispersive X-ray spectroscopy (EDX) to study the elemental composition of the prepared TEM samples. While the quantitative data from this technique was deemed unreliable, we did gather an important qualitative confirmation of particle linking. EDX analysis of $CoFe_2O_4$ NPs showed that both Co and Fe were present. More importantly, in the background signal no peaks relating to Pd were observed. EDX analysis performed on the linked particles however did show an appearance of a Pd peak as well as the Co and Fe peaks. Since this sample was magnetically separated (as noted in the previous section), and no Pd peaks were found in the background, the Pd signal could only be due to Pd NPs linked to the $CoFe_2O_4$ NPs.

3.4.3 Scanning Electron Microscopy

Due to the difficulty in obtaining high quality TEM images we explored using scanning electron microscopy (SEM) to further image the particles. A solution of magnetically separated $CoFe_2O_4$-Pd NPs was drop-cast onto a Si wafer for imaging.

While the images are not perfectly clear, it does appear that the particles exist in a type of “cauliflower” organization with larger particles decorated on the surface with smaller ones. This is what would be expected given our proposed linking arrangement. Larger aggregate clusters of these particles are also observed (most likely due to aforementioned cross-linking), which would further explain why the imaging and characterization of these NPs is difficult.

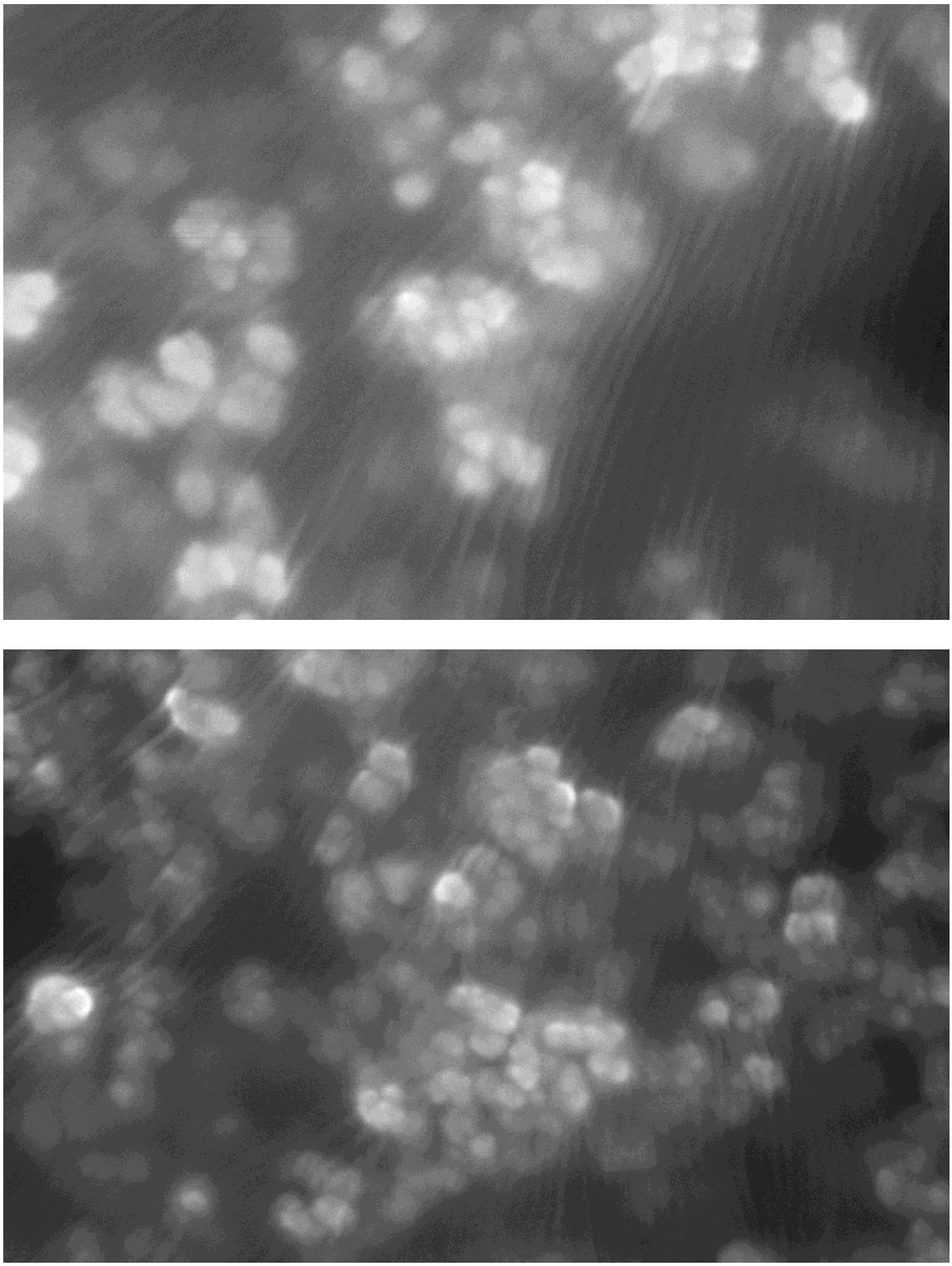

Figure 3.6: SEM images of $CoFe_2O_4$-Pd linked NPs

3.4.4 Thermogravimetric Analysis

One of the most difficult to characterize, and thus most often ignored, aspects of wet-chemically synthesized nanoparticles are the stabilizing ligands present on the surface. As opposed to bulk materials, or fabricated micro or nanoparticles, synthesized nanoparticles routinely have organic ligands present on their surface to prevent agglomeration. Additionally, in a typical synthesis there are an excess of ligands in solution, which are removed through purification. This makes it very difficult to determine the final ligand surface coverage on a typical particle. Thermogravimetric analysis (TGA) has been chosen as a means to try to begin to understand the amount of these ligands present on the suface of synthesized $CoFe_2O_4$, Pd and linked NPs.

A solution of NPs was placed in a watchglass and dried under vacuum for 24-48 hours to remove all solvent. Then 2-3 mg of the dried particles was weighed in a crucible and placed on the TGA balance. The oven was closed and the particles were heated from 25 – 900 °C at a rate of 10 °C per minute. Initial measurements were performed under compressed air flow, however it was found that the mass would actually increase slightly during the initial heating, which was attributed to oxide formation on the surface of the particles. To combat this, subsequent measurements were carried out under nitrogen flow. During the heating, the organic ligands present on the particles would be removed leaving behind only the metal. By subtracting the final weight from the initial weight, the mass of the ligands present in a known sample mass can be determined.

The TGA curves for as-synthesized and MUDA stabilized $CoFe_2O_4$ NPs, as well as synthesized Pd NPs are found in Figure 3.7. By subtracting the final mass of the particles from the initial we find the overall loss in mass, which we attribute to the

organic ligands present on the surface of the NPs. We then can find the percentage of the initial mass, which is attributed to stabilizing ligands.

For these samples we find approximately 11% ligands/mass for the Pd NPs, 21% for the as-synthesized $CoFe_2O_4$ NPs, and 30% for the MUDA stabilized $CoFe_2O_4$ NPs. This data illustrates that the MUDA stabilized particles contain a significantly higher percentage by mass of stabilizing ligands, which is most likely due to the fact that the large excess of MUDA used in ligand exchange prevents almost any bare sites from being present on the surface of the NPs.

Additionally, the shape of the curves shows only one major decrease in mass for both the Pd and as-synthesized $CoFe_2O_4$ NPs. In the case of the Pd NPs this is due to the fact that only n-dodecyl sulfide resides on the particle surface. For the synthesized $CoFe_2O_4$ NPs, both oleic acid and 1,2-hexadecandiol have similar boiling points (360 and 364 respectively) and were found to evolve at approximately the same time on the TGA curves thus only one major decrease is found. The MUDA stabilized particles demonstrate a more drawn out trace with what appears to contain at least two distinctive drops. Though the temperatures of the second drop appear significantly higher than one would expect given the boiling point of MUDA (350) it certainly appears that more species of ligands are found on the MUDA stabilized $CoFe_2O_4$ NPs, which is what would be expected.

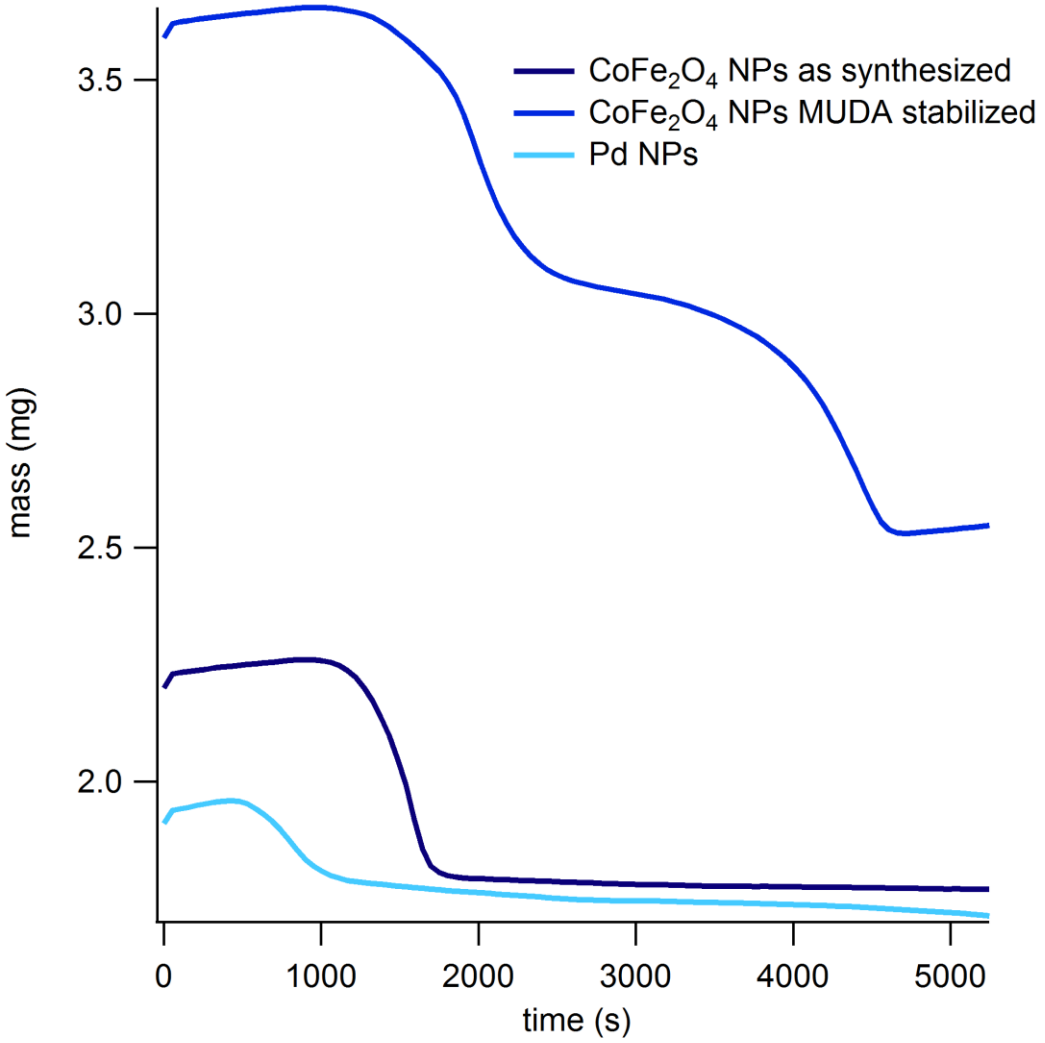

Figure 3.7: TGA curves for as-synthesized and MUDA stabilized $CoFe_2O_4$ NPs as well as Pd NPs

3.4.5 IR Spectroscopy

Due to the addition of the ligand exchange step for these particles we also examined IR spectroscopy as a means to witness the ligand exchange occurring on the surface of the NPs. Samples of each of Pd, $CoFe_2O_4$, and $CoFe_2O_4$-Pd NPs were dried overnight in a vacuum oven. The stage of the spectrometer was cleaned with acetone, force gauge set to 50 and a background scan was collected. IR spectra were collected for each NP sample as well as for all possible stabilizing ligands.

While giving far from conclusive results, the IR spectra in Figures 3.8 and 3.9 demonstrate a few features. First, it is readily observed that the Pd NPs are stabilized solely by n-dodecyl sulfide. Additionally it appears that the MUDA stabilized $CoFe_2O_4$ NPs have a similar IR spectra to the MUDA alone. However due to the similarities between the structures of the various organic ligands and the weak IR peaks it is almost impossible to draw any meaningful conclusions about the surface ligand coverage. Finally the $CoFe_2O_4$-Pd linked NPs appear to quench almost all of the IR features of the organic ligands thus making it even more difficult to determine their ligand structure.

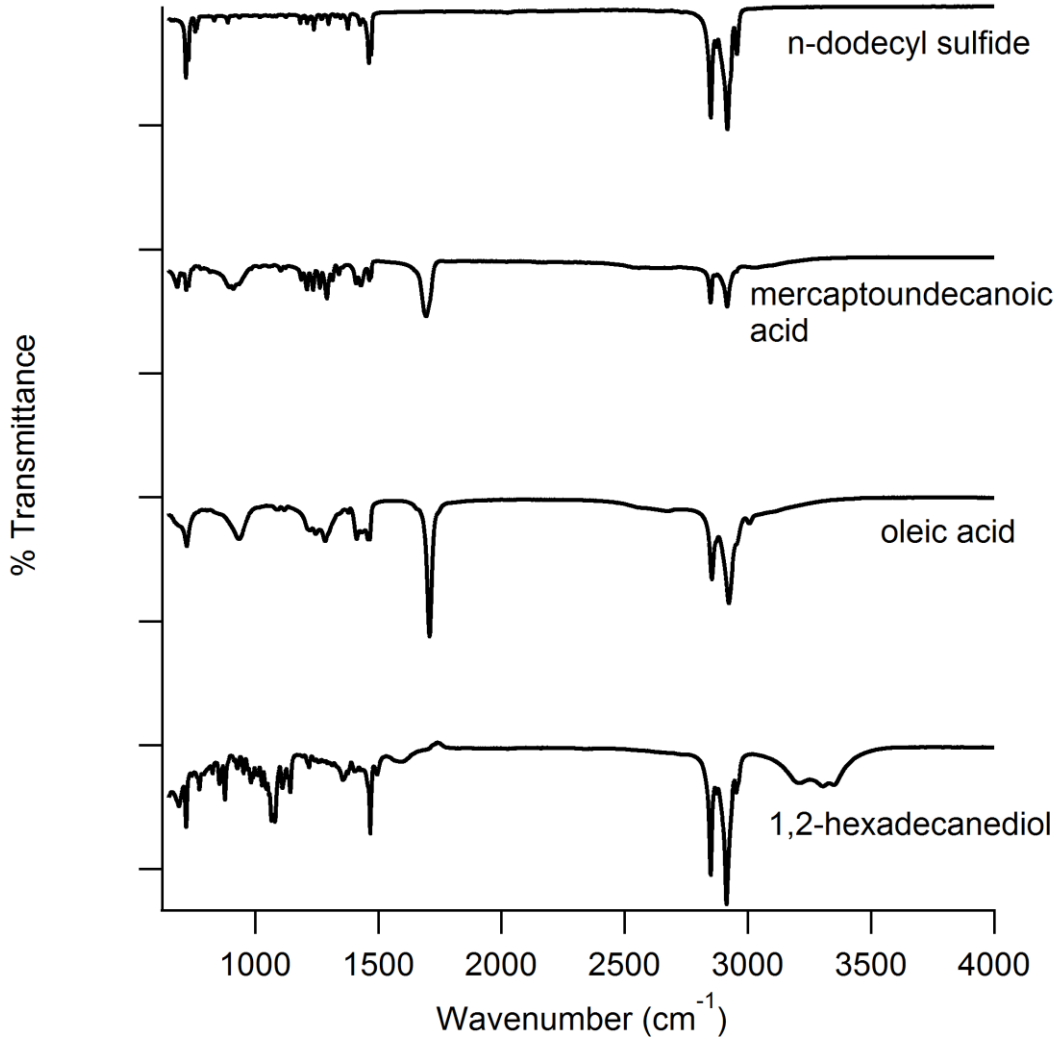

Figure 3.8: IR spectra for the four possible ligands present (n-dodecyl sulfide, mercaptoundecanoic acid, oleic acid, 1,2-hexadecanediol) in linked $CoFe_2O_4$-Pd NPs.

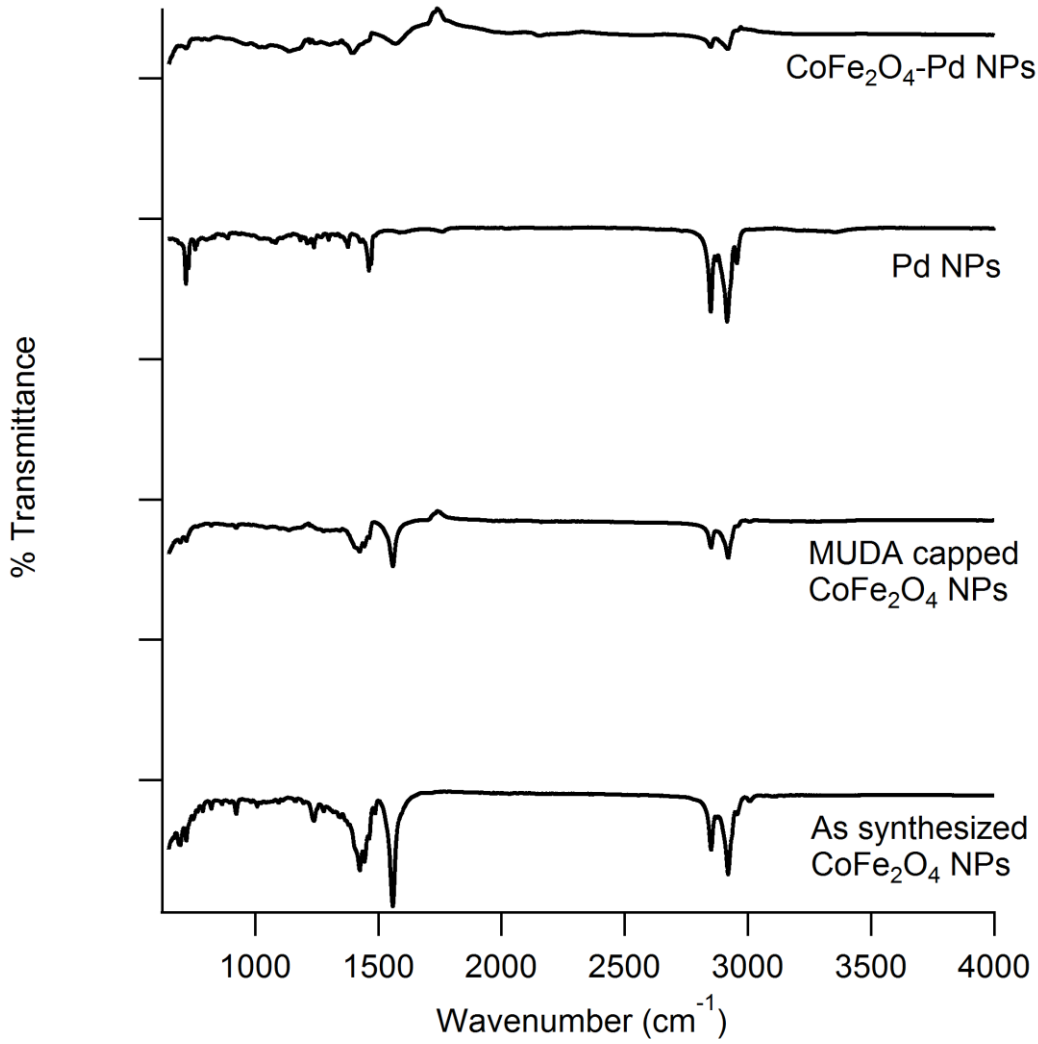

Figure 3.9: IR spectra for synthesized $CoFe_2O_4$ NPs before and after ligand exchange, Pd NPs, and $CoFe_2O_4$-Pd linked NPs.

3.4.6 Characterization conclusions

We have found that it is extremely difficult to fully characterize these $CoFe_2O_4$-Pd linked NPs. This is not all that surprising as the structure is most likely not-uniform between various particles and could become quite complex. We have determined that the most likely orientation is some type of clustering where one or more MUDA stabilized $CoFe_2O_4$ NPs are linked to multiple Pd NPs. To determine if this type of arrangement gives us the desired catalytic properties we explored their use in a set of hydrogenation experiments.

3.5 Proposed catalytic cycle for hydrogenation with Pd nanoparticles

We propose that the catalytic cycle for hydrogenation across a C-C double bond with Pd nanoparticles follows closely with what would be expected in organometallic Pd catalysts, or other transition metal organometallic catalysts such as the well known Wilkinson's catalyst $[Rh(PPh_3)_3Cl]$.

Two hydrogen atoms bind to two open sites on a Pd(0) NP via oxidative addition, leading to a Pd(II) particle. Alkene insertion leads to a Pd(II) NP with two hydrogen molecules as well as a coordinated alkene. Subsequent hydrogen insertions occur before finally a reductive elimination leads to the desired alkane and the original Pd(0) NP catalyst.

Though Figure 3.10 demonstrates only one such reaction per particle, it is entirely possible and more than likely that the above cycle could occur on multiple sites on the Pd NPs simultaneously. This helps to illustrate how the large surface area to volume ratio of the Pd NPs aids in their catalytic efficiency relative to bulk Pd catalysts.

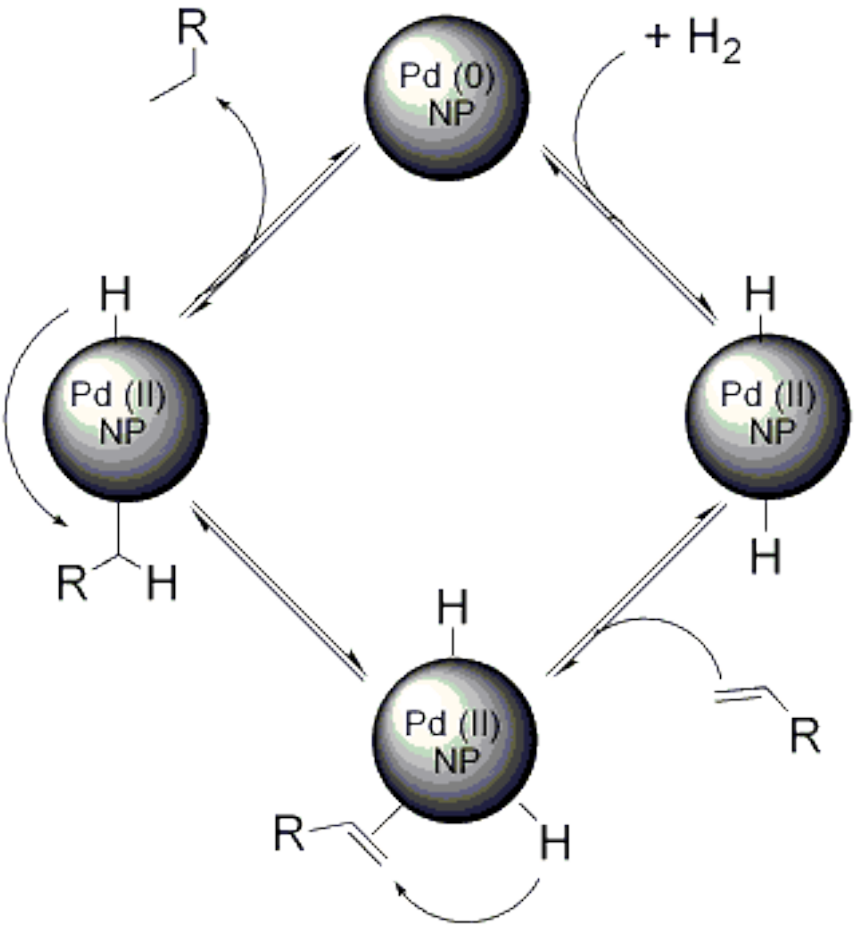

Figure 3.10: Proposed catalytic cycle for the hydrogenation across a C-C double bond using Pd NP catalysts

3.6 Conversion of 1-hexene to hexane

The first catalytic reaction carried out was the conversion of 1-hexene to hexane in which hydrogenation across a carbon-carbon double bond in a straight chain molecule occurs.

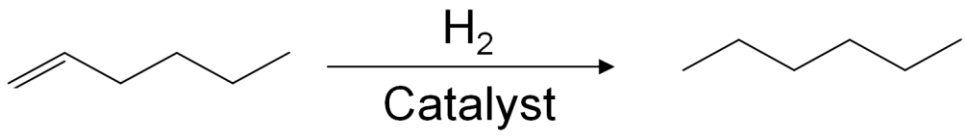

Figure 3.11 : Conversion of 1-hexene to hexane

To a 25 mL round bottom flask were added, 0.1 mL of $CoFe_2O_4$-Pd linked nanoparticles in toluene, 0.1 mL of 1-hexene, and 10 mL of toluene. This solution was placed under vacuum and flushed with hydrogen three times for 10 seconds. The solution was kept under hydrogen atmosphere under vigorous stirring at room temperature for 30 minutes. Afterwards the solution was placed in a vial and subjected to a magnetic field for 30 minutes to remove the nanoparticles to the sides of the vial. The solution was removed for analysis. The $CoFe_2O_4$-Pd NPs were then reused for another catalytic experiment in the same fashion as above. This process was repeated for 5 consecutive cycles.

This same process was carried out in the same fashion replacing the $CoFe_2O_4$-Pd NP catalyst with $CoFe_2O_4$ NPs alone, Pd NPs alone, and a blank addition of toluene.

After each catalytic reaction, GC analysis was run and compared to standards of the product and substrate, and percent conversions were determined. It was observed that

for the reactions without any catalyst present less than 5% conversion to hexane occurred. Likewise with only $CoFe_2O_4$ NPs alone, conversion was no higher than without any catalyst present. This observation leads us to determine that since the $CoFe_2O_4$ NPs alone exhibit no catalytic activity, any conversion from the $CoFe_2O_4$-Pd NPs must be due to the Pd NPs. To determine the reusability of the $CoFe_2O_4$-Pd linked particles as catalysts, they were directly compared to the conversion from the Pd NPs alone. These results are shown in Figure 3.12.

It can be seen that both particles act as very effective catalysts for the hydrogenation of the 1-hexene double bond, providing conversion yields of over 90% for the first cycle. However in the first reuse of the particles a noticeable difference occurs. While the linked particles still exhibit high conversion efficiencies in excess of 90%, the Pd NPs alone yield only a 25% conversion. With subsequent cycles, the linked particles lose some conversion efficiency (most likely due to unlinked Pd NPs present being lost) but still allow for hydrogenation in excess of 80%. Meanwhile, the Pd NPs alone provide less than 10% conversion by the third cycle and prove to be no more useful than no catalyst at all with subsequent uses. This is due to the fact that by the 3rd cycle almost no Pd NPs are able to be collected from solution. However the magnetic properties of the $CoFe_2O_4$-Pd linked particles allow for their removal of solution and thus subsequent reuse.

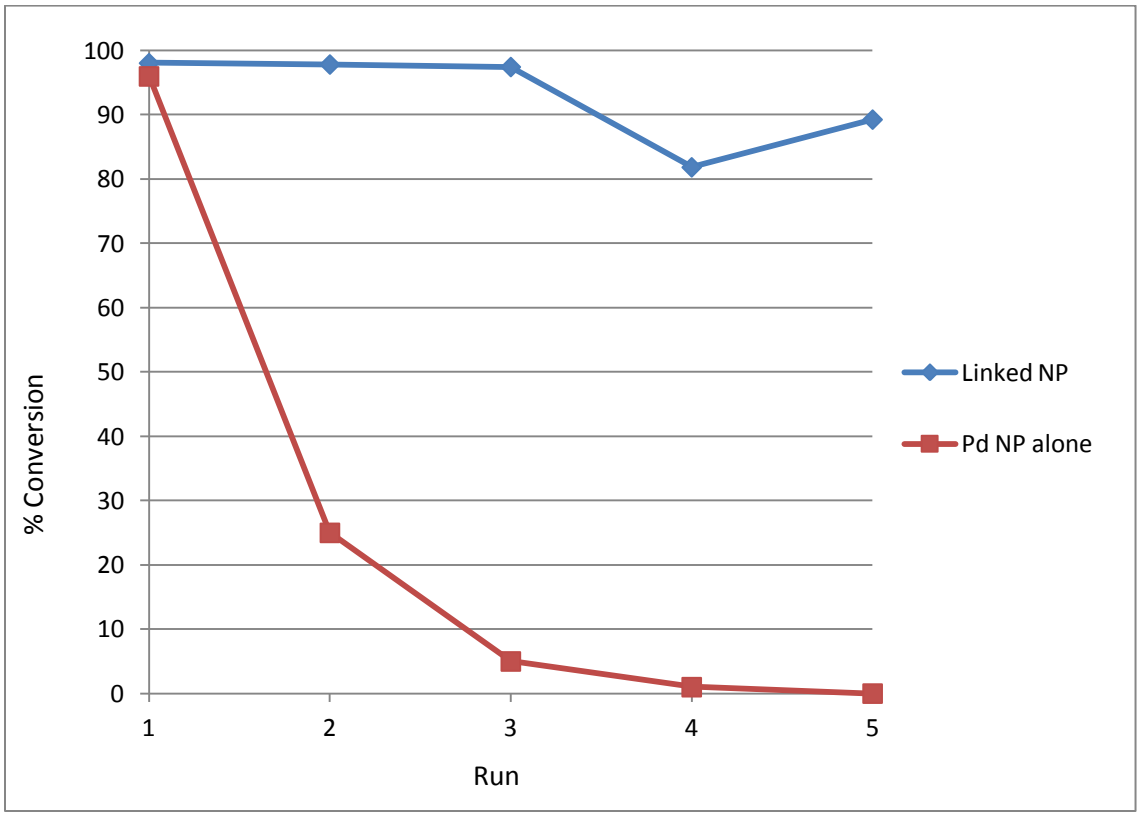

Figure 3.12: Percent conversion of 1-hexene to hexane using $CoFe_2O_4$-Pd linked NP catalysts and Pd NP catalysts alone for 5 cycles.

3.7 Conversion of styrene to ethylbenzene

To test these catalysts on an aromatic system, the hydrogenation of styrene to ethylbezene was chosen. This hydrogenation was selected to demonstrate the ability to hydrogenate across a double bond while not affecting the C-C bonds present in the benzene ring.

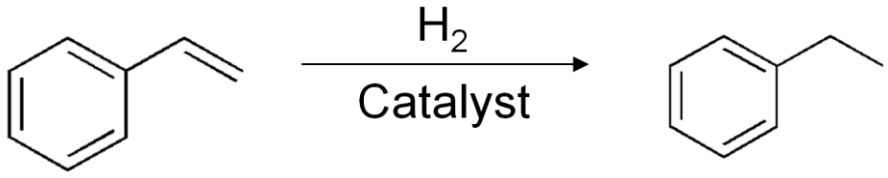

Figure 3.13 : Conversion of styrene to ethylbenzene

Experiments were carried out in the same fashion as for the 1-hexene conversion. In this case, the experiments without catalyst present and with $CoFe_2O_4$ NPs alone both showed no measureable conversion.

As with the 1-hexene conversion experiments, both the Pd NPs alone and $CoFe_2O_4$-Pd linked NPs provided conversion efficiencies in excess of 90%. While subsequent runs for the $CoFe_2O_4$-Pd linked NPs did not have exhibit quite as high conversion as with the 1-hexene (only about 85%) they still were reusable for up to 5 consecutive cycles without losing any further efficiency. The Pd NPs alone showed an 80% decrease in conversion by the second cycle and little to no conversion after 3 cycles, as observed in Figure 3.14.

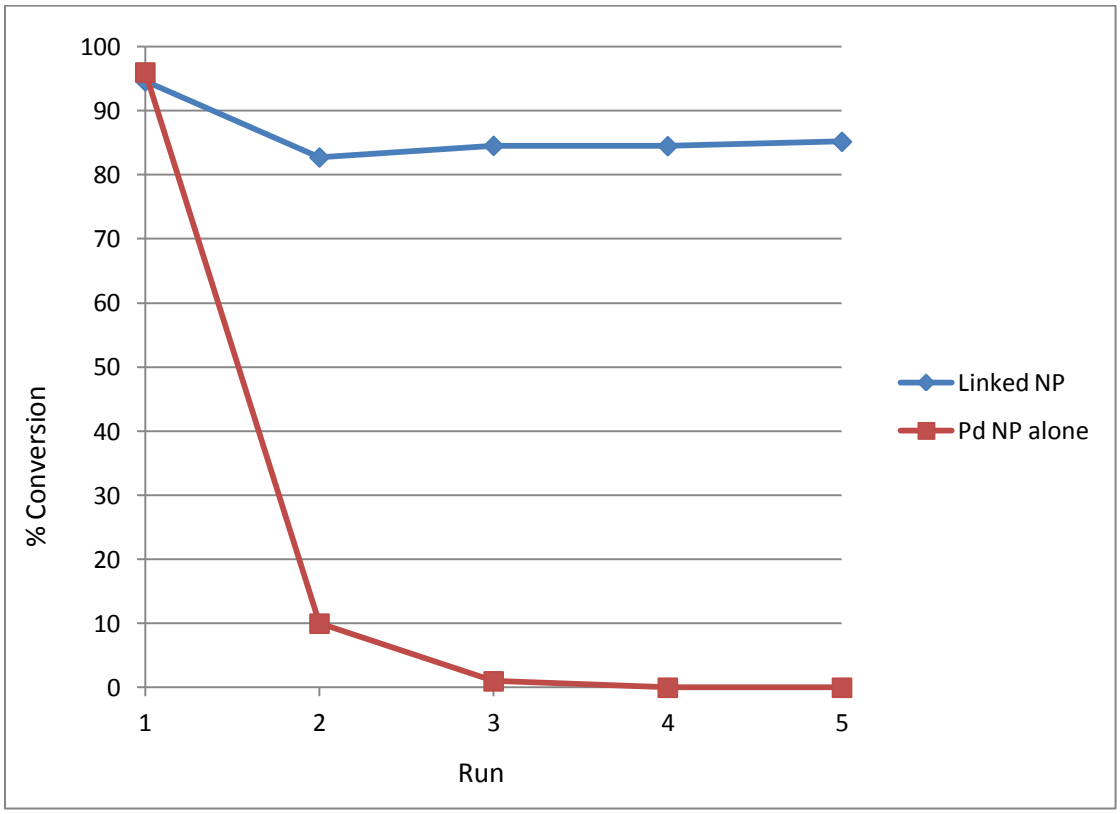

Figure 3.14: Percent conversion of styrene to ethylbenzene using $CoFe_2O_4$-Pd linked NP catalysts and Pd NP catalysts alone for 5 cycles.

3.8 Conversion of 6-bromo-1-hexene to 1-bromohexane

The final catalytic reaction examined with these particles was the conversion of 6-bromo-1-hexene to 1-bromohexane. This reaction was chosen to examine the selectivity of the $CoFe_2O_4$-Pd catalyst to the C-C double bond.

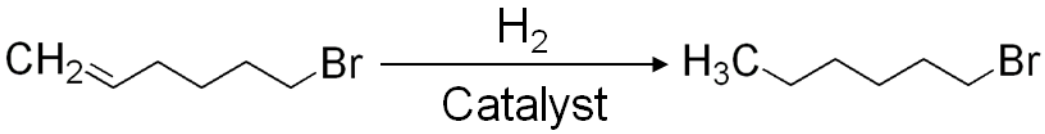

Figure 3.15 : Conversion of 6-bromo-1-hexene to 1-bromohexane

Experiments were carried out in the same fashion as for the 1-hexene and styrene conversions. Again in this case, the experiments without catalyst present and with $CoFe_2O_4$ NPs alone both showed no measureable conversion. $CoFe_2O_4$-Pd linked NPs again demonstrated a conversion efficiency of approximately 90% with high recoverability and reuse over 5 cycles.

3.9 Conclusion

We developed a new method for recovering NP catalysts by linking Pd NPs to magnetic $CoFe_2O_4$ NPs. We demonstrated the recovery and reuse of these NPs for 3 distinct hydrogenation reactions, for up to 5 cycles. This work is important as it has the potential to greatly improve the reusability of precious metal catalysts.

CHAPTER 4: CHARGE TRANSFER FROM TiO_2 TO Pt NANOPARTICLES

4.1 Introduction

At the nanoscale, many materials display unique properties from their bulk counterparts. Monolayer protected nanoclusters (MPCs) have shown an ability to display quantized capacitance charging.[66] Murray and Chen have been leaders in the field of studying the basic science behind capacitance charging of nanoparticles. It has been shown that when Au nanoparticle core sizes decreases, a transition into molecule like redox behavior is exhibited.[67] Once particle radii are reduced beyond a certain size, the shrinking size of the nanoparticle core results in the evolution of a HOMO-LUMO energy gap. Experimentally this is observed as a transition of the nanoparticles quantized charging from classical double layer charging to molecule-like redox behavior.

Careful theory has been developed to illustrate these transitions, as well as the behavior of Au nanoparticles throughout the various size regimes. Work by Murray demonstrated the transition from a continuum of density of states (DOS) in a metallic structure, to metal like quantized charging, and finally to a molecule-like energy gap as the size of Au nanoclusters decreases.[68]

The theoretical basis for quantized MPC charging begins with simple electrostatic interactions. This analysis considers neutral metallic clusters, MC, that form a series of anionic species, MC^n where n is negative via one electron transfers depicted as:

$$MC^n + e^- \leftrightarrow MC^{n-1}$$

With n = 0, -1, -2, etc. and the standard electrode potentials for first and subsequent electron-transfer steps denoted as E_n^f. These metallic clusters can be treated similarly to the conventional description for charging of gas-phase clusters for which electron addition or loss is given by:

$$\Phi_r = \Phi_{WF} + \frac{(n-0.5)e^2}{r}$$

Where e is the electronic charge, r is the radius of the conducting sphere, Φ_r is electron affinity, and Φ_{WF} is the work function of the corresponding metal-vacuum interface. This gas-phase system, through a series of relationships can be derived into an equation for the energy of electron-transfer steps in metallic clusters:

$$E_n^f = E(r \to \infty) + (n-0.5y)e/\varepsilon_s r$$

Here E_n^f is the electrode potential of redox couple in a solvent of dielectric ε_s. $E(r \to \infty)$, which corresponds to Φ_{WF}, refers to electode potential of an infinitely large cluster (bulk material) of the same material.[69] This electrostatic model has been used as the theoretical basis for the more commonly used capacitance model for MPCs.

To determine the potential steps at which single electron charging of the MPC occurs a solution of monodisperse MPCs in equilibrium with a working electrode with the potential of the MPC (E_p) is given by:

$$E_P = E_{PZC} + \frac{ze}{C_{CLU}}$$

E_{PZC} is the potential of zero charge of the nanoparticle, z is the number of electronic charges on the particle (if $z > 0$ the particle is oxidized, if $z < 0$ the particle is reduced), and e is the electronic charge. The capacitance (C_{CLU}) of the MPC with a uniform monolayer (dielectric constant ε) in an electrolyte solution can be expressed by:

$$C_{CLU} = A_{CLU}\frac{\varepsilon\varepsilon_o}{r}\frac{r+d}{d} = 4\pi\varepsilon\varepsilon_o\frac{r}{d}(r+d)$$

A few groups have extensively studied the relation between TiO_2 and metal nanoparticles. The Kamat group has been leaders in this area of research and have also studied systems involving metal nanoparticles other than gold.[70] Improved photoelectrochemical performance has been shown for TiO_2/metal (Au, Pt, and Ir) composite films, which was attributed to shift in quasi-Fermi level to more negative potentials. Additionally, this work showed chemical changes at the semiconductor-metal interface after continuous irradiation. Irradiation was also shown to cause aggregation in gold-capped TiO_2 nanoparticles where the stability of the composite was directly related to the [TiO_2]:[Au] ratio. At low ratios (<1:1) composites tend to be large and readily aggregate. When the ratio of [TiO2]:[Au] was ≥ 1:10 the particles were found to be relatively stable to 532 nm laser irradiation.[71] Kamat has also examined the effect on metal nanoparticle size on Fermi level equilibration in TiO_2/Au nanocomoposites, showing an increased shift from 20 mV for 8 nm particles to 60 mV for 3 nm gold nanoparticles.[72] In addition to these TiO_2 composites, Fermi level equilibration using ZnO/Au nanoparticle systems has been examined,[73] as well as the growth and electronic structures of Au nanoclusters on NiO compared to Au on TiO_2.[74-75]

Though far less studied than TiO_2/Au systems, other metal nanoparticle/TiO_2 composites have been explored. After gold, silver nanoparticles have been the most widely studied metal nanoparticles so it is no surprise that they have been examined in similar systems with semiconductor particles. TiO_2/Ag nanocomposites have demonstrated enhanced photocatalytic[76-79] and bactericidal[80-81] activities. Likewise,

Kamat *et. al.* has examined charge separation in TiO_2/Ag nanocomposites demonstrating charge transfer in these core-shell particles.[82]

Arguments have been made against similar electron storage in Pt nanoparticles. There have been two major arguments posed. Work by Mulvaney *et. al.* utilizing 5 nm ZnO particles with Pt islands demonstrated that with Ohmic contact induced quick transfer of the electrons to surrounding solvent.[83] Kamat *et. al.*, using similar theoretical analysis to the work they analyzed with Au particles, determined that the "electron sink" property of the Pt would not allow electrons, once stored, to discharge.[72] Neither of these theories however were examining the same system that we propose, which utilizes small (less than 3 nm), monodisperse particles not directly on the semiconductor surface.

Previously proposed systems utilizing TiO_2 and Pt for the photochemical splitting of water employ Pt doped TiO_2, most commonly using either deposition[84-85] or impregnation[86] methods of synthesis. Work by Gratzel *et. al.* in 1983 was one of the first explorations of multielectron storage for hydrogen generation by colloidal particles.[87] While this work focused on colloidal TiO_2 with co-deposited Pt surface catalyst and amphiphilic viologen derivatives for hydrogen generation, it was part of the foundation for TiO_2/Pt multi-electron storage systems. Since this early work, wide varieties of these types of systems have been investigated, including iodide or other sacrificial agent addition,[88-89] photosensitization,[90] sulfuric acid decomposition,[91] coal-hydrogen production,[92] hybrid systems[93-94] and various photocatlysts.[86, 95-101] All these systems require that the water splitting occurs under irradiation. For the utilization of monodisperse nanoparticles in these types of systems, the issue of continuous irradiation must be addressed. This has been shown recently in work by Eisenberg *et. al.* Pt

complexes [Pt(4,4′-dicarboxyl-2,2′-bipyridine)Cl_2] have been shown to be precursors to colloidal Pt after irradiation at wavelengths ≥ 455 nm. This work argues that the colloidal platinum formed after irradiation are the true catalysts for hydrogen production, not the Pt precursors.[102] Additionally though not key to this research it should be noted that TiO_2/Pt and TiO_2/Pd systems have been examined for a variety of uses, a few of which include, the mineralization of sucrose,[103] the degradation of oxalic acid, [104] the photooxidation of xylenol orange,[105] and the oxidation of carbon monoxide. [106]

4.2 Electrochemical study of Pt nanoparticles

Differential pulse voltammetry (DPV) was chosen to study the electrochemistry of the Pt NPs. A solution of Pt NPs in a 0.1 M tetrabutylammonium hexafluorophosphate ($TBAPF_6$) electrolyte solution was prepared. The solution was degassed and blanketed with ultra-high purity N_2 gas during the experiment. A glassy carbon working electrode, Pt wire counter electrode and Ag/AgCl reference electrode were placed into the solution. The voltammogram in Figure 4.1 Shows distinct peaks for the Pt NPs with $\Delta V = 0.16 \pm 0.07$ V vs. Ag/AgCl. Given that $\Delta V = e/C_{CLU,}$ the Pt NPs have a $C_{CLU} = 0.1$ aF.

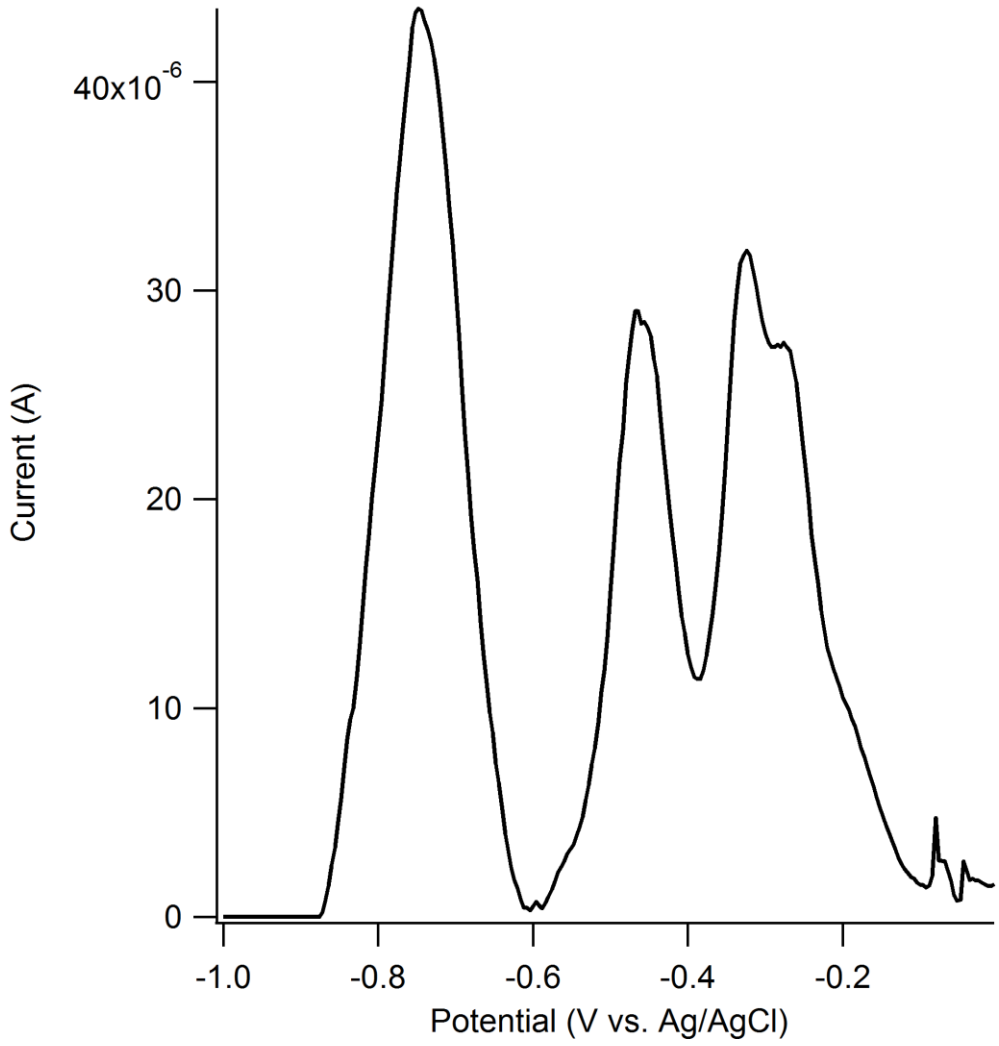

Figure 4.1: Differential pulse voltammogram of Pt NPs

4.3 Charging of TiO_2 and discharging with Pt nanoparticles

As mentioned in the introduction to this chapter, TiO_2 is a broadly used and readily synthesized wide-bandgap semiconductor with a bandgap of 3.2 eV. In the last few decades it has become a staple in the solar cell and energy industries. Due to its availability and wide use, it was decided to follow literature examples and use nanoparticle TiO_2 as the electron donor for studying charge transfer to Pt nanoparticles in solution.

TiO_2 nanoparticles were synthesized following a sol-gel method and coated onto glass slides or used in solution.[107] Additionally, commercial Degussa 10 nm TiO_2 powder was purchased and also used for these studies. The TiO_2 nanoparticles (with an approximate concentration of 1×10^{-5} M) alone were placed in a methanol solution and flushed with inert gas (either nitrogen or argon). The sealed solution was then placed in front of a 400W xenon lamp solar simulator for a 60 minute irradiation. During irradiation, charge separation within the TiO_2 occurred. The benefit of irradiating these solutions in methanol is that it is able to act as a hole scavenger, oxidizing to formaldehyde, before the exciton in the TiO_2 can recombine. This allows for the accumulation of electrons in the TiO_2 conduction band with time. To confirm that this reaction was occurring, gas chromatography of the methanol solution was conducted before and after irradiation showing the appearance of a formaldehyde peak after TiO_2 irradiation.

To study this accumulation of conduction band electrons, UV-visible absorbance spectroscopy was carried out on the TiO_2 samples before and after irradiation. These spectra displayed an increased absorbance in the region between 400-800 nm indicating

electron accumulation (i.e. [$TiO_2(e^-_{CB})$]). Additionally a characteristic color change of the particles from white to blue was observed. This process has been well documented in the literature.

In order to study charge transfer, a solution of 5×10^{-5} M of 2.5 ± 0.1 nm colloidal Pt nanoparticles in methanol was deaerated with inert gas (nitrogen or argon). Aliquots of this solution were injected into the TiO_2 sample, which immediately resulted in a loss of the blue coloration. UV-visible absorption also showed a loss of absorption intensity at 400-800 nm corresponding to a decrease in the [$TiO_2(e^-_{CB})$] population as observed in Figure 4.2. This disappearance of the TiO_2 absorption peak with increasing Pt nanoparticle addition is attributed to electron transfer from the TiO_2 conduction band to the Pt nanoparticles. It is important to note that for subsequent experiments, Pt nanoparticles were titrated into solution until the TiO_2 absorption from 400-800 nm was brought down to pre-irradiation intensity levels, thus ensuring that only electrons stored in Pt nanoparticles would be investigated.

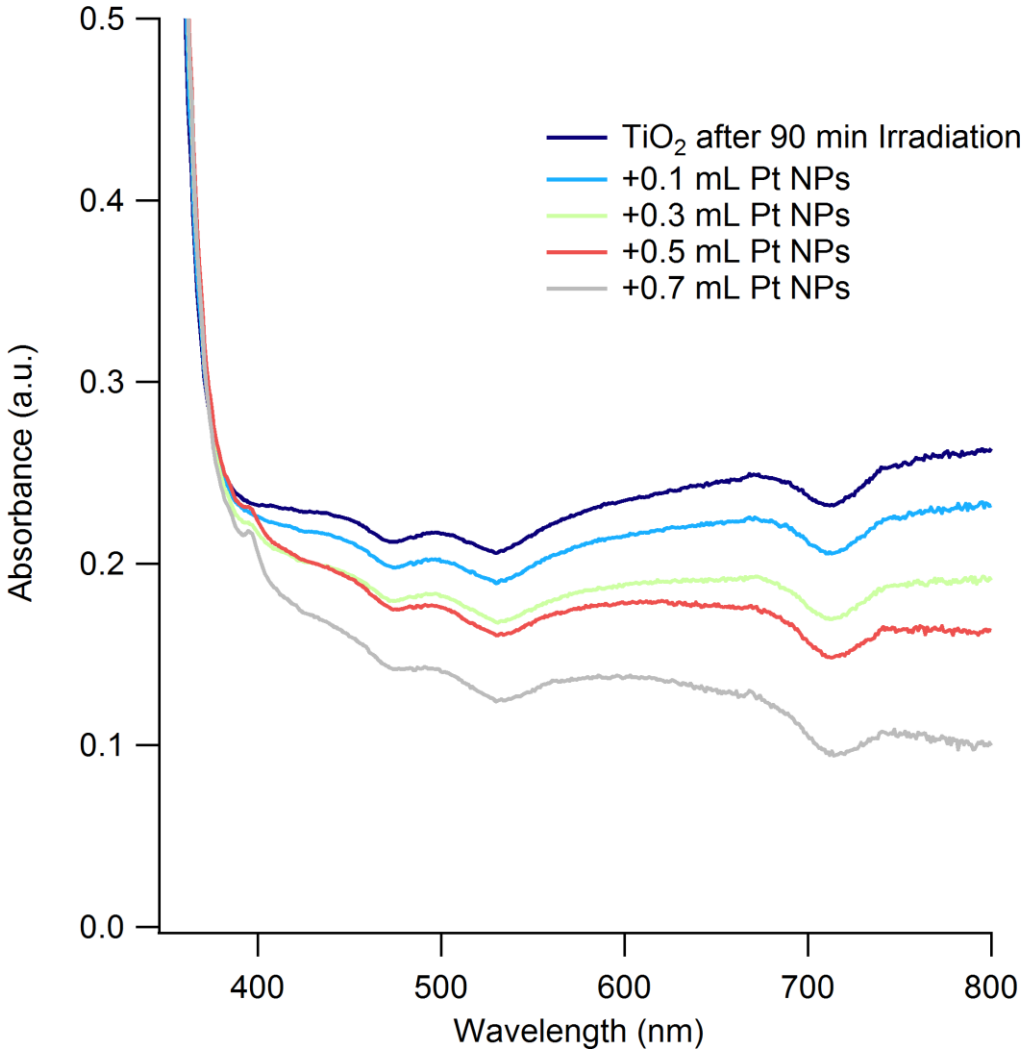

Figure 4.2: UV-visible absorption spectra of TiO_2 slide after 90 minute irradiation and after addition of 0.1 mL, 0.3 mL, 0.5 mL, and 0.7 mL of a Pt NP solution.

A variety of control experiments were also conducted to confirm that these results did in fact indicate charge transfer from the TiO_2 to Pt nanoparticles. Deaerated solutions of both the n-dodecyl sulfide stabilizing ligands and solvent alone (without any nanoparticles) were added to excited TiO_2, neither of which affected the [$TiO_2(e^-_{CB})$] population as observed through UV-visible absorbance intensity. Similarly a solution of deaerated Pt black was added to excited TiO_2 and again no change in the absorption intensity was observed. These results indicated that the 2.5 nm Pt nanoparticles possess specific ability for electron transfer of excited electrons from the TiO_2 conduction band.

4.4 Reduction of methyl viologen with charged Pt nanoparticles

Once confirmation of charge transfer to Pt nanoparticles was achieved it was necessary to determine a means to study whether any stored electrons could be discharged in a useful fashion. Based on literature examples of similar systems, the reduction of methyl viologen (1,1'-dimethyl-4,4'-bipyridinium dichloride) was chosen as a probe molecule. Electron transfer to the pyridinium can occur, which causes an observable color change making this molecule an ideal probe candidate.

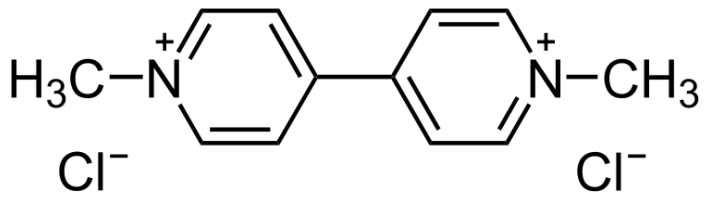

Figure 4.3 : Structure of methyl viologen

To examine this charge transfer, a solution of TiO_2 was again irradiated and Pt nanoparticles were added. To this system, a deaerated solution of methyl viologen (MV^{2+}) was injected, shaken, and allowed to equilibrate for 30 seconds. Upon addition of the colorless MV^{2+} solution the color changed to a vibrant deep blue, which is characteristic of the reduced methyl viologen radical ($MV^{+\cdot}$). UV-visible absorption spectrum showed the emergence of two peaks at 397 nm and 607 nm, which also indicated the formation of $MV^{+\cdot}$.

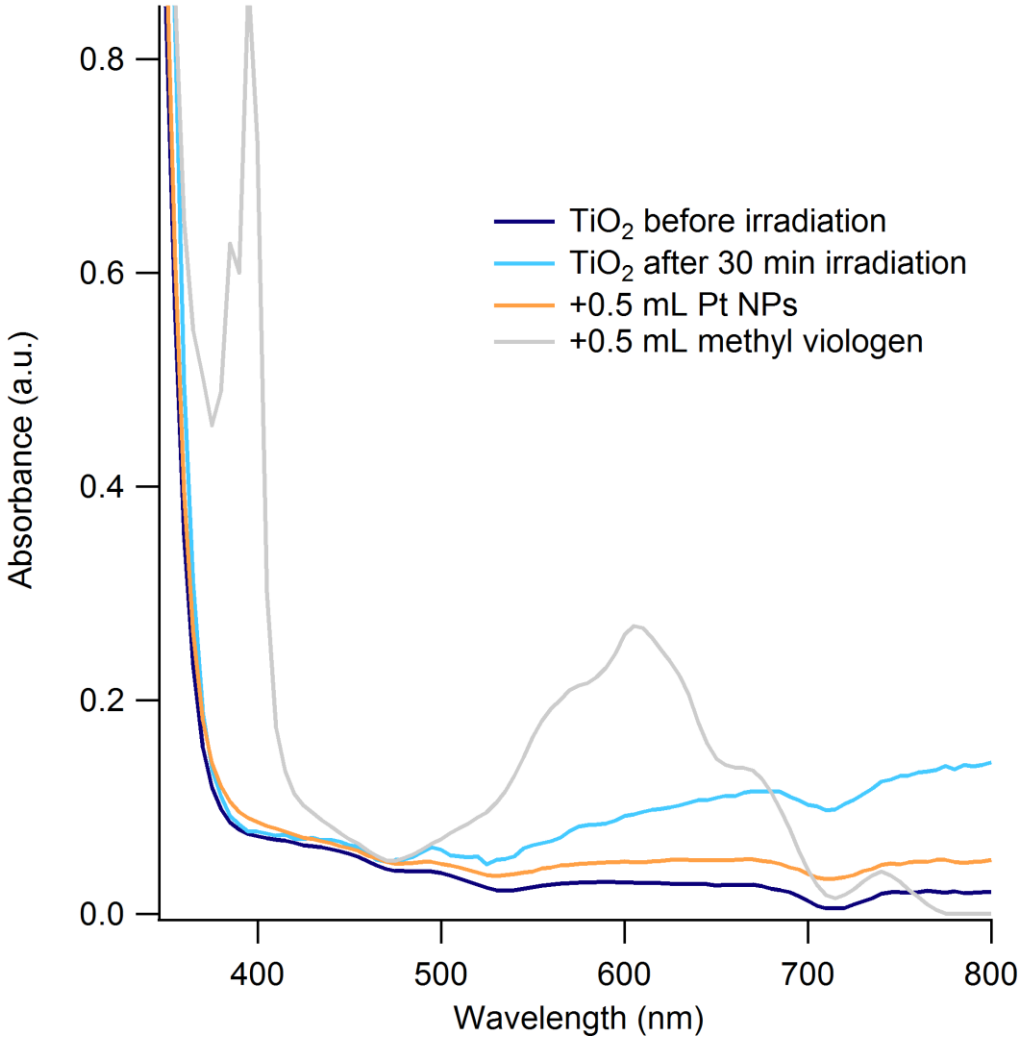

Figure 4.4: UV-visible absorption spectra of a TiO_2 slide: before irradiation, after 30 min irradiation, after addition of a 0.5 mL aliquot of Pt NPs, and after addition of a 0.5 mL aliquot of methyl viologen.

This observation led us to hypothesize that if it was possible for electron storage on these Pt nanoparticles then it could be possible for multiple electron transfer upon demand. One of the most important processes that require the transfer of multiple electrons is the production of hydrogen from water.

4.5 Water splitting with TiO_2-Pt nanoparticle system

Upon studying the water-splitting reaction, the importance of particles that exhibit multi-electron transfer capability becomes immediately apparent as the splitting of water to hydrogen and oxygen is a two electron per water molecule reduction.

$$2H_2O_{(l)} \rightarrow 2H_{2(g)} + 2O_{2(g)}$$

$$4H^+ + 4e^- \rightarrow 2H_2$$

$$2H_2O \rightarrow O_2 + 4e^-$$

To study if our Pt nanoparticles could be effective multi-electron charge catalysts for water splitting an experiment was conducted exploiting the electron storage ability of the Pt particles. In this experiment, a colloidal solution of 10 nm TiO_2 particles in dry methanol was purged with argon in a 25 mL round bottom flask. This solution was irradiated at 400W for one hour as described previously. After removal from the solar illumination, a 1×10^{-5} M aliquot of purged Pt nanoparticles was then injected into this solution allowing for electron transfer and storage on the Pt. Argon purged water was then injected into the round bottom flask and stirred vigorously before being allowed to sit. As soon as one minute after the injection, bubbles were noticed on the walls of the flask, indicating gas production. Headspace GC-analysis of this gas produced was then conducted and compared against gas standards, using the same parameters, thus confirming that the gas produced is indeed hydrogen from the water splitting, as shown in

Figure 4.5. The plots have been normalized so that they could be easily compared, which is why the production test curve appears noisy.

Additionally, standards of air, pure nitrogen, dry methanol vapor, and water vapor were all injected into the GC. None of these standards showed peaks similar to the hydrogen peak, thus confirming that we were in fact measuring hydrogen from our water splitting set up and not residual vapor from any other source.

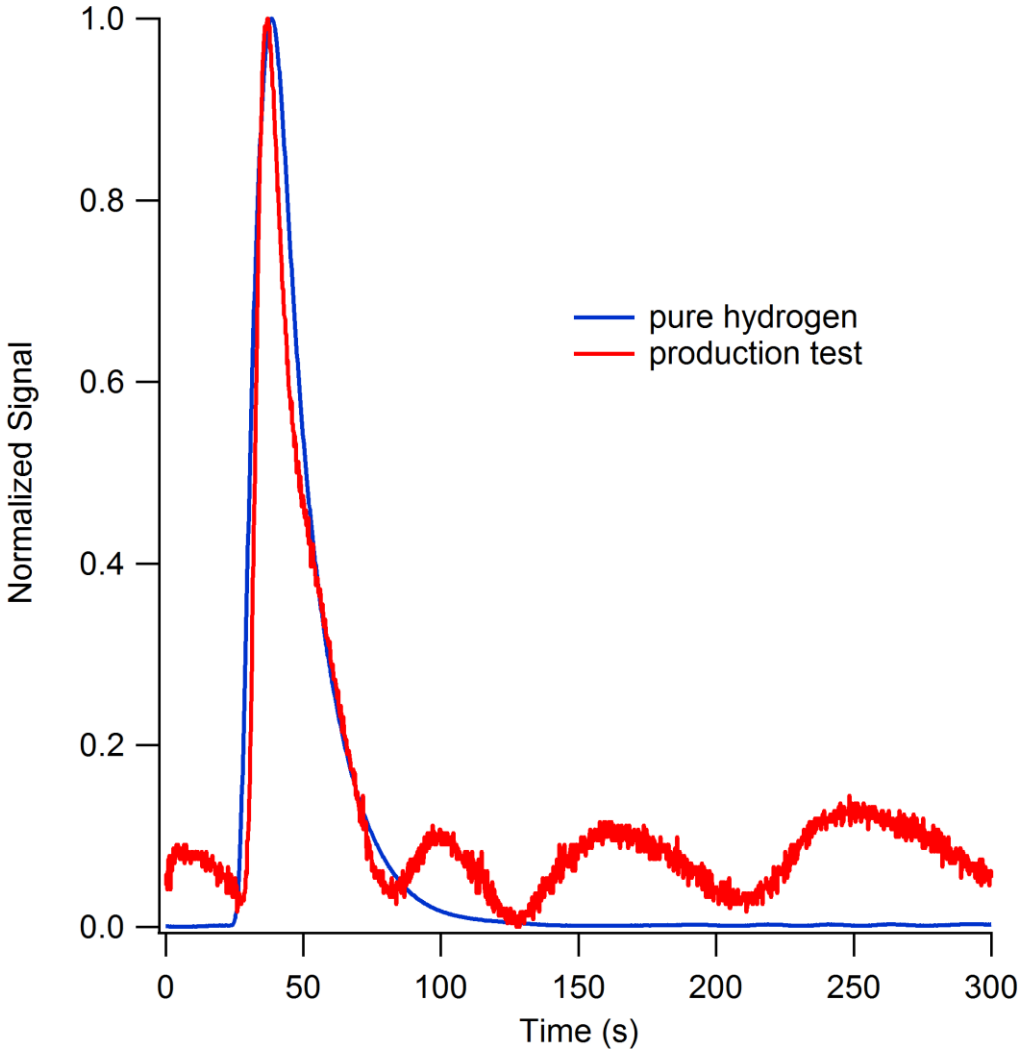

Figure 4.5: Normalized GC traces of a sample of pure H_2 and a headspace analysis of a TiO_2-Pt-water splitting production test

A variety of other experiments were conducted in a similar fashion to further examine this water splitting set-up. The first experiment conducted was to determine if Pt particle size played any role in the production of hydrogen using this set-up. We began by synthesizing Pt particles as in Chapter 2, with different reaction times of 30, 60 and 90 minutes. We then utilized these particles, as well as a sample of bulk Pt black, in water splitting exactly as before.

The GC traces collected for all of these samples showed a peak at approximately 50 s, which we have attributed to air. None of these samples showed a strong peak at 36 seconds, which is where we previously noticed the evolution of hydrogen.

These interesting results led us to further refine the particle sizes examined by conducting another set of Pt NP syntheses. In this case we narrowed the reaction times (centered around the previous heating time of 45 minutes) to 5 minute intervals ranging from 35 to 55 seconds. These 5 samples were then used for water splitting as before.

Interestingly, the strongest hydrogen evolution peak was witnessed for the 40 minute sample, which was slightly less than the particle time utilized before. Both the 35 minute, and 45 minute (the same particle time utilized before) samples showed weaker hydrogen peaks.

These results show that these synthesized Pt NPs have a unique ability for water splitting in this set-up. Additionally, the amount of hydrogen produced is highly correlated to the NP particle growth time and very specific Pt NPs are required for water splitting.

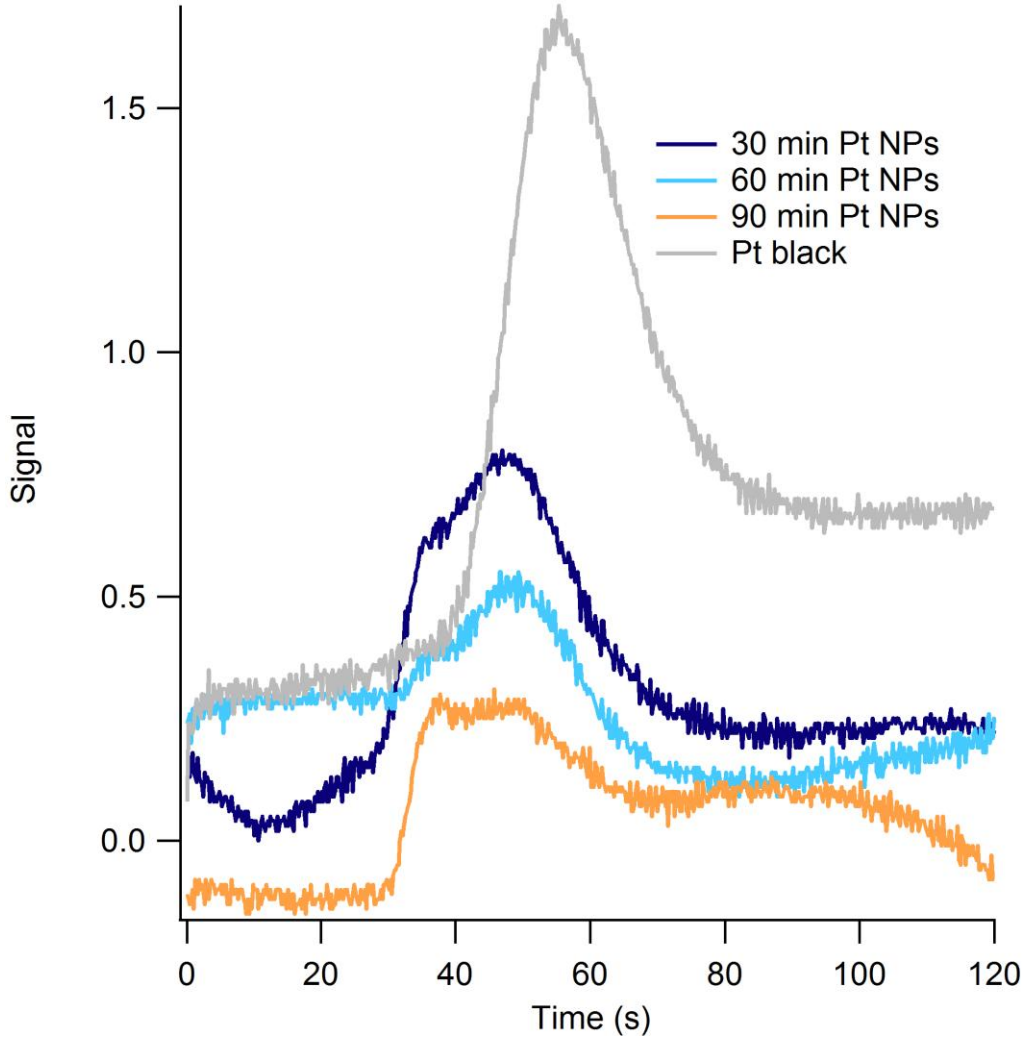

Figure 4.6: GC headspace analysis of TiO_2-Pt-water splitting hydrogen production tests for 30 min Pt NPs, 60 min Pt NPs, 90 min Pt NPs, and Pt black.

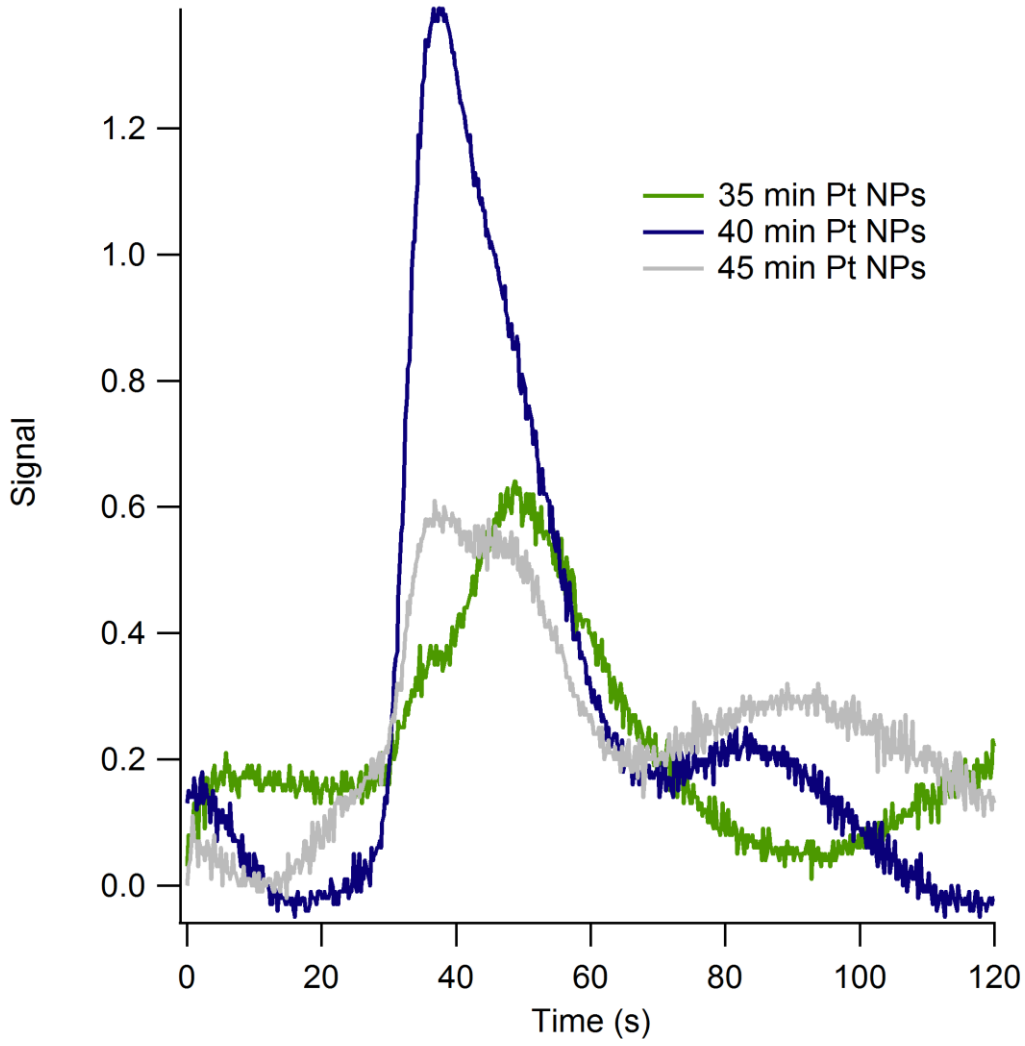

Figure 4.7: GC headspace analysis of TiO_2-Pt-water splitting hydrogen production tests for 35 min Pt NPs, 40 min Pt NPs, and 45 min Pt NPs

4.6 Examining charge transfer properties of Pd NPs

Since Pt and Pd have many similar properties we also wanted to examine the charge transfer properties of the Pd NPs that we synthesized as described in Chapter 2. We again studied these particles utilizing both the reduction of methyl viologen and the production of hydrogen through water splitting. All experiments were carried out as previously detailed, replacing Pt NPs with Pd NPs.

The reduction of methyl viologen proved to be difficult to observe with Pd NPs. Pt NPs have a more pronounced absorption as measured by UV-visible absorption spectroscopy and demonstrate measureable absorbance in the 500-700 nm range where the reduced methyl viologen peak ($MV^{+\cdot}$) appears. Additionally it is difficult to observe the decrease in the $TiO_2(e^-_{CB})$ absorbance. These problems are illustrated in the spectra in Figure 4.8. It was possible however to visibly witness the proper color changes (i.e. bluing/whitening of TiO_2 slide and bluing of methyl viologen solution) so it did appear that the Pd NPs were able to charge via the TiO_2 and discharge to reduce the methyl viologen radical.

Water splitting reactions were then conducted as before, replacing Pt NPs with Pd NPs. The Pd NPs were found to be able to produce hydrogen, giving similar signals to the 40 or 45 minute Pt NPs discussed in the previous section.

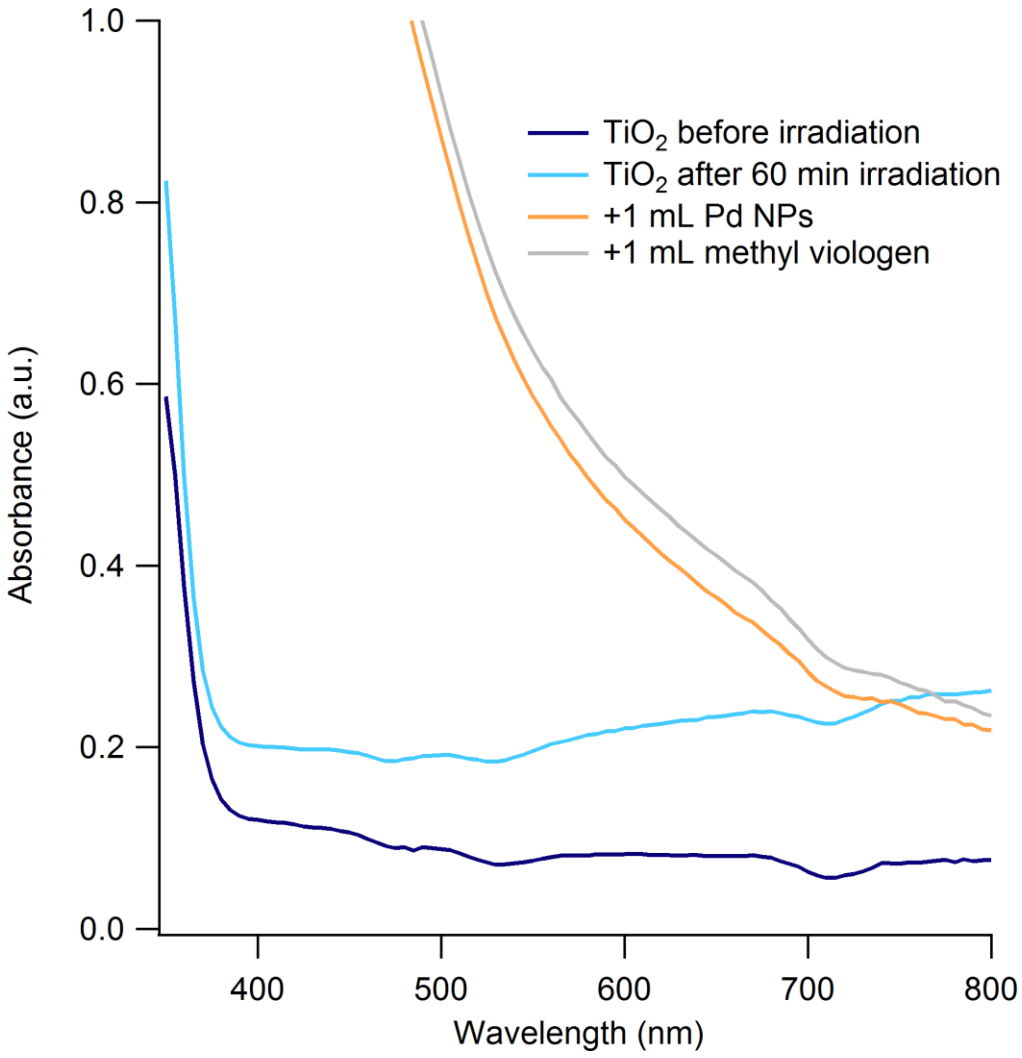

Figure 4.8: UV-visible absorption spectra of a TiO_2 slide: before irradiation, after 30 min irradiation, after addition of a 1 mL aliquot of Pd NPs, and after addition of a 1 mL aliquot of methyl viologen.

4.7 Conclusions

We have demonstrated the charging and discharging of Pt and Pd NPs. We have found a unique ability for these metal NPs to accept and store charges from irradiated TiO_2 NPs, which can then be used in the reduction of methyl viologen or the production of hydrogen from water splitting. These unique properties of sub 5 nm Pt and Pd NPs open up new avenues of exploration in various charge and energy transfer schemes. One such system involving CdSe quantum dots will be explored in the final chapters of this dissertation.

CHAPTER 5: EFFECTS OF STABILIZING LIGANDS ON THE PHOTOLUMINESCENCE PROPERTIES OF CdSe QUANTUM DOTS

5.1 Introduction

When a semiconductor particle is synthesized or fabricated with a radius that is smaller than its Bohr exciton radius (the physical distance between an electron and hole in a particle), a unique effect called quantum confinement occurs.[108-109] The materials science community terms these particles quantum dots (QDs) (when they are spherical), and extensive resources are being devoted to unlocking their photophysical properties. With a potential for use in a wide range of applications from energy to biology, the interest in QDs is only projected to increase.[110-117]

Because of our developed knowledge in Pt and Pd NPs, we wanted to examine the interaction of those metal nanoparticles with QDs, with an eye for future photocatalytic applications. The study of cadmium selenide (CdSe) QDs - Pd NPs systems is discussed in Chapter 6 of this dissertation. While preparing experiments to examine this metal NP-QD interaction however, we realized that we first needed to further understand the photophysics of the QDs themselves.

The vast majority of QDs are synthesized using a wet-chemical procedure, much like the ones previously described for Pt and Pd NPs.[54, 63, 118-121] Also, like the metal NPs, these synthesized QDs are stabilized in solution by organic ligands, which assist in particle growth and help to prevent agglomeration. Most QD syntheses are performed in a

solution with a large excess of stabilizing ligands. After synthesis, the QDs are then isolated and purified by a variety of methods. Most commonly, the QDs are precipitated with either methanol or acetone and multiple centrifugations.[122-123] These isolated particles are then usually stored in a pristine organic solvent.

For experimental fluorescence studies, an aliquot of this QD solution is removed and further diluted by multiple orders of magnitude. Additionally, for some experiments the QDs must be placed into a completely different solvent environment. When we began to study the fluorescence of these dots we found that for samples prepared in precisely the same fashion, we observed large deviations, outside of expected experimental errors, in their recorded steady-state photoluminescence (PL) and fluorescence lifetimes.

These results led us to question how the multiple steps from synthesis, to purification, to storage, to experiment may be affecting the surface of the QDs. It is well known that chemically synthesized QDs exhibit trap states where either electrons (e^-) or holes (h^+) can transfer to after excitation. Once an e^- or h^+ is trapped it can exit the trap in a variety of ways. Therefore these trap states greatly affect the dynamics of the QDs.[124-128] Common thought is that traps exist in both the core and on the surface of the QDs. While core traps should not be affected in any way upon QD dilution, surface traps could be greatly altered. Since the surface of the QDs is stabilized by organic ligands, purification and dilution of the QDs has the potential to remove some of these ligands. Besides preventing agglomeration, stabilizing ligands also remove dangling bonds on the surface of the QDs resulting from unpaired electrons on surface atoms. The removal of a ligand reintroduces a dangling bond, which is believed to be the primary cause of QD surface traps.

We hypothesized that the observed fluctuations in PL intensity and lifetimes of the QDs upon dilution was due to the introduction of these surface traps via ligand desorption. To confirm this hypothesis, we designed and conducted a full set of experiments to understand the role of native ligands on the fluorescence dynamics of QDs.

Some groups have conducted similar work, which examine changes in the steady-state PL of the QDs as the surface ligand composition is modified. The most common systems explored involve strongly-binding, non-native quenching ligands.[129-139] These studies rely on the ability to see drastic decreases in PL of the QDs as these quenching ligands bind to the surface of the particles. The two key differences with our studies are that we are studying native binding ligands, and that we are focusing our study on changes in the dynamics of the QDs. These differences make this system uniquely challenging as dynamics changes are often harder to correlate and any changes observed are not nearly as drastic as with strong quenchers. However, since nearly all QDs are capped with some native stabilizing ligands, it is vital to gain as much understanding of the QD-native ligand interaction as possible.

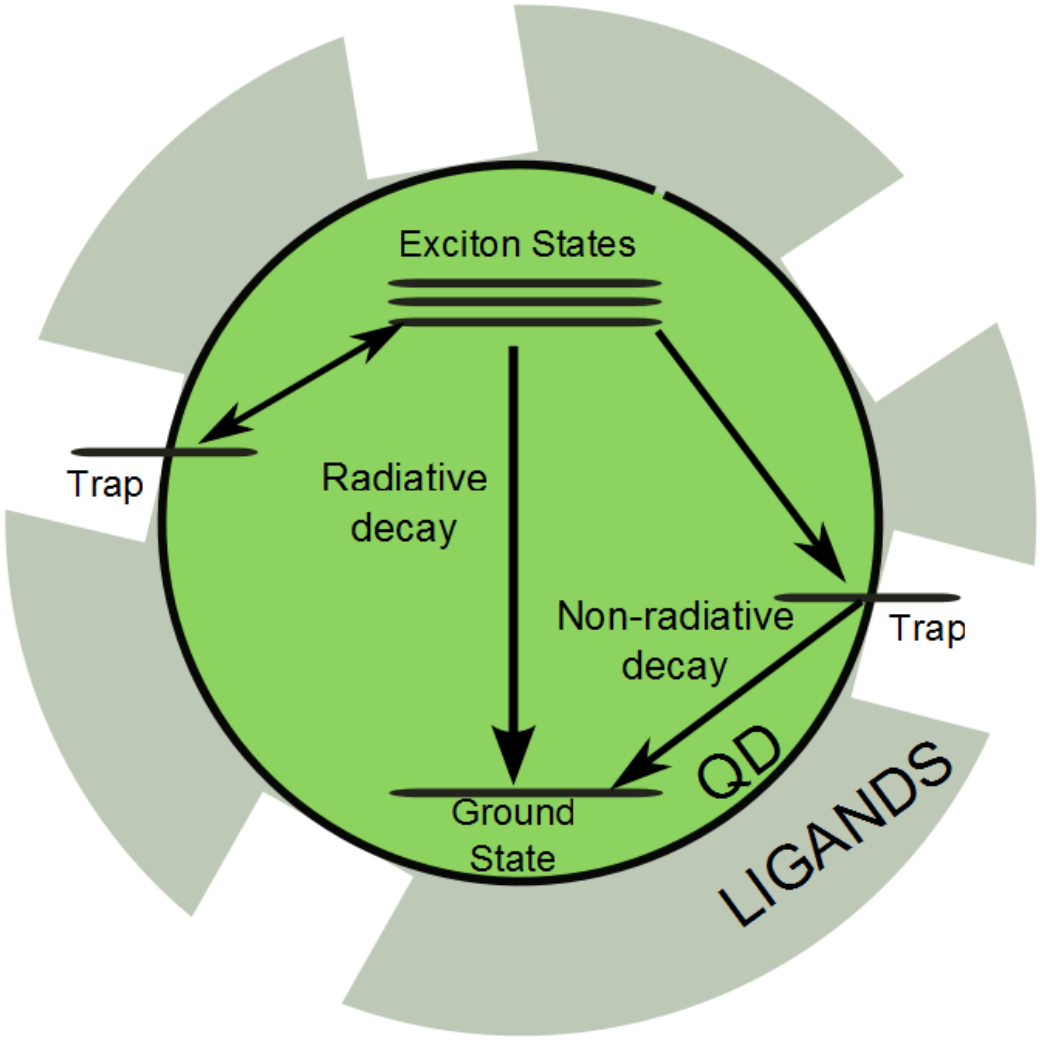

Figure 5.1: Illustration of a core only CdSe QD with incomplete surface ligand coverage. Demonstrates formation of surface traps due to gaps in the ligand coverage as well as potential dynamic pathways.

5.2 Synthesis and stabilization of CdSe QDs

CdSe QDs were synthesized using an established synthetic method, which is described in Appendix B.[121] The synthesis calls for the use of three stabilizing ligands, trioctylphosphine oxide (TOPO), hexadecylamine (HDA) and trioctylphosphine (TOP), with a majority excess of TOPO. It is expected that the TOPO and HDA bind to surface Cd atoms, while TOP coordinates to Se atoms. All three of these ligands are in excess during synthesis.

5.3 Importance of pristine solvents

The first observation we made through this work was the importance of using pristine solutions when preparing QD samples. It stands to reason that since QD samples must be diluted by many orders of magnitude, the effect of any impurities present in the solvents will increase the more the QDs are diluted. We observed that the PL of QDs diluted in technical grade toluene or hexanes would quench overtime. Attributing this quenching to impurities binding to the surface of the QDs, we then prepared samples of the same concentrations in pure anhydrous hexanes ($\geq$ 99%) and pure anhydrous toluene (99.8%). With these samples we observed much smaller changes in the PL of the QDs. However, though we did not observe the fast quenching (within minutes of sample preparation) anymore, we still observed changes in both the PL and fluorescence lifetimes of the QDs with increasing time.

Our first hypothesis was that these changes in PL dynamics were due to oxygen dissolved in the sample binding to the QDs. To study this possibility, we prepared samples in cuvettes with an 80/20 adapter fitted with a septum allowing us to purge the samples with inert nitrogen to flush out any oxygen present. After 10 minutes of purging,

steady state PL and fluorescence lifetimes were collected on the samples. By examining multiple samples prepared with purging, we found that both the steady-state fluorescence and dynamics of the QDs still fluctuated, thus leading us to conclude that dissolved oxygen was not the problem. Additionally, we found that purging the samples actually led to increased error as the organic solvents (most notably for the dots dissolved in hexanes) would evaporate under purging, thus changing the concentration of the dots. Therefore no further samples were purged with inert gas for any future studies.

With additional tests we determined that the QDs were reaching an equilibrium with bound and unbound ligands over time, causing the observed changes in the PL dynamics. To investigate this equilibrium process we designed a set of experiments to observe the changes in PL dynamics over time. To gain a more complete understanding of the equilibrium process we chose to study the changes in fluorescence dynamics overtime focusing heavily on time-correlated single photon counting (TCSPC) measurements. We chose to study the QDs with and without excess stabilizing ligands present in solution, as well as in various experimental solvents.

5.4 Experimental methods

We prepared samples by diluting a stock solution of synthesized CdSe QDs in solutions containing excesses of various stabilizing ligands. We chose to examine the three stabilizing ligands (TOPO, HDA, TOP) expected to be present on the QD. To prepare the ligand solutions a calculated mass of ligand was placed in a 10 mL volumetric flask. The flask was then filled with either pristine hexanes or toluene. A sample of the ligand solution was removed (so that it could be used to run a blank for UV-visible absorption). Finally a 16 µL aliquot of a 6.9×10^{-7} M stock CdSe QD solution

was added to the volumetric flask, which was then refilled using the removed ligand solution.

UV-visible absorption spectroscopy and time correlated single photon counting were used to examine all of the prepared samples. For each sample, the solution was divided between two cuvettes so that both techniques could be run simultaneously. This allowed for observation of any changes in the absorption and the fluorescence lifetimes of the QDs immediately after being diluted.

UV-visible absorption spectra were collected using a Cary-50 spectrometer from 600 to 200 nm at 0.5 nm intervals with integration time of 0.5 s. The spectrometer was set to run consecutive spectra so that any changes in absorption overtime could be observed over the length of the experiment.

TCSPC measurements were conducting using a Jobin Yvon Fluorolog spectrometer. The samples were excited with a 341 nm LED diode pulsed at 1 MHz. The emission monochromator was set to the determined QD emission maximum at 597 nm with a 12 nm bandpass. The TAC was set to 500 ns. Up to 50 consecutive lifetimes were collected for each sample by collecting data until 20,000 counts in the maximum peak channel and then immediately starting the next lifetime measurement. (The procedure for collecting these simultaneous lifetimes is given in Appendix C).

We were also able to determine changes in the relative quantum yield of the samples over time using the TCSPC data. By determining changes in the amount of time taken for each subsequent lifetime to be collected, we were able to quantify whether the quantum yield of the sample was increasing or decreasing with time. The Igor Pro

procedure code, which was developed to generate a collection time wave is provided in Appendix D.

5.5 Results and discussion

5.5.1 Displaying fluorescence lifetimes as contour plots

In order to better display and examine changes in the collected fluorescence lifetimes we plotted subsequent runs as contour plots. Often, fluorescence lifetimes for molecular or biological fluorophores follow one specific decay pathway, and can thus be fit to a single exponential decay function. QDs however typically have a variety of decay pathways, due to the previously discussed traps and other complicated decay processes not present in molecular fluorophores. Thus, QD fluorescence decays need to be modeled using a multi-exponential decay function.

The most commonly reported value determined by this function is the average PL lifetime. This value is the average time between excitation of the QD and detection of an emitted photon. The average PL lifetime <τ>, is given by[140]

$$< \tau >= \sum_{n} \frac{\int_0^{t_{exp}} \alpha_n \tau_n \exp\left(-\frac{t'}{\tau_n}\right) dt'}{\sum_m \int_0^{t_{exp}} \alpha_m \exp\left(-\frac{t''}{\tau_m}\right) dt''}$$

Where α_n and α_m are pre-exponential fitting constants and t_{exp} represents the time window for the PL decay experiment and is typically set to infinity.

The downfall of reporting only the average lifetime for a QD fluorescence decay is that it does not give the full picture of how the dynamics change over time. For instance, 2 QDs, which have very different looking decay curves could in theory have the same average lifetime values by the above formulation, as no information about the shape of the decay curve is given. We therefore calculate the average lifetime of the QDs as a

function of the time window, t_{exp}, ranging from approximately the minimum time resolution of the instrument to the TAC rise time. For example, the average lifetime calculated for a time window of 1 ns is the average lifetime that would be calculated if the dynamics in the first 1 ns were to continue, unchanged, for the rest of the decay.

A visual representation of this process is provided in Figure 5.2. If we fit a decay to a single-exponential function, we find that it is a straight line when plotted on semi-log axes. Using the procedure explained above, we then find values for the average lifetime as a function of t_{exp}. As shown in the bottom graph in Figure 5.2, this results in a flat line: the average lifetime remains constant across all time-windows. For a multi-exponential fit, we find that the value for τ_{avg} changes depending on the time-window. This is easily conceptualized by observing the decay in the top graph within the first ~ 10 ns. One can imagine that if the decay continued to follow these dynamics over the life of the experiment, the shape of the multi-exponential fit would closely resemble the single-exponential fit. As observed in the bottom graph, at a time window of 10 ns the two fits provide the same value for τ_{avg}, representing this fact.

Using this method, we can easily plot subsequent decays as an image demonstrating how the dynamics of the QDs are changing with time. This allows for easy comparison of any changes in the lifetime across different samples. Therefore, all of the lifetime image plots presented in this dissertation should be interpreted as follows. The x-axis represents the sample number, which will be based on the needs of the experiment. (Commonly we have used experiment time, Pd NP concentration, solvent percentages, and ligand concentration as x-axes). The y-axis represents the time window for which the average lifetime, τ_{avg}, was calculated. The color scale (height of the plot) represents the

value for τ_{avg}. Contours, labeled with number values for τ_{avg} (always in units of ns) are also provided on top of the image plot to assist in observing the changes in lifetime dynamics across the decays. It should be noted that when the contours have a decreasing slope τ_{avg} is increasing, and vice-versa. Though this appears to be a complicated method for displaying PL dynamics, it becomes crucial to fully observe small changes between samples.

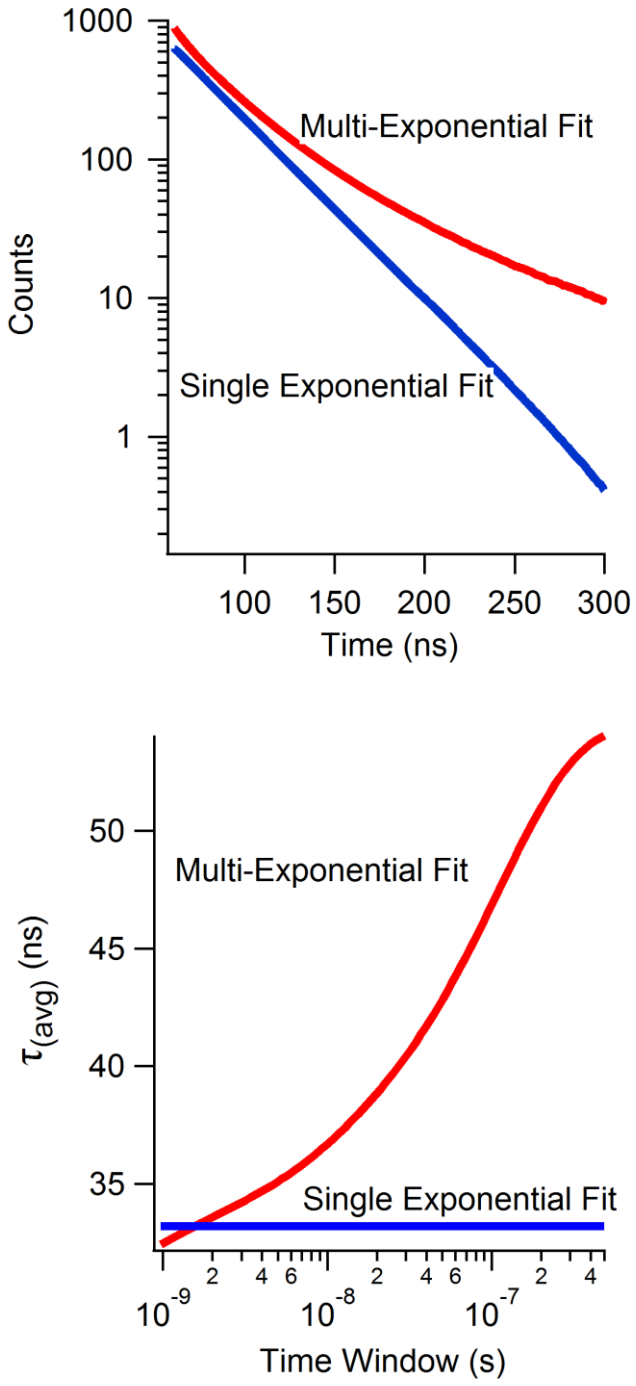

Figure 5.2: Example of a multi-exponential and single exponential fit for a fluorescence decay (top). Plot of τ_{Avg} versus time window for the two fit curves (bottom).

5.5.2 Differences between CdSe QDs diluted in toluene and hexanes

The first experiment performed was to dissolve the CdSe QDs into pristine toluene or hexanes alone, which are two of the most commonly used solvents for QDs. Consecutive lifetimes were collected for 10 hours on each sample. Two major differences were observed between QDs diluted in the two solvents. First, the sample prepared in hexanes appeared to equilibrate much faster (within about 1 hour) than the toluene sample (between 8-10 hours). This led us to believe that the organic ligands tended to be more soluble in the toluene, which allowed for more desorption from the surface of the QDs, and thus a longer equilibration time. Additionally, even after stabilization the hexanes sample had a slightly longer average lifetime (about 2-4 ns), which could either be due to differences in the surface coverage of the QDs (due to the ligand's solubility in different solvents) or could be simply due to effects of the different refractive indices of the two solvents.

Experiments were also performed using a mixture of hexanes and toluene as the solvent. CdSe QDs diluted in 70:30 and 50:50 hexanes:toluene mixtures were prepared and studied over time. These experiments yielded some interesting results. Both samples show an overall decrease in lifetimes of about 20 ns. This appears to indicate that a mixture of hexanes and toluene is even more prone to removing ligands from the surface of the QDs than simply either solvent alone. Additionally the equilibration process seems to take longer in both of these samples. In the 50:50 mix for instance, the lifetimes have just begun to start their decreasing trend after the 10 hour experiment. Thus, a mixed solvent environment was deemed too complicated for current ligand stabilization studies.

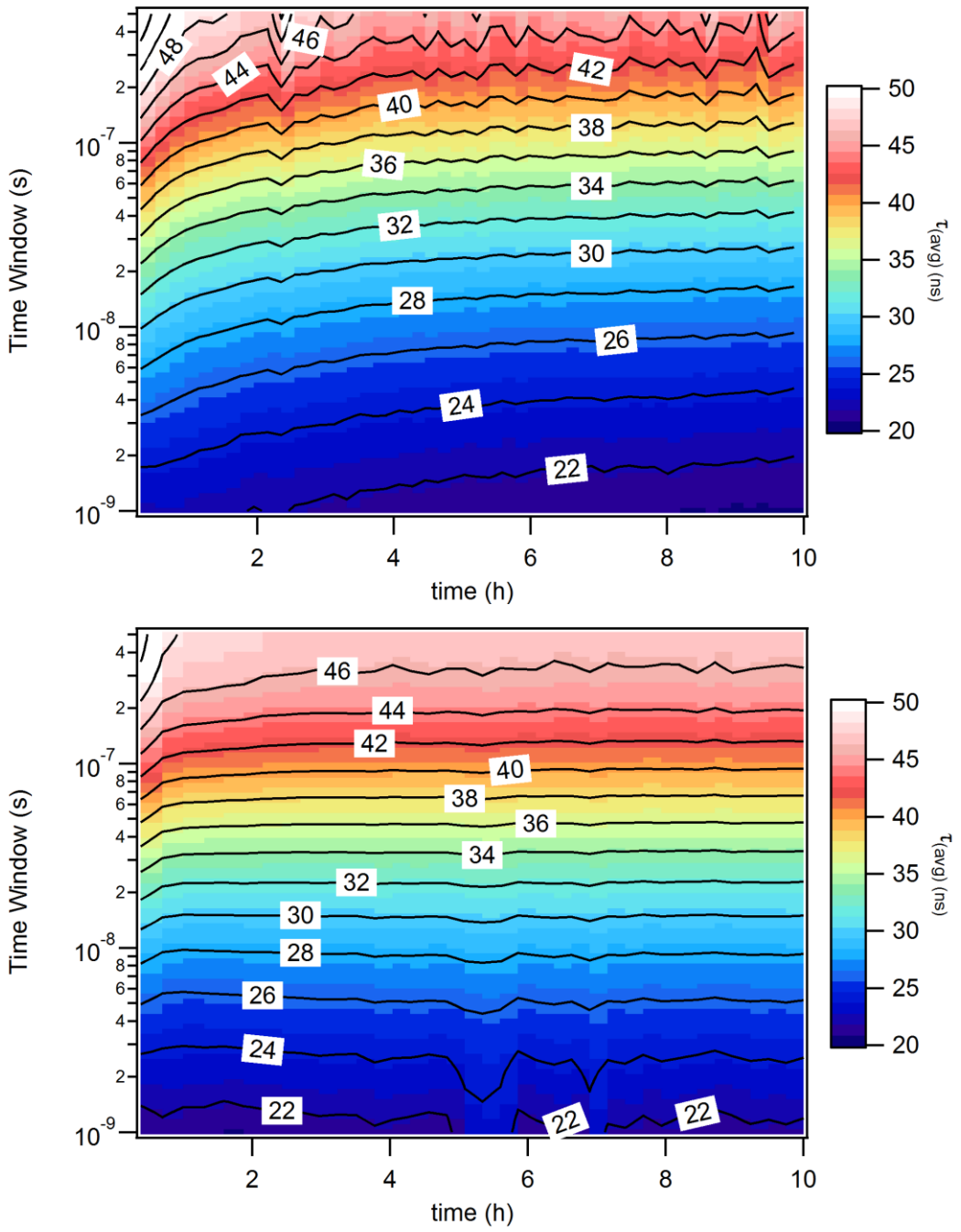

Figure 5.3: Average lifetime plots for CdSe QDs diluted in toluene (top) and hexanes (bottom) over time.

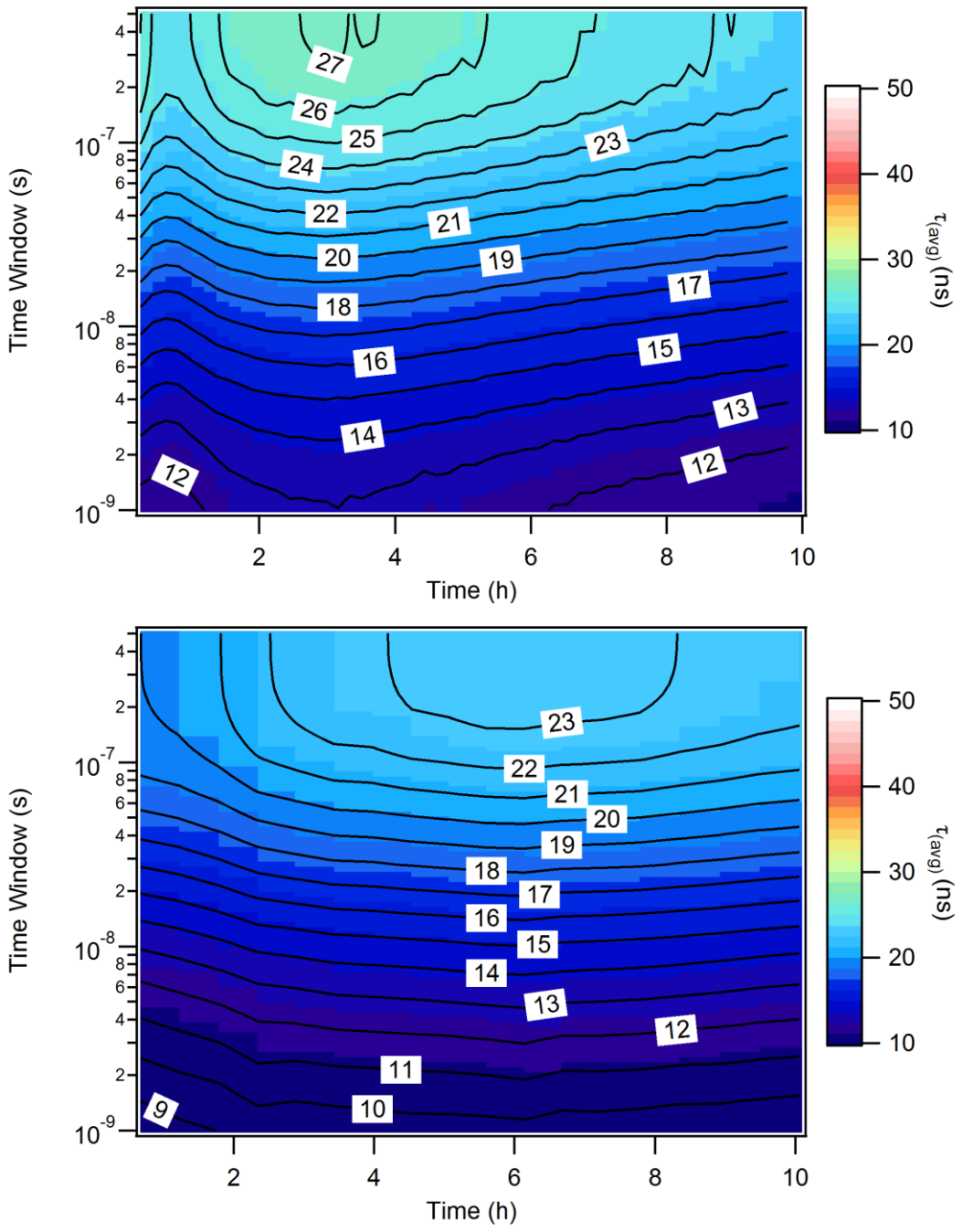

Figure 5.4: Average lifetime plots for CdSe QDs diluted in 70:30 (top) and 50:50 (bottom) hexanes:toluene mixture over time.

5.5.3 Differences between technical grade and 99% pure TOPO

The first set of experiments conducted to determine the effects of additional surface ligands on QD lifetimes was examining increasing concentrations of technical grade trioctylphosphine oxide (TOPO), which is one of the main stabilizing ligands present in solution to coordinate to the Cd in the QDs. Solutions of 0.5 M, and 5 mM TOPO in hexanes were prepared for these studies. It was quickly observed that the additional TOPO drastically shortened the lifetimes of the particles. The lifetime plots in Figure 5.5 demonstrate these much shorter lifetimes. For the 0.5 M sample, the QDs immediately show a drastically shortened lifetime (about 5 ns) compared to the almost 50 ns average lifetimes previously witnessed. The lifetimes of these QDs demonstrate no measureable changes over the 4 hour experiment. The 5 mM sample also shows a shorter lifetime initially, however with increasing time the lifetimes also increase and after stabilizing around 4 hours, the average lifetime of the QDs has rebounded to nearly 30 ns.

The relative quantum yields of these two samples also follow different trends. The 0.5 M sample shows a decrease in relative quantum yield over the 4 hour experiment, while the relative quantum yield of the 5 mM sample increases over the same time period.

UV-visible spectroscopy was also used to examine any changes in the absorbance of the QDs over time, as shown in Figure 5.6 for the 0.5 M TOPO sample. The first absorption peak of the particles significantly blue shifted and decreased over time, completely disappearing after 4 hours. It was hypothesized that the particles were actually being etched and destroyed by impurities present in the tech. grade TOPO. Previous research has shown that these impurities are integral to the production of high

yields of QDs due to their strong binding to the Cd.[141-143] However in the large excess of TOPO present in these solutions, the impurity levels became high enough to destroy the dots.

This theory also helps to explain the differences in PL lifetimes and quantum yields between the two TOPO concentrations. In the 0.5 M sample, the number of strong-binding impurities would be high, and thus most of the QDs would be drastically affected. This is why the lifetimes immediately decrease and show little change over time as well as why the relative quantum yield simply decreases. For the 5 mM sample however the number of impurities is two orders of magnitude less and thus does not lead to as high coverage. This prevents the complete etching and destruction of the QDs and instead allows them to become more stabilized and thus demonstrate increased quantum yields, along with the changes observed in PL lifetimes as an equilibrium is reached.

To confirm that it was in fact the impurities responsible for these effects, the same experiments were rerun with the same concentrations of 99% TOPO in solution. It was observed that the absorption spectra of the QDs demonstrated no noticeable changes over time, indicating that the dots were not being etched as before. Additionally, the average lifetimes collected demonstrated an increase of over 20 ns from the particles diluted in a solution of blank hexanes.

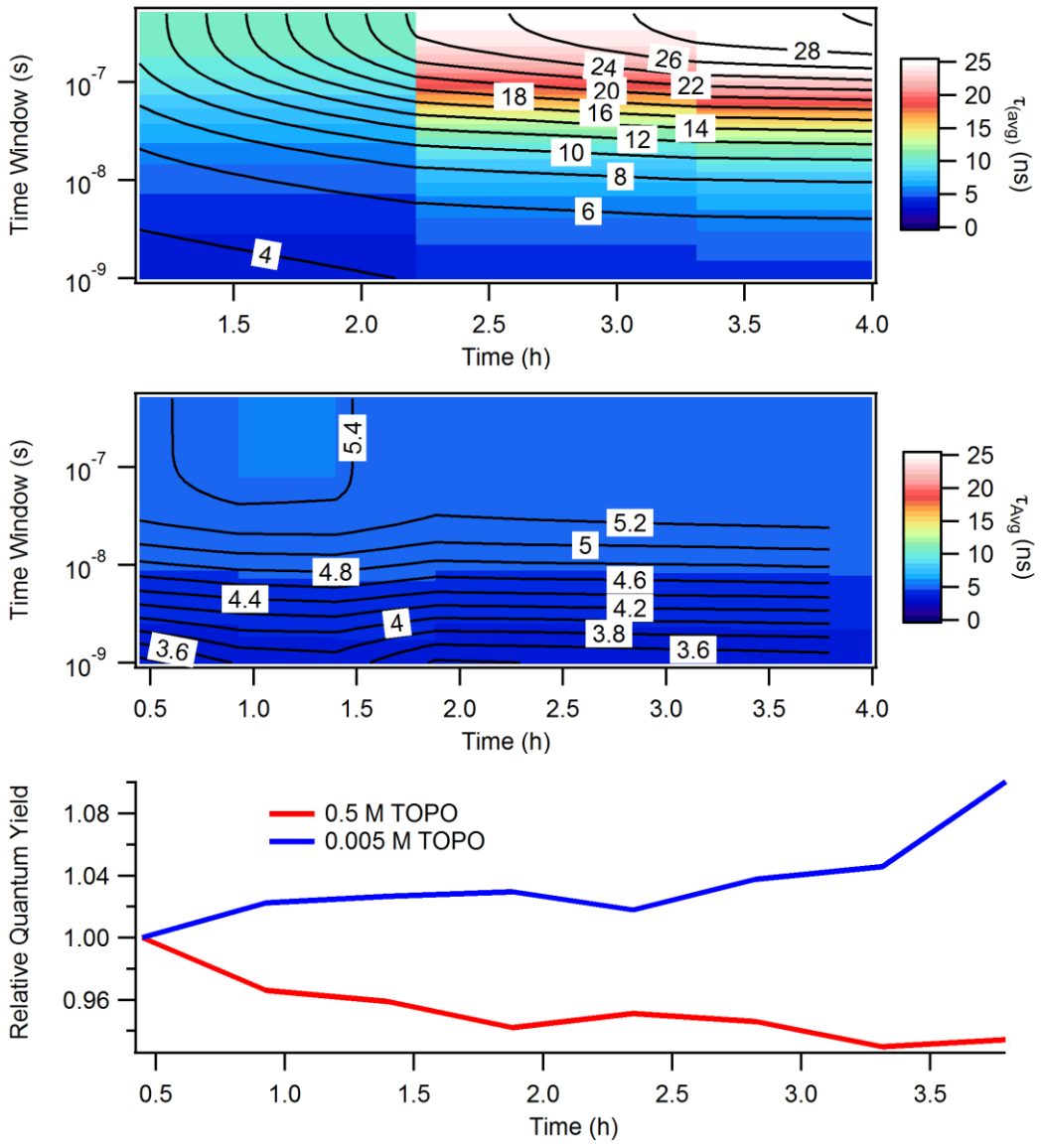

Figure 5.5: Lifetime plots for CdSe QDs with 5 mM tech. grade TOPO (top) 0.5 M tech grade TOPO (middle) over time. Changes in relative quantum yield for both solutions (bottom).

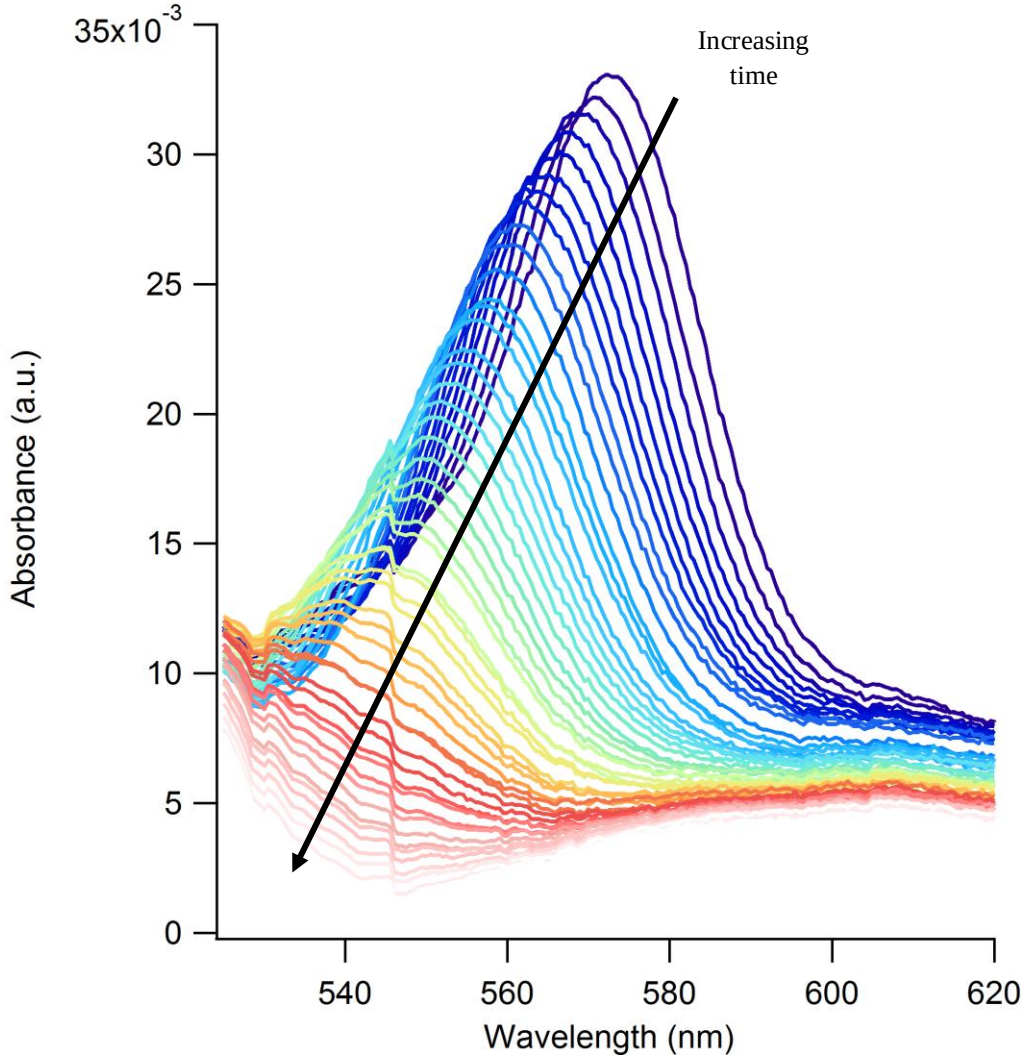

Figure 5.6: Absorbance of CdSe QD diluted in 0.5 M tech. grade TOPO solution over time.

5.5.4 Effects of increasing TOPO in solution

To further examine the effects of increasing amounts of TOPO present (without adding any more impurities) in solution, smaller intervals were chosen and solutions were prepared with 1.25 mM, 2.5 mM, 5 mM, 10 mM, 20 mM TOPO(99%) along with a blank solution of dots diluted in hexanes. By using 99% pure TOPO we expect that any of the destructive effects on the dots caused by TOPO impurities will be eliminated, thus allowing us to study the effects that additional TOPO alone has on the QD PL. The blank solution shows a decrease in lifetimes within the first 30 minutes and then a subsequent increase in lifetimes. By the 4 hour mark, the lifetimes have essentially stabilized about 4 to 6 ns longer than at time zero. Similar features are observed at low concentrations of TOPO with the "peak" of decreasing-increasing lifetimes occurring at later times (just under 1 hour for 1.25 mM, and slightly over 1 hour for 2.5 mM) and beginning to broaden and flatten out. Additionally the overall lifetimes of the dots increase by approximately 4 and 6 ns respectively over the blank solution.

Increasing the TOPO concentration from 5 mM to 10 mM continues the flattening out of the "peak" and thus the lifetimes simply decrease over time Additionally the increase in lifetimes overall compared to the blank solution continues to be observed, up to a 14 ns increase by 10 mM TOPO present. Pushing the concentration even higher continues to increase the overall lifetime relative to the blank solution up to a maximum of about 75 ns (compared to the starting lifetime of approximately 50 ns). Additionally within the first hour, a slight immediate increase in lifetimes is now observed as opposed to the initial decrease, and the lifetimes quickly stabilize and level out.

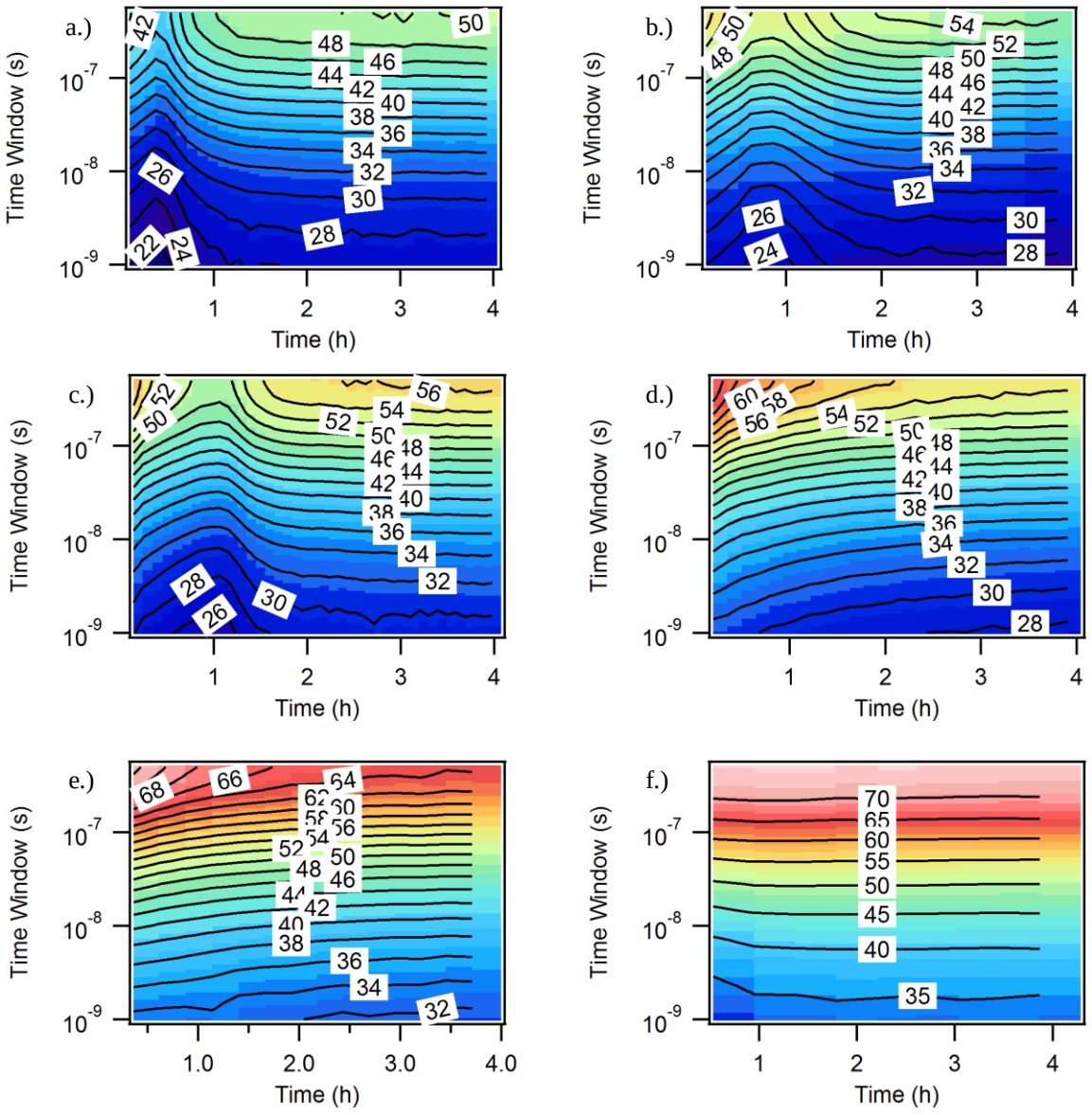

Figure 5.7: Lifetime plots over time for CdSe QDs diluted in TOPO solutions of a.) 0 mM, b.) 1.25 mM, c.) 2.5 mM, d.) 5 mM, e.) 10 mM, and f.) 20 mM in order, prepared in hexanes.

These results appear to indicate that two distinct processes are occurring. Initially, the particles seem to be aggregated to an extent in the stock solution and when diluted in solvent, they are able to dissociate from each other. In an aggregate state only well passivated QDs will be emissive, leading to longer decays and low PL. As the aggregates begin to dissociate, a dynamic quenching regime is entered leading to shorter lifetimes. Once the aggregates have broken up, then the lifetimes would start to increase as the bare sites on the surface of the now smaller QDs are covered by any ligands that fall off during this process. As the ligands – particle equilibrium occurs the lifetimes stabilize. With the presence of additional amounts of TOPO present, the lifetimes increase. This was surprising, since our original hypothesis was that additional TOPO would remove dangling bonds (surface traps) and thus non-radiative recombination pathways, we expected that our lifetimes would decrease (as they approached the radiative rate (k_r) of the QDs, which is expected to be around 10-20 ns.[144] We discuss this observation further in the modeling section of this chapter.

Additionally, with higher and higher concentrations of TOPO this effect of the ligand stabilization appears to occur within a significantly shorter time frame. This effect does appear to follow our hypothesis that deaggregation is occurring. With more TOPO present in solution, the deaggregation/stabilization would happen at a faster rate as QDs, which are not fully capped (and thus are aggregated at the start) will achieve more complete ligand coverage in a shorter time.

We chose to re-run the above experiment with a new QD sample. A new CdSe QD sample was synthesized and purified as previously described. Diluted samples with increasing amounts of TOPO were prepared as before using these new QDs. The main

difference between the two sets of QD samples is the amount of time from synthesis to experiment. The previous samples were prepared and studied months after synthesis, whereas these new QD samples were prepared and studied as soon as possible (within one week) after synthesis. We expected that the new samples would have less loss of ligands from the start, and demonstrate less aggregation due to the fact that they were allowed to sit in solution for significantly less time after synthesis. The lifetime plots for these samples are given in Figure 5.8.

Examination of the lifetimes for these new QD samples confirms our hypothesis. Fist, there appears to be no drastic decrease/increase in lifetimes within the first hour as witnessed in the previous sample. If the QDs have less time stored in solution before experiments are run, it stands to reason that less aggregation will occur, and thus no drastic de-aggregation effects are witnessed. Additionally, all of the samples show relatively steady lifetime plots with next to no changes in the average lifetime of the dots with time, which appears to indicate a more uniform starting surface coverage. The final observation is that the lifetimes change very little with addition of TOPO until the 10 mM and 20 mM samples.

These experiments directly illustrate that over time, QDs stored in solution begin to lose their surface ligands. Once enough ligands have been lost, the QDs will aggregate into larger clusters, which can be dissociated by dilution, especially into a ligand solution. Newly synthesized QDs have not gone through this process and therefore little aggregation effects are observed. Additionally, since less open sites remain, it takes a larger excess of additional ligands in solution to observe changes in the PL dynamics.

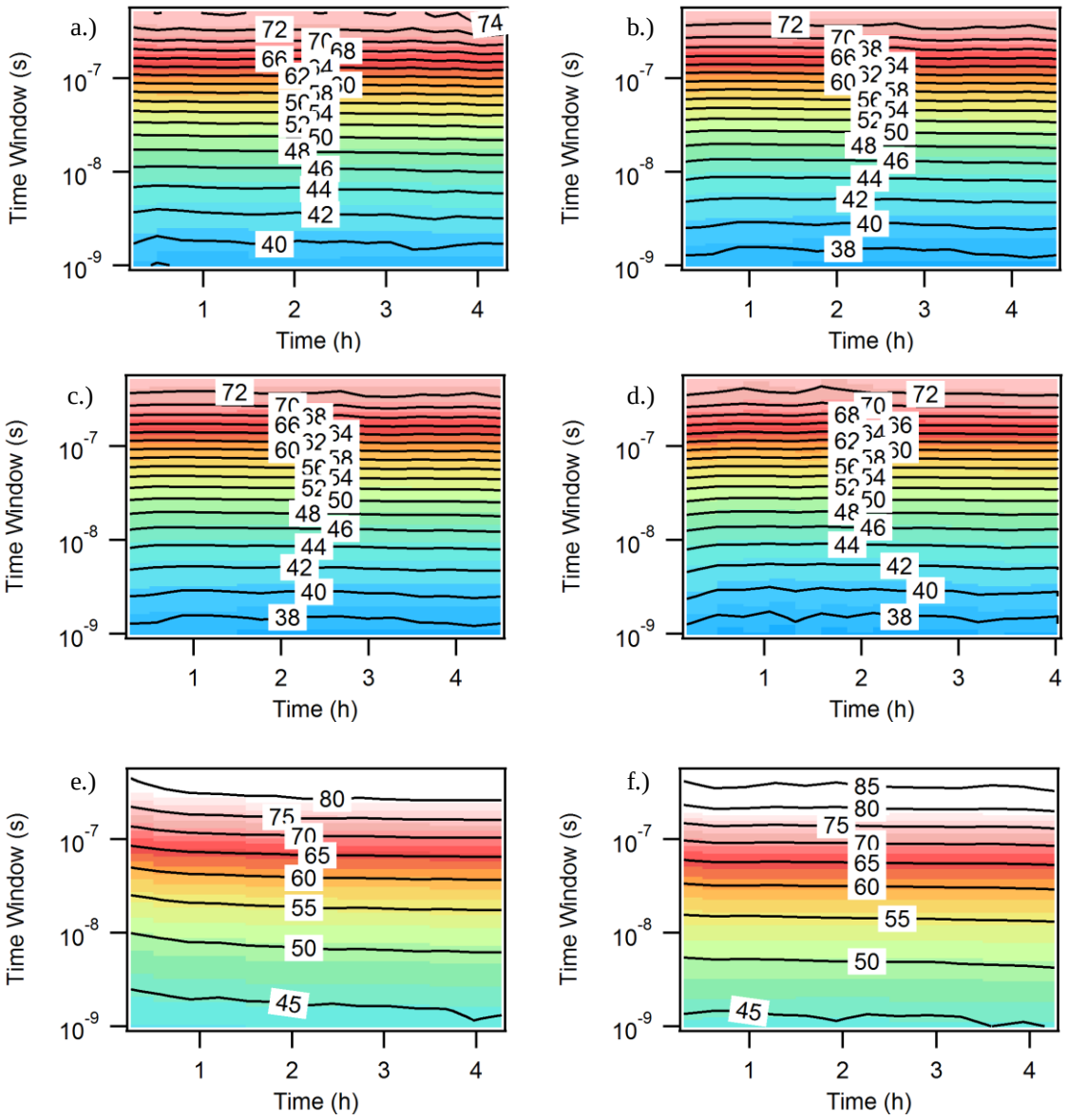

Figure 5.8: Lifetime plots over time for CdSe QDs diluted in TOPO solutions of a.) 0 mM, b.) 1.25 mM, c.) 2.5 mM, d.) 5 mM, e.) 10 mM, and f.) 20 mM in order, prepared in hexanes.

5.5.5 Injection of TOPO to stabilized QD solutions

To help to further elucidate the difference between the dissociation and equilibration processes another experiment was run where lifetimes were collected on a sample (of the original CdSe QDs studied) diluted in hexanes for 2 hours. This allowed for the initial breakdown of aggregates to occur. Afterwards, 0.019 g, (equivalent to 20 mM solution) of 99% TOPO was added to the solution and vigorously shaken to dissolve. Lifetimes were then run in a similar fashion for at least an additional 2 hours. This experiment showed an immediate increase in lifetimes upon the addition of TOPO, with final lifetimes that are longer than the 20 mM TOPO experiment run above. This lends credence to the idea that both processes are occurring in the previous samples at the same time. In this experiment, all aggregates are dissociated before any additional stabilization with excess ligands occurs. Since the stabilization process appears so rapidly, it suggests that in the previous experiments some of the larger aggregates become stabilized by the excess ligands before they have a chance to dissociate into solution.

Additionally, the relative quantum yield plot demonstrates two distinct increases. Initially the relative quantum yield of the QDs increases as the particles de-aggregate as seen before. A second jump in the relative quantum yield occurs upon addition of the TOPO, corresponding to the increase in lifetimes. This experiment conclusively shows that addition of TOPO to these CdSe QDs increases both their fluorescence lifetime and quantum yield.

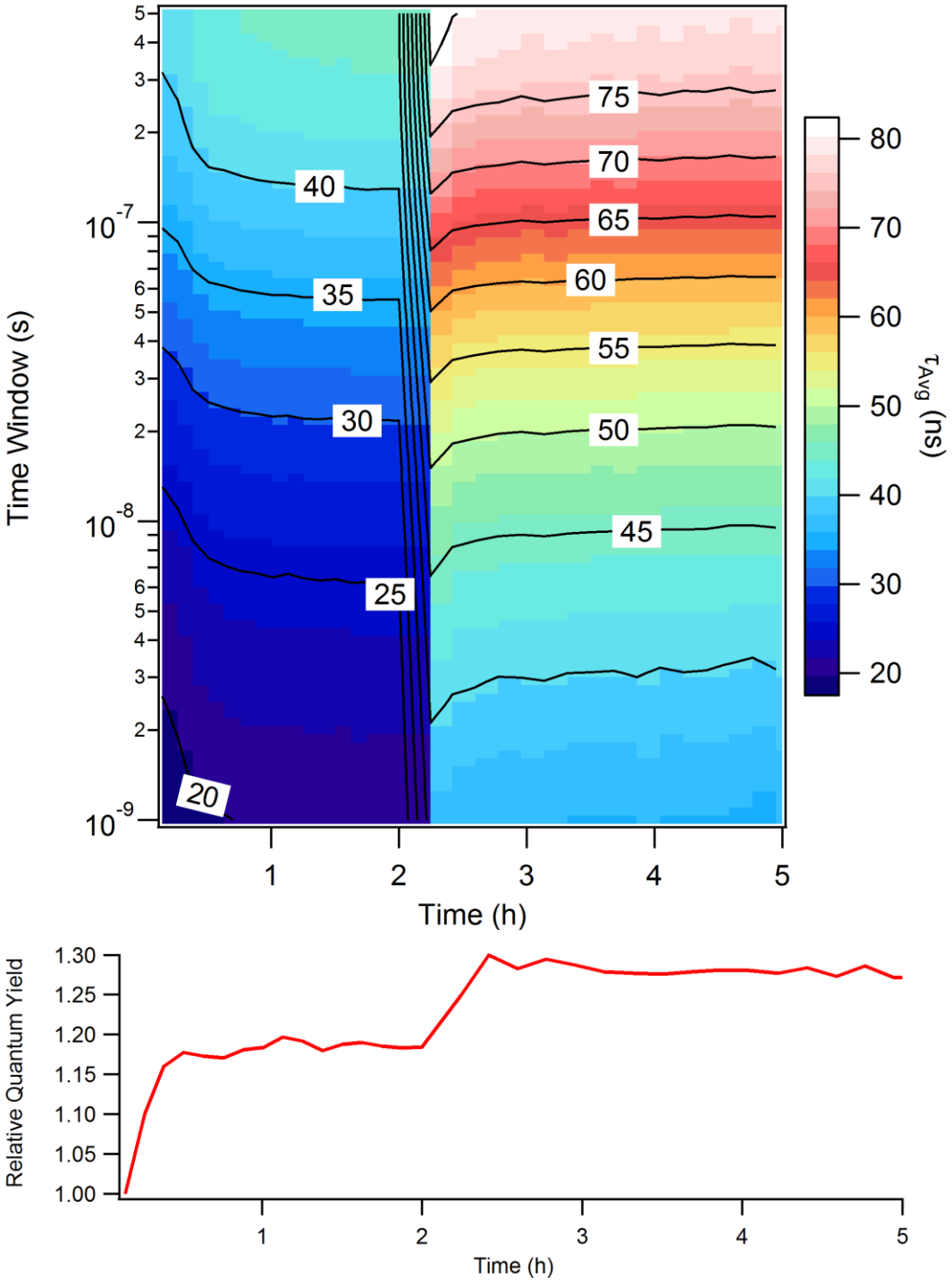

Figure 5.9: Lifetime plot and relative quantum yield for CdSe QDs diluted in hexanes over time with an injection of 0.019 g TOPO at 2 hours.

5.5.6 Differences between TOPO and HDA

A similar set of experiments was conducted using an excess of HDA in solution. With increasing concentrations of HDA, the results were markedly different than for the TOPO. The first noticeable difference occurs at low concentrations of HDA added. The initial decrease/increase "peak" in the lifetimes is no longer observed. For 1.25 mM HDA the lifetimes simply decrease and stabilize after about 2 hours in solution. With 2.5 mM and 5 mM HDA added the lifetimes of the QDs increase, up to a maximum of about 62 ns, which is an overall increase of about 12 ns from the blank solution. Additionally, with the 5 mM HDA solution, equilibrium was almost immediate as there was very little change in the lifetimes across the 4 hours.

The addition of further amounts of HDA provided some interesting results. As opposed to the TOPO solutions, the overall lifetimes with 10 mM and 20 mM HDA actually began to decrease again, and in fact were up to 8 ns shorter than in the blank solution. Also the QDs no longer exhibited an initial increase in lifetimes, instead simply decreasing across the 4 hour time frame.

Absorbance measurements demonstrated that with increased HDA concentration, the absorbance peak of the QDs decreased with time. This drop in absorbance was not accompanied by any shift and seemed to be correlated to the amount of ligand present. In cases with low excess of HDA the drop was less drastic whereas with a large excess of ligand (such as the 10 mM or 20 mM samples) the absorbance peak significantly dropped within the first few scans. In addition to the decreased absorbance, an excess of HDA was observed on the bottom of the cuvette with time, suggesting that the excess ligands fell out of solution with time and pulled QDs out of solution as well.

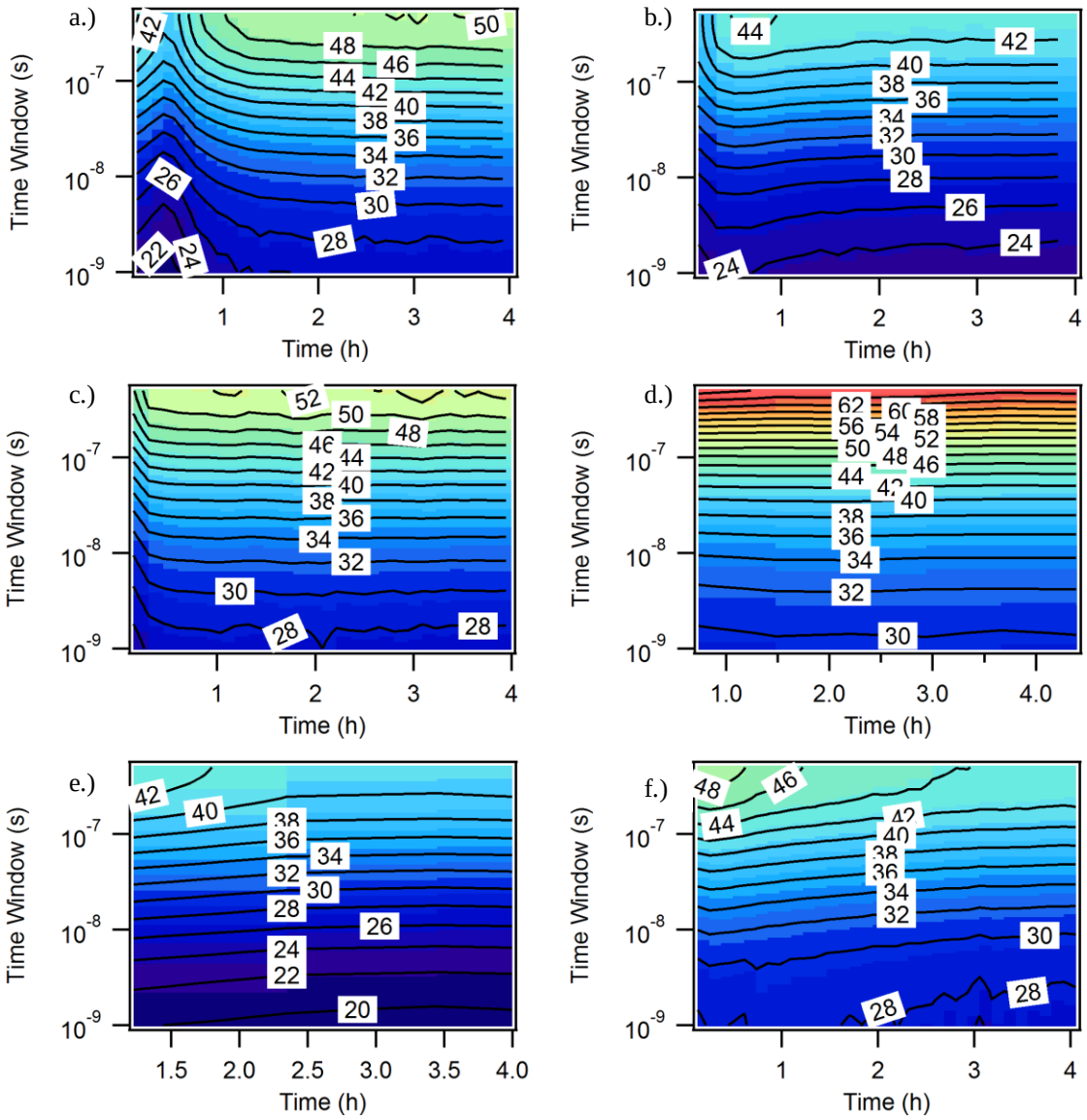

Figure 5.10: Lifetime plots over time for CdSe QDs diluted in HDA solutions of a.) 0 mM, b.) 1.25 mM, c.) 2.5 mM, d.) 5 mM, e.) 10 mM, and f.) 20 mM in order, prepared in hexanes.

We also conducted a ligand injection experiment with HDA (Figure 5.11). Examination of the lifetime plot demonstrates similar effects to the TOPO injection experiment. Initially as aggregates break down, the lifetimes of the QDs decrease followed by an increase and stabilization by about 2 hours. Upon injection of 0.012 g (equivalent to 20 mM solution) HDA at 2.5 hours, the lifetimes of the QDs immediate increase by 2-4 ns. This value corresponds to the previous experiment.

Corresponding to the increase in lifetimes, the relative quantum yield of the QDs also greatly increases upon injection of HDA. This demonstrates perhaps the most drastic difference between addition of TOPO and HDA in solution. Comparing the two injection experiments, injection of TOPO drastically increases the lifetime of the QDs (by 20+ ns) while also increasing the relative quantum yield. The HDA injection results in only slightly longer lifetimes, but a much more drastic increase in relative quantum yield (up to a 3-fold increase).

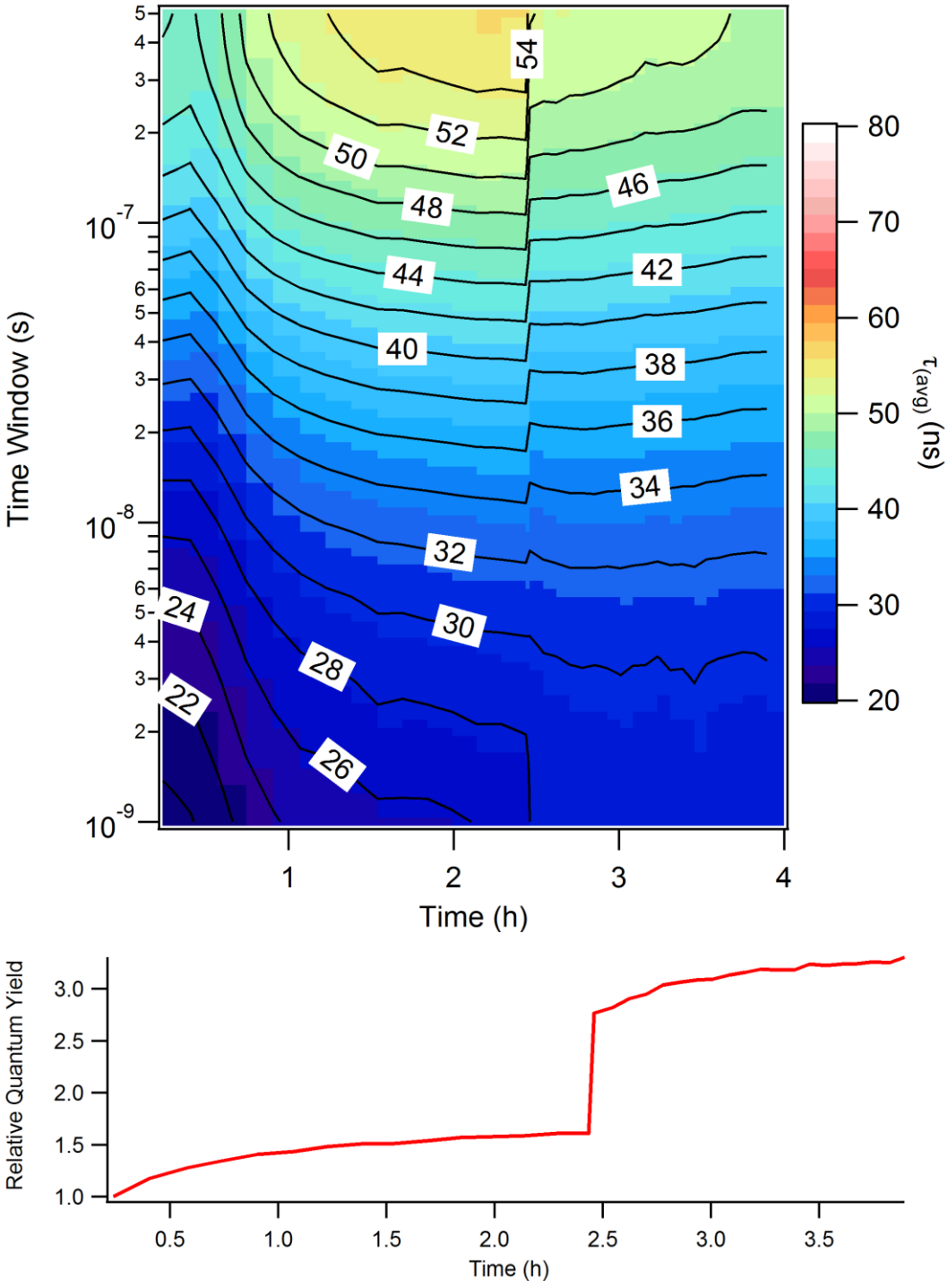

Figure 5.11: Lifetime plot and relative quantum yield for CdSe QDs diluted in hexanes over time with an injection of 0.012 g HDA at 2.5 hours.

5.5.7 CdSe QD lifetime changes with added TOP

The last potential native ligand on the surface of the QDs is trioctylphosphine (TOP). We expect that the TOP present would be more likely to bind to any Se sites on the surface of the QDs. It has been surmised that the effects of surface Se sites do not play a significant role in the dynamics of CdSe QDs and thus TOP should have much less of an effect on the lifetimes of CdSe QDs compared to TOPO or HDA.

We observe that in fact TOP does not seem to drastically change the lifetimes of the QDs. Though there is an initial slight increase in lifetimes, the lifetimes reach a maximum of approximately 42 ns after 7 hours, which is comparable to that witnessed in solutions of dots alone. Additionally, observation of the changes in the relative quantum yield of the dots show an immediate increase, which then slowly flattens out (with some experimental fluctuations) back to the starting quantum yield. These results confirm that in fact the addition of TOP has a significantly less effect on the dynamics of CdSe QDs than either TOPO or HDA.

Because of these results we focused the remainder of our studies on TOPO. TOPO seemed to have the greatest, most discernable, and most consistent effects on the QD lifetimes of the 3 native ligands. Therefore, we chose to develop a model to fully examine the interaction between CdSe QDs and TOPO in solution to begin to understand the effect of ligand adsorption/desorption on the surface of QDs.

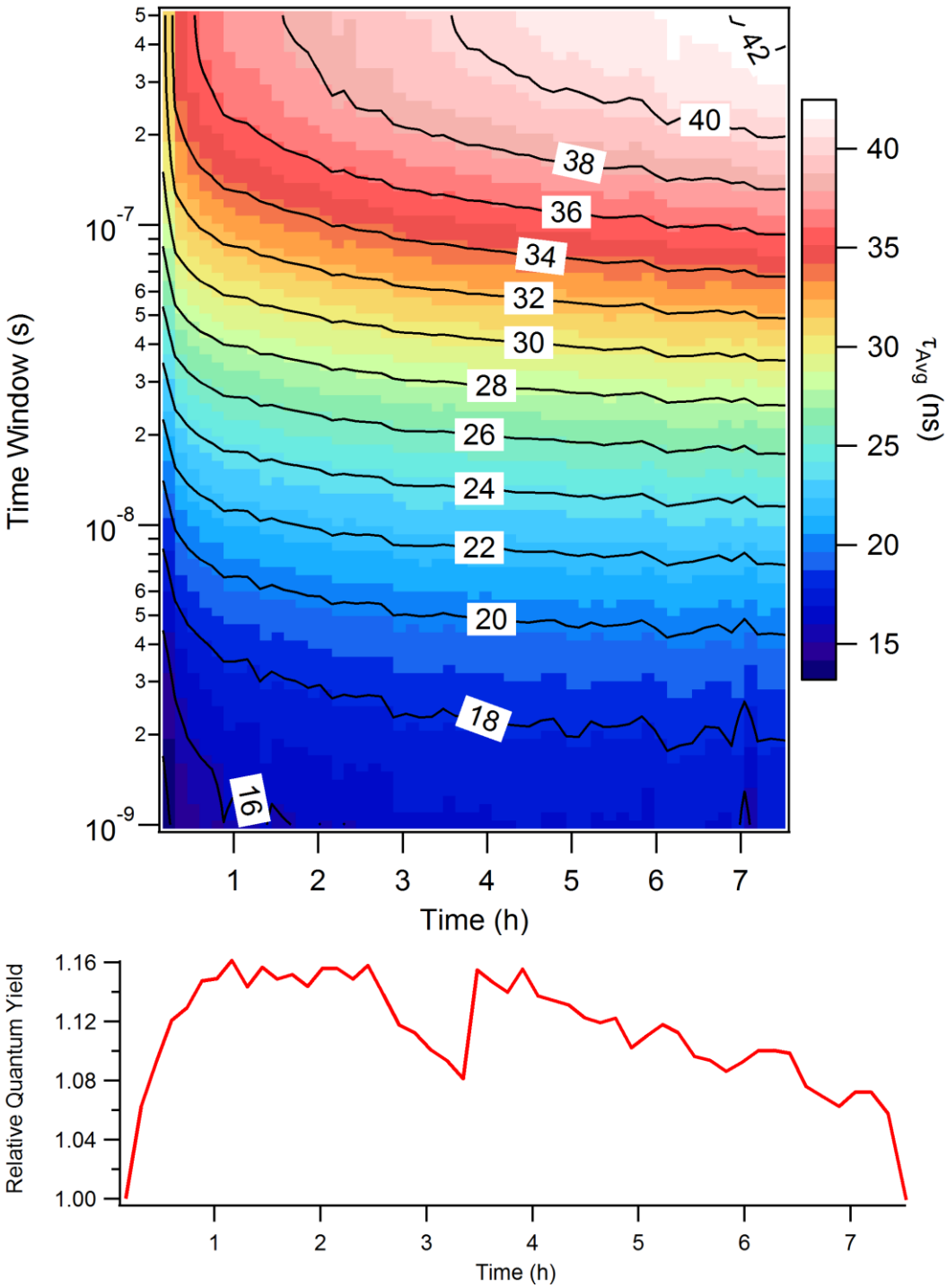

Figure 5.12: Average lifetime and relative quantum yield plots for CdSe QDs diluted in excess TOP over time.

5.5.8 Differences between purified and raw QDs

As a final experimental study, we synthesized another new sample of CdSe QDs. These dots were separated into two samples. One of the samples was purified as before, the other sample was left in the raw, unpurified solution. These QDs were then diluted as before in hexanes. Lifetimes of both samples were collected immediately after sample preparation for 6 hours.

The lifetime plots for these samples in Figure 5.13 demonstrate little change in either sample with time. This corresponds to our previous findings of the second set of TOPO experiments (Figure 5.8) that QDs examined shortly after synthesis appear to demonstrate less agglomeration/equilibration tendencies. Comparing between the two samples however demonstrates a 20 ns decrease in average lifetimes between the raw and purified dots. Additionally, while the relative quantum yield for both samples demonstrates an initial decrease (most likely due to some equilibration, which doesn't appear as drastically in the lifetime measurements), the raw solution stabilizes at almost the starting quantum yield after 6 hours, while the quantum yield of the purified solution continues to decrease. These findings are consistent with our previous ligand experiments. Since the raw solution should still have an excess of ligands present, the QDs demonstrate increased lifetimes and quantum yields, much like what we witnessed by adding excess ligands to samples of purified QDs.

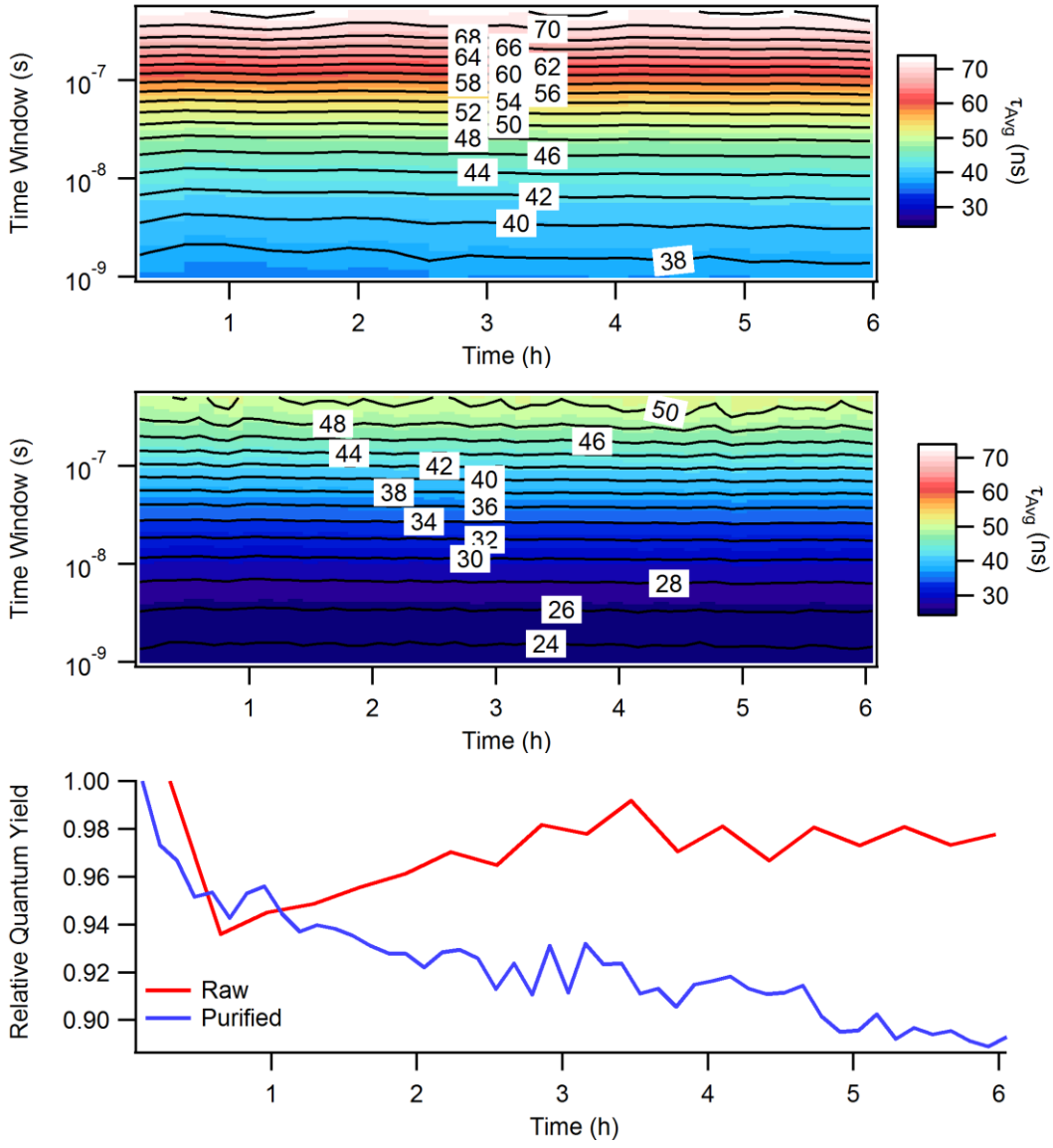

Fiugre 5.13 Lifetime plots for CdSe QDs in raw (top) and purified (middle) solutions. Relative quantum yield for both solutions (bottom).

5.5.9 Model for TOPO binding

Because of the importance of ligands on the photophysical properties of QDs, a variety of models to describe their binding, and subsequent optical effects have been developed. As mentioned in the introduction to this chapter, the majority of QD-ligand studies have been conducted with non-native strong quenchers, and thus the models in the literature have been designed for these systems. The common method for modeling ligand binding is based on the Langmuir adsorption model which assumes a flat surface of equivalent binding sites and thus is not directly applicable to QD systems.[145]

$$\theta = \frac{K_a[L]_{free}}{1 + K_a[L]_{free}}$$

Where θ is the fractional surface coverage, $K_a$is the adsorption constant, and $[L]_{free}$ is the concentration of free ligands in solution. For the case of a QD-ligand binding system the adsorption constant for QD-ligand binding is defined as

$$K_a = \frac{[QDL]}{[QD][L]}$$

and setting θ to be

$$\theta = \frac{[QDL]}{[QDL] + [QD]}$$

where $[QD]$, $[L]$, and $[QDL]$ define the concentrations of QDs with no ligands bound, unbound ligands, and QDs with a bound ligand respectively.

One of the first instances of using a Langmuir model to fit QD-ligand binding was reported by Mulvaney *et. al.*[146] This model has been expanded upon multiple times in recent years for various QD-ligand systems.[130, 133, 138, 147] Recently Weiss *et. al.* demonstrated potential flaws in using a simple Langmuir model for QD-ligand binding,

and instead proposed a modified Langmuir model, which is based on a binomial distribution.[137] The benefit of a binomial distribution, is that is limits the number of potential ligands bound, which holds more physical meaning as each open surface binding site on a QD can only be occupied by one ligand.

All of these Langmuir-based models, which we found in the literature, were then developed relating to the steady-state PL of the QDs. Commonly strong-binding ligands which quenched the QD PL were studied. This poses three problems for our experimental studies. We are first and foremost relating changes in the fluorescence dynamics (via changes in average lifetime) of the QDs upon ligand addition. Secondly, we are not observing a quenching phenomenon, but rather we witness an enhancement of the PL upon ligand addition. Finally, and perhaps most importantly, we expect that many TOPO ligand adsorption/desorption events will occur for each QD in solution. Each QD in solution does not have the same amount of ligands bound to its surface, but rather a distribution of ligand coverage exists. We expect that a QD with few open binding sites will have a much lower probability of additional ligand binding than a QD with many open sites. These differences in surface ligand coverage will relate to various effects observed in the fluorescence dynamics. We therefore developed a new way to relate changes in fluorescence dynamics upon ligand binding based on a series of equilibrium constants and corresponding charge trapping/detrapping.

For a sample of QDs with a maximum of N surface sites per QD, we define a series of equilibrium, with corresponding equilibrium constants:

$$QD + XL \xleftrightarrow{K_1} QDL + (X-1)L$$

$$QDL + (X-1)L \xleftrightarrow{K_2} QDL_2 + (X-2)L$$

…

$$QDL_{N-1} + (X - N + 1)L \xleftrightarrow{K_N} QDL_N + (X - N)L$$

A general expression for the equilibrium constant, K_j for the above series is:

$$K_j = \frac{[QDL_j][L]^{X-j}}{[QDL_{j-1}][L]^{X-j+1}} = \frac{[QDL_j]}{[QDL_{j-1}][L]}$$

At equilibrium the ratio of the forward, k_+, and reverse k_- rates is constant.

$$K_j = \frac{k_+}{k_-}$$

From the Arrhenius expression,

$$K_j = \frac{k_{+j}}{k_{-j}} = \frac{A}{B}\left(\frac{N + 1 - j}{j}\right) e^{-\frac{\Delta H}{RT}}$$

where A and B are the pre-exponential factors related to particle collisions, and $\Delta H$is the change in enthalpy of the system. Using the Arrhenius expression allows us to define the forward and reverse rates in terms of ΔH. We assume that ΔH is the same for each reaction and the difference between reactions is the amount of surface sites present for binding, related to the pre-exponential factors. Using our previously defined expression for K_j in terms of $[QDL_j]$, the concentration of QDs with j ligands bound is then given by

$$[QDL_j] = \left(\frac{N + 1 - j}{j}\right) K_0 [QDL_{j-1}][L]$$

where,

$$K_0 = \left(\frac{A}{B}\right) e^{-\frac{\Delta H}{RT}}$$

The benefit of this formulation is two-fold. First, we are not making any direct assumptions about the number of ligands on a specific dot, but rather we allow for a probability of a QD to have n number of TOPO ligands bound based on the starting

concentrations of QDs and TOPO. Since we are performing ensemble measurements, we expect that even though a sample of QDs may have some average number of TOPO ligands per QD, we allow that there is a measureable probability of finding a QD with anywhere from 0 to N TOPO ligands bound. Secondly, by treating each binding event as a specific reaction with a specific equilibrium constant, we make no assumptions about one general equilibrium constant for a QD-TOPO reaction. This means that while ΔH for each reaction is constant, we are allowing for differences in ΔG. This makes intuitive sense as it should be significantly more preferred for a TOPO molecule to bind on a bare QD than on a QD with only one open site, simply due to steric hindrances.

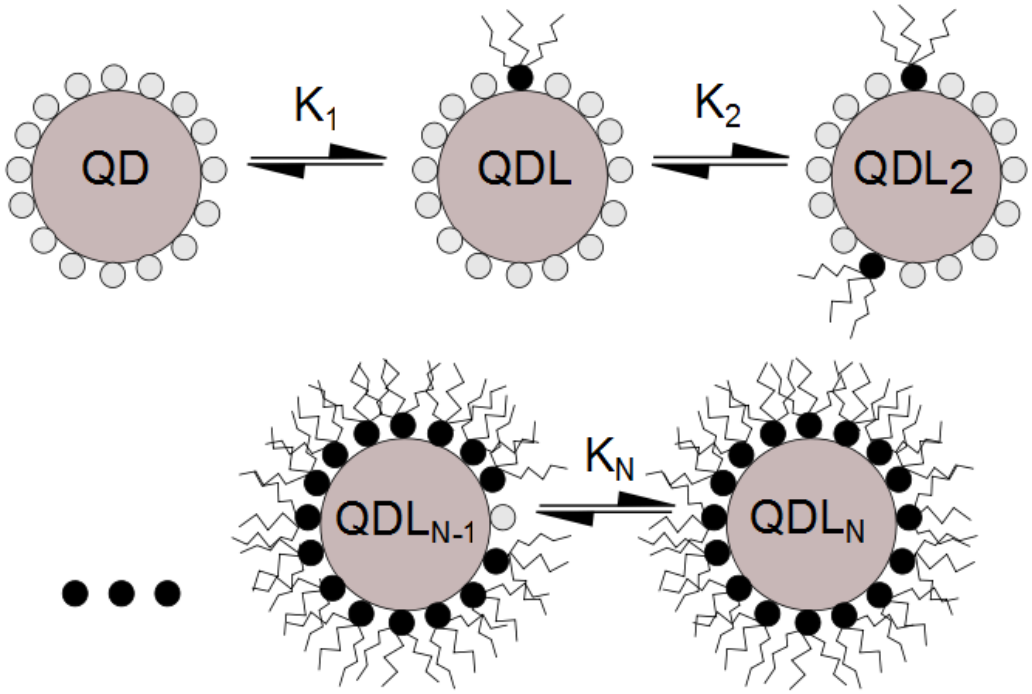

Figure 5.14: Proposed equilibrium series for binding of a ligand (L) to a QD with increasing surface coverage.

This allows us to generate a probability curve of finding a QD with n TOPO bound, based on the amount of TOPO in solution and a value for K_0, which we set as a fitting parameter. It should be noted that this value of K_0 technically relates to the equilibrium constant for the reaction binding a TOPO to a QD with half of its available sites (N/2) filled and does not correspond to K_a in the Langmuir model. Assuming a K_a as defined in by the Langmuir equation, we can relate the quantity K_1 in our model (the equilibrium constant for the binding of a single TOPO to a bare QD) to the K_a from the Langmuir model. Since for our experiments it takes a large excess of TOPO added to solution to observe changes in the dynamics we find values for K_0 that are quite low and usually much less than previously reported values for K_a from the Langmuir model for other QD-ligand binding systems. Reported values for K_a range from 8×10^3 to 1×10^9 for thiols and amines on CdSe QDs in chloroform.[138, 146] Viologen binding to CdSe and CdS have been found to have K_a values of 5.4×10^4 and 2.6×10^4 respectively.[130, 136] Lower values have been found for the binding of octylamine to CdSe QDs in chloroform (50 M^{-1} – 100 M^{-1}) and TOP/TOPO binding to CdSe (5.6 M^{-1} , 49.3 M^{-1}).[133, 148] We are then able to generate a distinct probability distribution for each TOPO concentration studied.

We then use this ability to determine probability distributions of a QD with n TOPO bound to determine average lifetimes of a QD ensemble. Based off of a previous method, we develop a three state scheme consisting of an exciton (X), surface trap (S), and ground state (G).[149] Assuming that the addition of a TOPO ligand to an open site removes a surface trap, we then are able to write differential equations to describe the populations of each of these states at a given time:

$$\frac{dX}{dt} = -(k_r^X + k_{nr}^X + nk_{ET}^+)X + nk_{ET}^- S$$

$$\frac{dS}{dt} = -(k_{ET}^- - k_{nr}^S)S + k_{ET}^+ X$$

$$\frac{dG}{dt} = k_r^X X$$

The above equations are then solved to determine an expression for the population of the exciton state:

$$X = C_1 e^{r_1 t} + C_2 e^{r_2 t}$$

Allowing us to calculate the average lifetime of the ensemble for a given number of identical surface traps (n) per quantum dot.

Using our formulated lifetime equation we then calculate the average lifetime of a QD ensemble by multiplying the probability of a QD having n traps by the average lifetime for a dot with n traps and finding the sum of these values from 0 to N.

$$\tau_{Avg_{Ensemble}} = \sum_0^N \tau_{Avg_{QD\ with\ n\ traps}} \times Prob_{QD\ with\ n\ traps}$$

With this approach we were then able to compare this model to our measured data. We began by selecting a reasonable value for N based off of the QD size as described in the literature,[136] as well as reasonable starting values for all of the rates. To assist in selection of these rate values we compared to our calculated quantum yield using the equation:

$$Quantum\ Yield = \frac{k_r^X}{k_r^X + k_{nr}^X + N(k_{ET}^+ + k_{ET}^- + k_{nr}^S)}$$

Once these rates have been set we then adjusted the value of K_0 until the calculated lifetimes best fit the experimental data.

With this formulation we then plot the average lifetime of the QDs versus concentration of TOPO added. Using a curve fitting routine, we were able to find a set of parameters, which generated a curve that closely fit our data. However, upon examination of these parameters a few red flags appeared. To obtain a proper fit, the value for k_r^X needed to be less than 1.25×10^8 s^{-1}, which translates to a radiative lifetime of 80 ns. Typical accepted values for the exciton radiative lifetime for CdSe QDs is in the range of several to tens of ns.[144] The reason that the exciton radiative lifetime has to be so long goes back to the fact that we observed significantly longer lifetimes with increasing TOPO concentration. If the addition of a TOPO ligand removes a surface trap it also removes a non-radiative pathway, which is the mathematical equivalent of decreasing k_{nr}. Therefore, as seen in the lifetime equation below, the average lifetimes of the QDs should begin to approach $1/k_r$.

$$\tau_{Avg} = \frac{1}{k_r + k_{nr}}$$

To accommodate the increase in fluorescence lifetime along with the increased quantum yield upon addition of TOPO, we needed to develop our model further such that the fitting parameters would have more physical meaning. After consideration, we decided to develop a model based off of 2 distinct types of traps: the previously explored normal surface traps (which are correlated to dangling bonds on the surface of the dots and thus would be removed upon addition of TOPO), and σ* orbitals formed by the interaction between the surface Cd atoms and TOPO. If, in this case, the non-radiative decay from the first type of trap is significantly faster than the return rate (signified by k_{ET}^-) and the opposite is true for the second type of trap, we would expect increased lifetimes with increased bound TOPO.

A four model system was developed to describe this process. Since the increase of an additional state adds another level of complexity, the assignment of rates had to be carefully chosen. Since the work from our 3-state model demonstrated that the exciton non-radiative rate (k_{nr}^{X}) exhibited little change in the PL lifetime, we chose to eliminate it from the 4-state model. This has a physical basis in the fact that any non-radiative processes should be accounted for via one of the two types of trapping. The return rate (k_{ET}^{-}) from the surface trap (S) to the exciton state was also removed, such that any trapping into this state would result in non-radiative recombination.

Essentially this is equivalent to setting the trapping rate (from exciton to surface trap) to be much slower than the rate of trap depopulation (from surface trap to ground). Assuming that any surface traps are at a significantly lower energy than the exciton state, it follows that this definition is valid. Additionally we did not add in a non-radiative rate from the σ* TOPO state (denoted L) to the ground state. Much like the previous assumption, this requires that the ligand to exciton return rate is much faster than rate from ligand to ground.

These assumptions were made due to the low starting quantum yield of the dots (approximately 5%) as well as the increasing lifetime with addition of TOPO. For both of these observations to occur, the overall non-radiative recombination rate must essentially decrease while the overall radiative rate is increasing. Since we do not expect the addition of ligands to change anything about the exciton to ground recombination, this four state model with the proposed assumptions becomes a necessity. This allows for the addition of a TOPO to a QD to increase the quantum yield of the dot (by reducing the non-

radiative recombination from surface trap to ground) as well as increasing the overall lifetime of the QD (by increasing the effective exciton to TOPO σ^* rate).

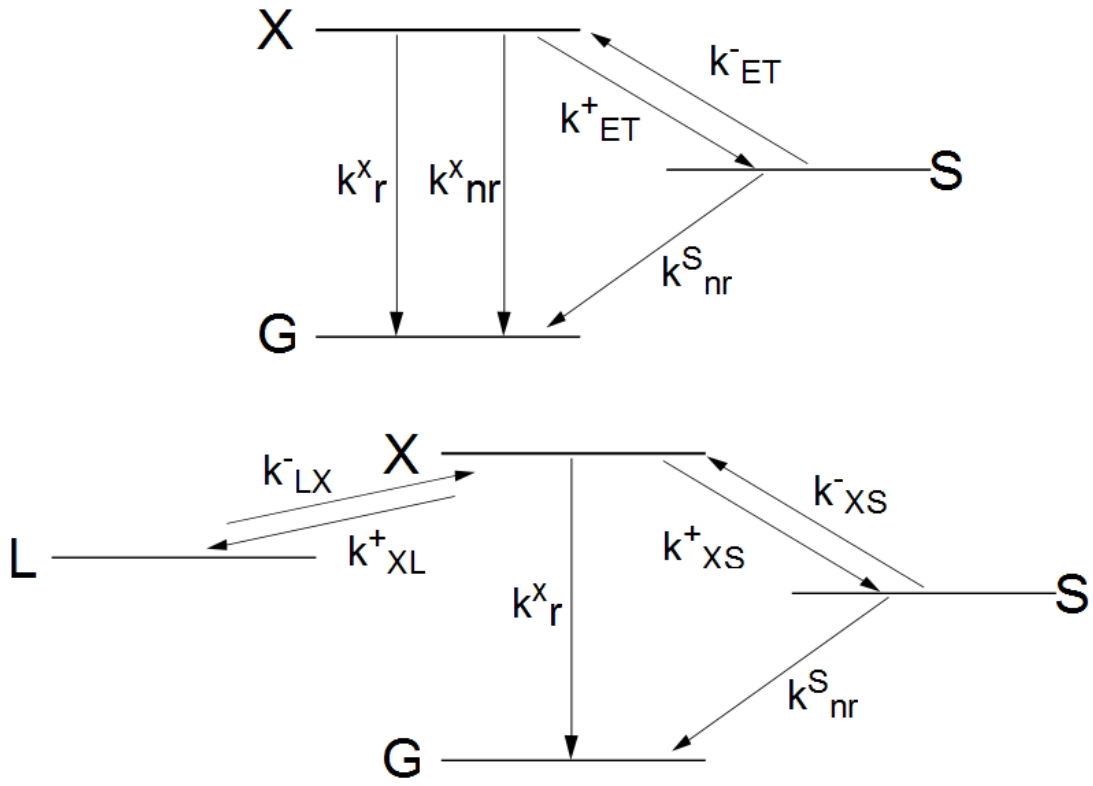

Figure 5.15: Proposed 3-state (top) and 4-state (bottom) diagrams displaying rates used for population state equations

We then developed an equation as before to describe the average lifetime of the QDs from the new population state equations.

$$\frac{dX}{dt} = -(mk_{XL}^{+} + nk_{XS}^{-} + k_r^X)X + k_{LX}^{-}L$$

$$\frac{dL}{dt} = k_{XL}^{+}X - k_{LX}^{-}L$$

$$\frac{dS}{dt} = k_{XS}^{+}X - k_{nr}^{S}S$$

$$\frac{dG}{dt} = k_r^X X + k_{nr}^{S}S$$

Where n refers to the number of surface traps on a QD and m is equal to the number of TOPO molecules bound (N-n) on a QD. Solving this system for the population of the exciton state yields

$$X(t) = e^{\frac{1}{2}(a_{11}+a_{22}-b)t} \times C_1 + e^{\frac{1}{2}(a_{11}+a_{22}-b)t} \times C_2$$

Where

$$C_1 = \frac{\left(-\frac{a_{11}}{a_{12}} + \frac{1}{2}(a_{11}a_{22} + b)\right)}{b}$$

$$C_2 = 1 - \frac{\left(-\frac{a_{11}}{a_{12}} + \frac{1}{2}(a_{11}a_{22} + b)\right)}{b}$$

$$b = \sqrt{a_{11}^2 + 4a_{12}a_{21} - 2a_{11}a_{22} + a_{22}^2}$$

$$a_{11} = -(mk_{XL}^{+} + nk_{XS}^{-} + k_r^X)$$

$$a_{12} = k_{LX}^{-}$$

$$a_{21} = k_{XL}^{+}$$

$$a_{22} = -k_{LX}^{-}$$

When solving for the average lifetime equations for this model, we chose to examine 4 specific time windows. As previously mentioned, reported values for average lifetime of QDs give no insight into the shape of the decay curve, and thus do not explore how the dynamics of the QDs may be changing over time. By examining the average lifetime of the QDs at different time windows we gain some insight into how the dynamics of the QDs are changing within certain time ranges. This added constraint gives our fitting parameters more physical meaning as the rates must now be chosen to not only fit for one average lifetime and quantum yield, but rather for 4 different average lifetime values. The equations for τ_{Avg} for the different time windows were solved as before, except we integrated from 0 to 50 ns, 100 ns, 500 ns, or 2 μs, rather than to infinity.

To assist in determining the validity of our chosen parameters we conducted similar experiments using the same concentration of QDs and TOPO diluted in hexanes, toluene, and chloroform. We found through observation that the solubility of TOPO is lowest in hexanes, more soluble in toluene, and significantly more soluble in chloroform. Therefore, by conducting experiments in all three solvents we can determine the value of K_{eq} for the different solvents. Since solubility of TOPO in solution follows: chloroform >>> toluene > hexanes, we would expect that K_{eq} would follow an inverse trend, as TOPO will be less inclined to bind to the QD surface in solvents in, which it is highly soluble.

We prepared sets of samples with increasing TOPO concentrations from 2 new CdSe cores of similar size. The stock solution for the first, 2.8 nm diameter core was stored in hexanes. The stock solution for the 2.7 nm core was stored in chloroform. The diluted samples were prepared as before, except in addition to the set diluted in hexanes,

we also prepared samples diluted into pristine toluene and chloroform. Lifetimes on all of these samples were collected and analyzed as before with one exception. Instead of a 500 ns TAC, both a 50 ns and 2 μs TAC were utilized. These two sets of collected data for each sample were then analyzed simultaneously, producing a single decay fit curve. This approach allowed us to better determine if there were any major differences in the dynamics of the QDs at short times, while still ensuring that we were collecting the full decay of the QD.

Before attempting to fit this data to our model, we plotted the collected lifetime curves, and as image plots to observe changes in τ_{Avg}. Our first observation was the difference between the two CdSe cores. The QDs that were originally stored in hexanes demonstrated significantly less changes with added TOPO than the QDs originally stored in chloroform. In fact, with the exception of the hexanes set, no measurable differences (outside of minor fluctuations) were found for the first QD sample. This follows with our proposed theory that the increased solubility of TOPO in chloroform over hexanes affects the surface coverage of TOPO on the QDs. The QDs stored in hexanes would be much more likely to retain their TOPO ligands than those stored in chloroform, and thus would have measurably less open sites for TOPO to bind. When these QDs are diluted, excess added TOPO is less likely to bind since there are few open sites available. These QDs only show any change (albeit relatively small) when diluted in hexanes, because eventually there is enough added TOPO so that some binding will occur. This is not observed in the toluene or chloroform dilutions since TOPO preferentially remains in solution.

The second observed effect is the drastically shortened lifetime of both QD samples when diluted in chloroform. Instead of lifetimes of approximately 50 ns, the QDs exhibit values of 5-6 ns for τ_{Avg}. Additional TOPO added to solution (up to 20 mM) seems to have little effect on the lifetimes of the QDs. This decrease in lifetimes is accompanied by a drastic decrease in relative quantum yield of the QDs, observed by steady-state PL measurements. We attribute these effects as well to the high solubility of TOPO in chloroform. As the QDs are diluted, the TOPO on the surface of the QDs rapidly disassociates into solution. This removes many of the longer exciton-TOPO rates, but more importantly adds exciton-surface trap pathways. This result validates our assumption that the surface trap to ground non-radiative recombination rate is much faster than the return S-X rate. Since this pathway becomes dominant when few TOPO molecules are bound, the quantum yield of the QDs is dramatically reduced and the lifetimes are significantly shortened as most of the decay occurs via a very fast non-radiative trapping mechanism.

To observe where the greatest changes in the average lifetimes were occurring with the addition of TOPO, we divided the average lifetime plot (for the full time window from 0 to 2 μs) for the 2.5-20 mM TOPO samples by the sample with no TOPO added. This allowed us to observe at which time windows the changes in τ_{Avg} were most pronounced. Since the hexanes stock sample showed little to no changes, this technique yielded little results. The chloroform sample however showed some interesting features. It appeared that there were two time windows at which the lifetimes showed the greatest increase. The first area of increase was within the 5-10 ns time window. We attribute this increase in τ_{Avg} to increased transfer from the exciton to TOPO σ^* orbital. The second

increase in τ_{Avg} is observed at much longer time windows of about 1-2 μs. We expect that this increase at longer times is due to increased PL from charges that go to and from a TOPO σ* orbital before emitting.

Using these observations to determine starting values for our fitting parameters for our 4 state model we fit the data collected for the second new sample of QDs. We began by calculating the average lifetime of the raw data for each TOPO concentration at the four different time windows. We then used a global fitting procedure to simultaneously fit the four average lifetime functions as well as the quantum yield function to the raw data. We first conducted a fit for the samples diluted in hexanes. After obtaining the closest possible fit, we then used these parameters as starting values to fit the raw data for the samples diluted in toluene as a check of the validity of our chosen parameters. We first held all parameters constant, except for K_0, since the main difference between the two samples would be the solubility of TOPO in solution, thus affecting K_0. Finally we allowed the ligand-exciton return rate to vary, since that should be the only other parameter that would possibly show any major changes between the two samples.

For the sample that was originally stored in chloroform, we were able to plot lifetime curves for all of the time windows in both hexanes and toluene (the diluted chloroform samples were unable to be fit due to the effects previously described). Though the fits have a fair amount of error, we do find that the correct trend is starting to be followed in both samples. Additionally it appeared that the tails (the highest TOPO concentration samples) appeared to fit much closer than at lower TOPO concentrations. Upon closer examination of the data this appears to be do to the fact that at lower TOPO concentrations, the average lifetime trend is less clear. It seems as though the changes in

average lifetime tend to follow a less defined trend. We wanted to confirm these effects and therefore prepared a new set of these samples, as well as a similar set from the original QDs studied in this chapter (which were now an additional 8 months older than when the previously presented data given in Figure 5.7 was collected). We observed that these fluctuations in average lifetime appeared across all older samples at low TOPO concentrations. We attributed some of these effects to additional aggregation/disaggregation processes occurring due to the advanced age of the QDs by the time these experiments were conducted. This prevents this type of modeling procedure from ever obtaining an accurate fit. Additionally it should be noted that trying to fit each of the average lifetime values across these different time windows simultaneously is quite difficult, as it simply magnifies the inherent issues with the formulation for τ_{Avg}.

The fits derived from this model and data however did garner some valuable information. By conducting these fits we were able to find acceptable ranges for the rates, as well as an estimate for the value of K_0. We found that in fact our value for K_0 did need to be much lower (2×10^{-4} M^{-1} and 1.2×10^{-4} M^{-1} for the fits presented) than other equilibrium constants reported in the literature, to even achieve a reasonable fit for the data. We expect that these measured differences are mainly due to the differences in the development of our model, which treats each QDL_X+L interaction as a unique reaction. This indicates that the binding interaction between QDs and TOPO is relatively weak, which has been further confirmed via some recent isothermal calorimetry (ITC) studies being conducted in our group.

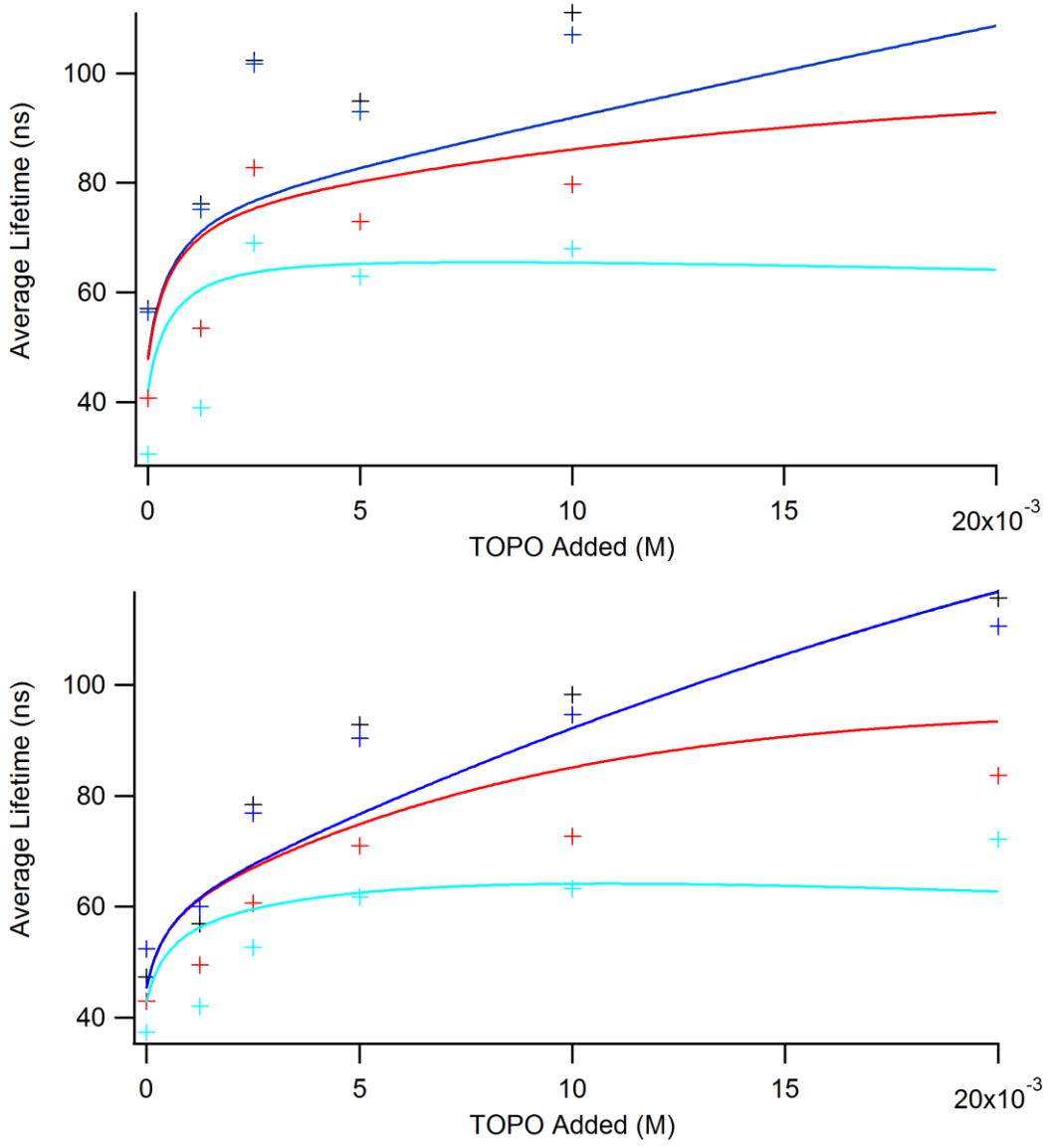

Figure 5.16: Average lifetime fits for CdSe QDs prepared in hexanes (top) and toluene (bottom) with increasing TOPO concentrations. Four different time windows were fit, with the lowest curves representing the shortest time window.

As a final step to improve on our model for QD-TOPO binding, we modified a previously developed lifetime fitting model[150] (based on a similar mathematical construct) using our probability distribution functions based on our QD-ligand equilibrium series. For this model we set energy levels for our four states (X, G, S, L), and define forward rates between the states as previously described. The reverse rates are defined by the energy difference between the two states.

This model also allows us to set the degeneracy of each state. The X and G states are singly degenerate. The degeneracy of the L and S states however will change based on the number of ligands bound per QD. We set the number of each states based on N. The values of K_0 and TOPO added for each sample determine the distribution of ligands bound per QD (as demonstrated in Figure 5.20). We then use a fitting procedure to model the fit decay functions for all the samples. We begin by adjusting the value for K_0 until we get separation between the fit curves for the different samples. Since all of the other parameters are the same across all samples, the only difference in the fits is due to the degeneracies of the L and S states based off of our ligand probability distributions. We then allow the values for the energy of the states and corresponding rates to fluctuate (excluding the energy for X and G) until the best fit is achieved.

Additionally, to prevent any additional complications from QD aging, we synthesized a new sample. Two aliquots of this sample were collected. The first raw aliquot was diluted down immediately into a full set of TOPO solutions (from 1.25 mM – 20 mM as before, as well as 30 mM, 40 mM and 50 mM samples) in both hexanes and toluene. The second (1mL) aliquot was washed with 10 mL methanol and centrifuged for

30 min. The collected QDs were diluted into 1 mL of hexanes. A full set of TOPO solutions was prepared from this sample in both hexanes and toluene.

A few initial observations are made from these samples. First, for both of the sets prepared from the raw QD solution, we see relatively minimal changes in τ_{Avg}. This is due to the fact that the surface of these raw QDs should be almost fully passivated. Therefore, adding additional TOPO to solution has less of an effect as few open sites for binding exist. The QDs, which were washed exhibited more distinct changes in τ_{Avg} between samples.

Though the overall values for τ_{Avg} does not show large changes, noticeable differences in the shape of the decays is observed as seen in Figure 5.17. Increasing TOPO appears to cause the lifetimes to drop at short times and increase at longer times. This follows with our previous deduction that adding TOPO removes a trap (which we attribute to the decrease at fast times) and adds an additional longer decay pathway due to trapping on the σ^* orbital.

To further illustrate the changes in fluorescence dynamics we generated a lifetime image plot as before however we then divided all of the traces by the trace with 0 mM TOPO added. Figure 5.18 shows this image, where numbers greater than 1 correlate to an increased lifetime and those less than one show a decrease in the lifetime. The decrease in PL lifetimes at short time windows and increase in lifetimes at long time windows is clearly visible in this image, especially at higher TOPO concentrations. We observed similar effects with the washed QDs in hexanes samples as well, however since there is more separation between the lifetimes (since more open binding sites are available) the two distinct changes are not quite as visually apparent. The samples prepared in toluene

also show changes to the shapes of the lifetime decay curves, though much like before, the changes are less uniform, and tend to be much more complicated to understand based simply from PL decays.

We then utilized our new lifetime fitting routine to fit the washed samples prepared in hexanes. These samples showed the most discernible trend and large enough changes between the samples that we were able to obtain a proper fit. The fit from the raw data and fitted curves from our model are given in Figure 5.19.

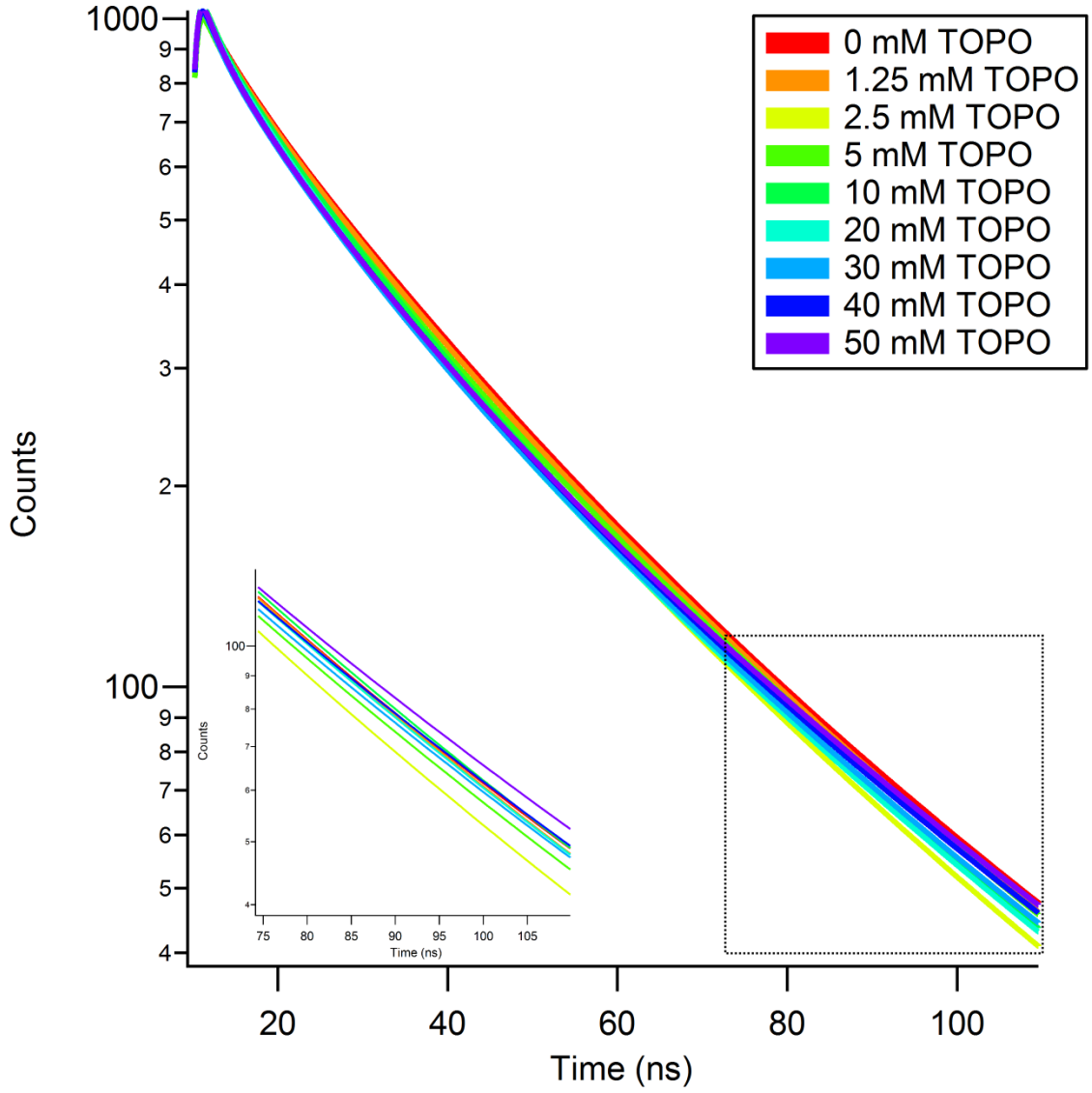

Figure 5.17: Fitted lifetime decays for unwashed QDs diluted in TOPO solutions prepared in hexanes. The inset is an expanded view of the traces from 75-105 ns to visually increase the separation between the curves.

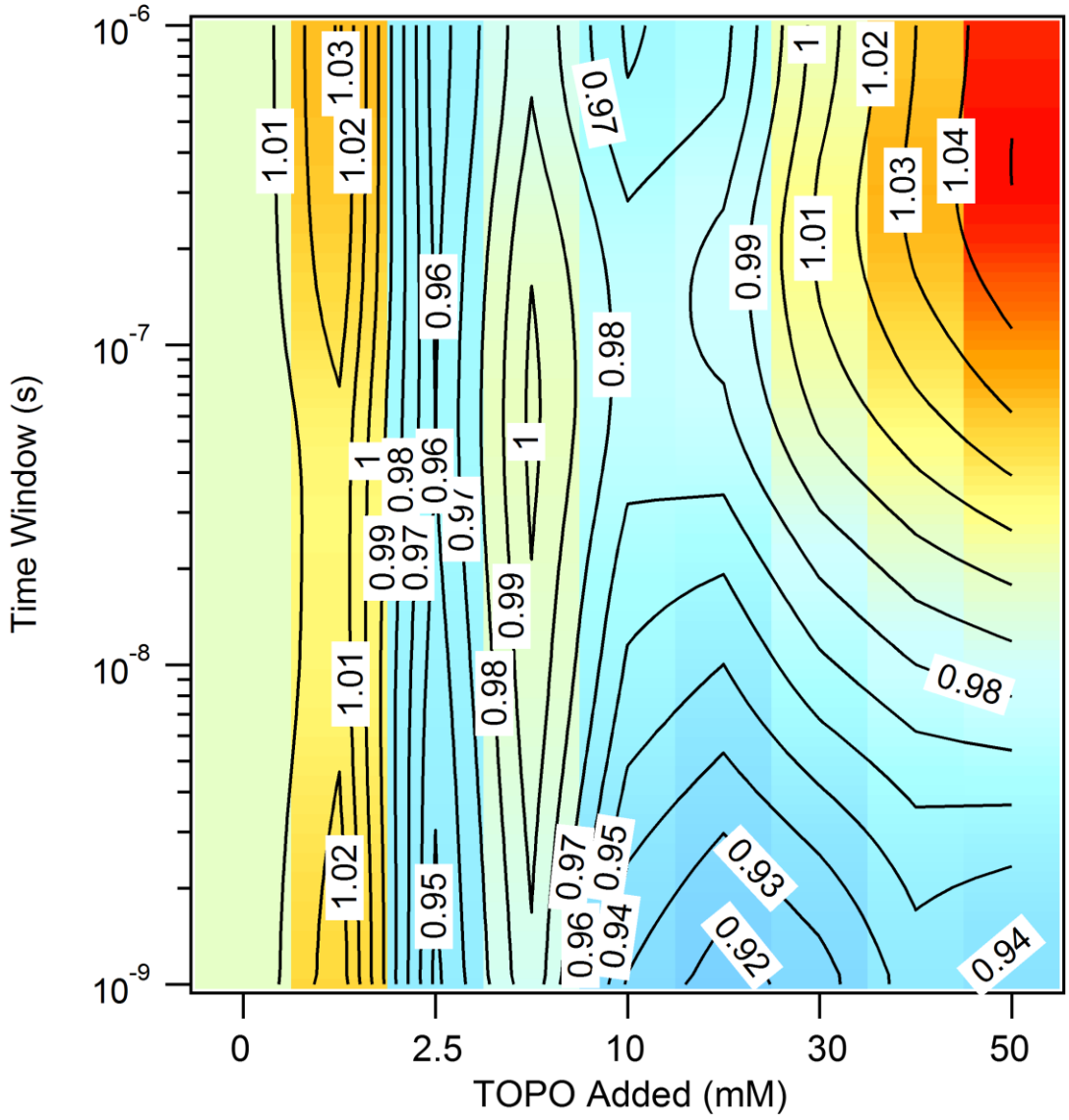

Figure 5.18: Plot of lifetime changes for newly synthesized unwashed CdSe QDs and diluted into TOPO solutions in hexanes.

We find that our fit data shows good agreement with the collected lifetimes across all samples. Our value for K_0 is found to be 1×10^{-4} M^{-1}, which again is quite low, suggesting that TOPO does not bind preferentially to the QDs. Additionally this value for K_0 is in relative agreement with the values determined from our original model fitting to τ_{Avg}.

We find a radiative lifetime of 12.4 ns, which is quite reasonable when compared to the literature values for CdSe. The exciton to surface trap rate is found to be much faster than the exciton to ligand rate. This follows from the fact that there is more TOPO bound per QD than traps (due to the relatively large amount of TOPO in solution), and these rates are multiplied by the number of potential pathways.

Figure 5.20 shows how the distribution of bound TOPO changes for this model with increasing TOPO concentration. It is apparent that as TOPO is added, the amount of surface traps decrease, and the distribution of traps also narrows for this fit.

The fact that this model provides an accurate fit for the lifetime data collected for these 9 different concentrations of TOPO is quite significant. We are simply only changing the number of TOPO per QD in solution while leaving all of the other variables constant and still are able to obtain an accurate set of fits. This demonstrates the power of such a model, not only for this system but for a variety of QD dynamics systems to be explored in the future.

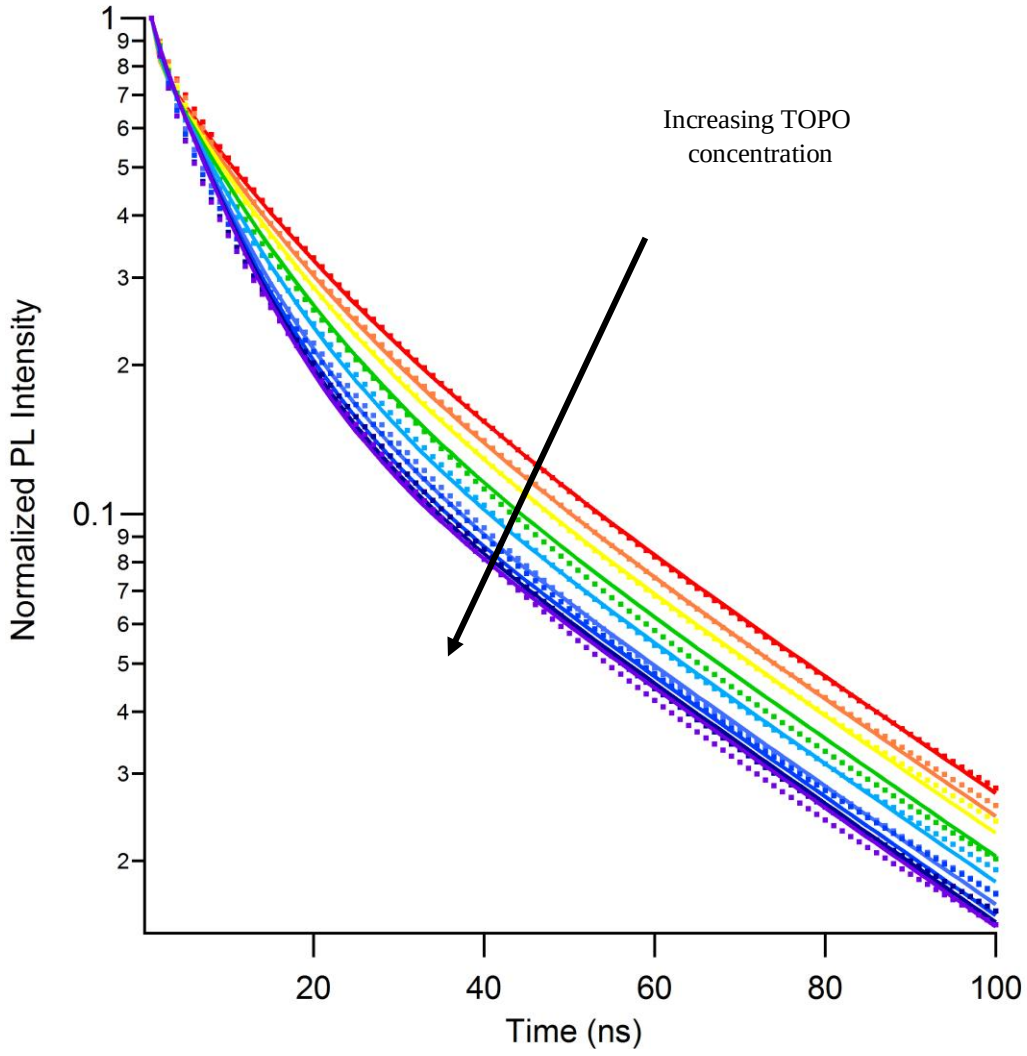

Figure 5.19: Plot for the fitted data (lines) and raw data (+) for the newly synthesized and washed once CdSe QDs prepared in TOPO solutions (0mM to 50 mM) in hexanes.

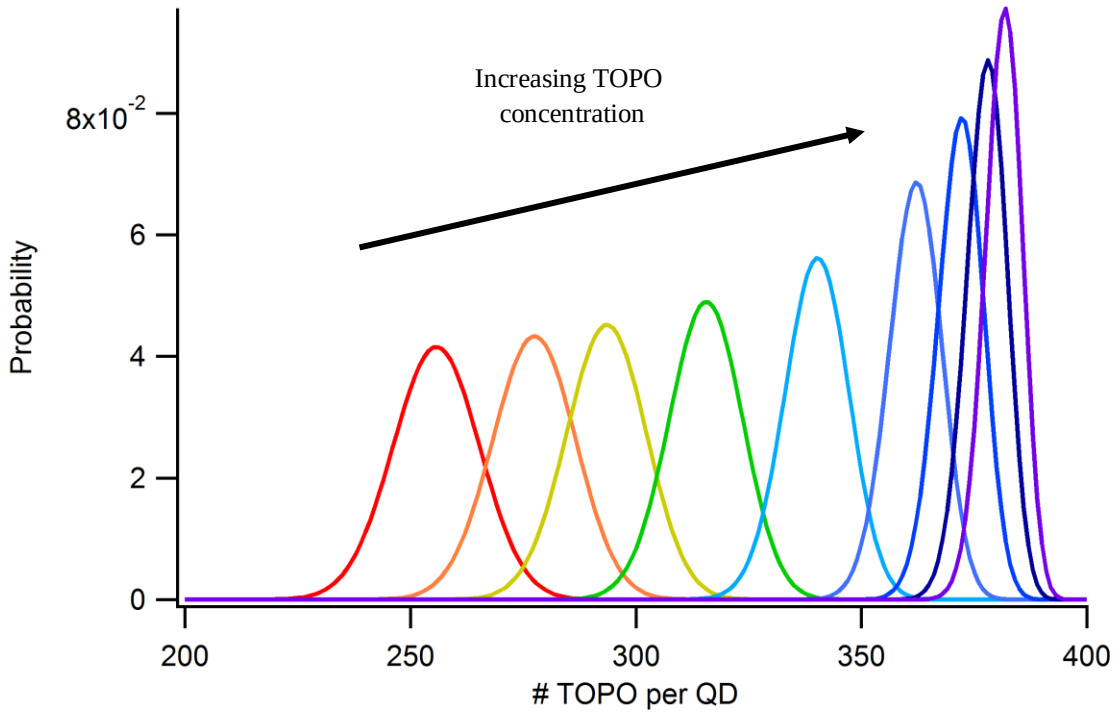

Figure 5.20: Plot of the probability of finding a QD with a certain number of attached TOPO and fitting parameters for the fit data in Figure 5.18.

Table 5.1: State energy values and transition lifetimes used to obtain the fit data in Figure 5.18.

Energies (ev)		**Lifetimes (ns)**	
Exciton (X)	1.9	k_r^X	12.4
Ground (G)	0	k^+_{XS}	131
Trap (S)	2.03	k^+_{XL}	5750
TOPO (L)	2.06		

CHAPTER 6: INTERACTION OF Pd NANOPARTICLES WITH CdSe QUANTUM DOTS

6.1 Introduction

Charge separation is one of the greatest challenges to using QDs to improve solar cell or photocatalytic device performance.[132, 151-156] After excitation with light of greater energy than the bandgap, an electron-hole pair, referred to as an exciton, is formed in the QD. The electron resides in the conduction band of the QD, while the hole (a particle formulation of the absence of an electron) resides in the valence band. After excitation, it is only a matter of time before the attraction of the electron and hole causes them to recombine and emit a photon. In the case of LEDs this process is desired. However for solar cells or photocatalysts, we need to prevent this charge recombination so that useful work can be accomplished with either the electron or hole before spontaneous recombination. Therefore, the study of ways to facilitate this charge separation in QDs is an intense area of research.[132, 151, 153, 157-158]

Current research is exploring the use of metal nanoparticles as charge acceptors from QDs to facilitate this charge separation. Within the last few years a variety of systems have been explored utilizing Au nanoparticles as charge acceptors from QDs. Banin *et. al.* developed a unique CdSe-Au "nanodumbbell" consisting of a CdSe nanorod with Au particles at either end.[159] These particles were found to be efficient charge separators as the Fermi level of the Au resided just slightly below the conduction band of

the CdSe. This allowed for efficient electron transfer from the CdSe to the Au. Once in the Au ends, electrons were utilized in the degradation of methylene blue dye. These particles demonstrated sufficient catalytic enhancement over similar CdSe quantum rods alone, which was attributed to this increased charge separation.

Additional QD-Au systems further showed this charge separation effect. Lin *et. al.* examined CdS decorated Au NPs, compared to CdSe QDs alone.[160] Again, due to differences in the band structure between the two materials, they found that after excitation a photoinduced charge separation occurred. This produced an electron charged Au core with a hole enriched shell. Time-resolved photoluminescence showed a decrease in PL lifetimes indicating electron transfer from shell to core.

Mattoussi *et. al.* demonstrated non-radiative quenching of QD fluorescence via Au NPs connected by a rigid polypeptide linker.[161] The linker allowed for precise control over the distance between the QD and Au particle as well as the amount of Au NPs attached per dot. Using this structure they found that the quenching of CdSe is Förster resonance energy transfer (FRET), similar to QD-molecular dye interactions.

FRET is a non-radiative transfer of electronic excitation from a donor to an acceptor. The mechanism for FRET arises from dipole-dipole coupling, and has been observed at relatively long distances (when compared to other electronic coupling) usually up to about 10 nm, depending on the coupling pair. FRET has been studied with many different QD systems with an eye towards potential biological applications, especially for protein studies.[162-166] The majority of these systems involve energy transfer from a QD to a molecular fluorophore.

Though these, and various other QD/Au[37, 167-171] (and to a lesser extent QD/Ag[171-175]) systems have been explored, other metal nanoparticle/QD systems have mostly not been developed. The reason for this is two-fold. First, simply Au and Ag NPs have been more widely synthesized and therefore a wealth of synthetic techniques exist for these particles allowing for precise control over NP size, shape, and reproducibility. Secondly, and probably part of the reason that Au and Ag NPs have been widely studied, is their unique plasmonic properties as described in the introduction to this dissertation. Au and Ag NP plasmons have been exploited in a variety of systems with QDs.[36-37, 167, 169, 173-174, 176] We wanted to expand this field and study a system that had yet to be explored. Also, since Pd is a well known catalyst (and our Pd NPs were shown to be efficient catalysts as described in Chapter 3), the potential for photocatalytic particles and systems based off of QDs and Pd NPs exists. The development of any potential applications however, requires a fundamental understanding of the interaction between the two particles. Therefore we chose to specifically examine the effects on the PL dynamics of CdSe QDs upon the addition of Pd NPs.

Based off of their bulk electronic structures (using the band gap for bulk CdSe and the work function of bulk Pd shown in Figure 6.1) the potential for a variety of mechanisms exists. Since the Fermi level (E_f = 5.6 eV relative to vacuum) of the Pd lies within the bandgap of CdSe (valence band = 6.2 eV, conduction band energy = 4.5 eV, relative to vacuum), the potential exists for either electron or hole transfer to occur. If single charge transfer occurs we would expect the hole to be more prone to transfer as the Pd E_f lies closer to the CdSe valence band energy. The potential for both electron and

hole to transfer also exists via either sequential charge transfer, or by some energy transfer mechanism such as FRET.

Because in our system, the particles are freely in solution at very low concentrations, we expect that negligible direct interaction (via particle touching due to collisions) between the particles will occur. Since charge transfer mechanisms typically require a direct contact between 2 particles we expect that any interaction will be dominated by longer-range energy transfer. The purpose of the experiments presented in this chapter is to lay the groundwork for potential QD-Pd NP systems in the future by developing an understanding of the most basic interactions between the two particles.

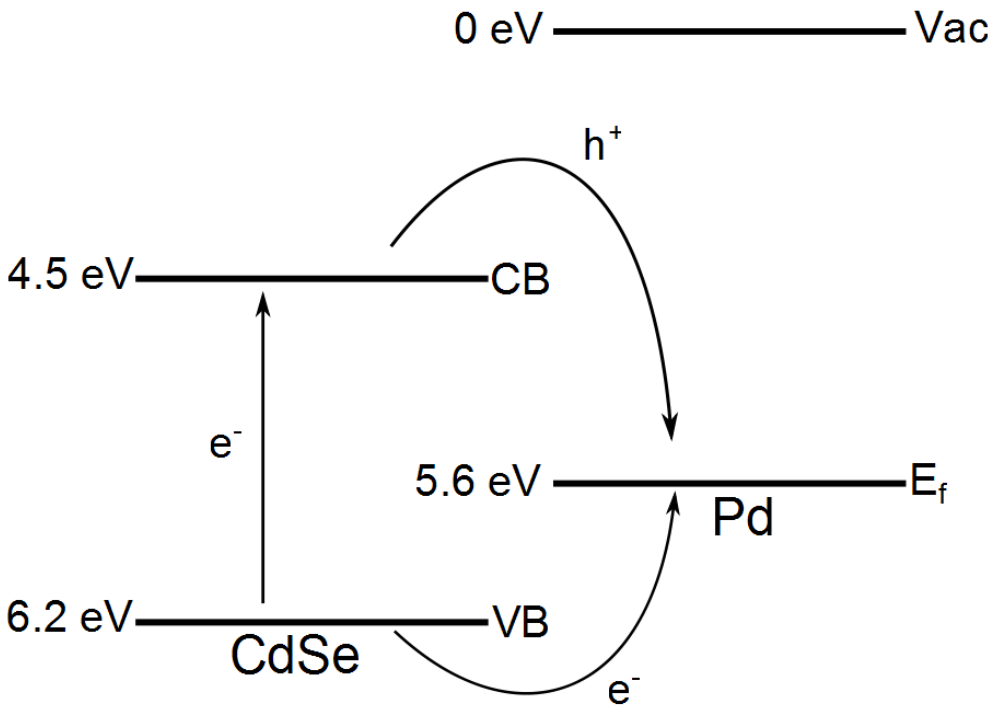

Figure 6.1: Band diagram for bulk CdSe and Pd demonstrating the potential for either electron or hole transfer after excitation of the CdSe. All energy values are given related to vacuum.

6.2 Experimental Methods

Steady-state and time-resolved photoluminescence were used to examine changes in the PL of the QDs in the presence of Pd NPs. All fluorescence measurements were conducted using a Jobin Yvon Fluorolog spectrometer. Steady-state PL spectra were collected with an excitation wavelength of 400 nm, excitation slit widths of 1 nm and emission slit widths of 5 nm to allow enough light through, due to the low concentration of particles used. The reason for using these low concentrations (approximately $10^{-5} – 10^{-4}$ mM) of both CdSe QDs and Pd NPs was to eliminate any scattering influences off of the Pd NPs. When the particles are diluted to these concentrations, they are not visible in solution. Therefore we assume that any possible scattering of the excitation light should be negligible. To obtain fluorescence lifetimes, time correlated single photon counting (TCSPC) measurements were conducted using a nano-LED pulse of 341 nm, 500 ns TAC rise time, and a wide band-pass emission filter of 29.4 nm (again due to the low concentration of QDs thus giving low signal).

As opposed to more complicated particle arrangements we chose to simply examine the interaction between the two particles in solution. By simply increasing the number of Pd NPs added, we shorten the average distance between the NPs and the QDs.

While this technique allows us to examine the NP-QD system in its most basic state without any further perturbations, it does not allow precise control over the distance between the particles. Instead we can only estimate the average distance, while assuming that a constantly changing distribution of radii between the particles actually exists.

We prepared QD solutions by dissolving 100 µL of 8×10^{-7} M CdSe QDs in 10 mL pristine hexanes. We then collected steady-state PL and lifetime measurements on

this sample. A measured aliquot of a 7×10^{-7} M Pd NP solution was added to the sample and shaken vigorously. Steady-state PL and lifetime measurements were again collected. Further aliquots were added and spectra were collected until the PL of the QDs was thoroughly quenched.

We also prepared solutions by preparing a large stock solution of QDs by diluting 100 μL of 4×10^{-4} M CdSe QDs in 100 mL pristine hexanes. From this stock solution, samples with increasing amounts of Pd NPs were prepared by adding the desired volume of Pd NPs to a volumetric flask and filling with the CdSe QD stock solution.

Both sample preparation methods have pros and cons. With the first method, the number of QDs is guaranteed to remain unchanged, however the total volume of solution will change. Additionally it becomes prohibitive to allow for long equilibration times between addition of the Pd aliquots. The second method allows for any desired equilibration time, as well as leaving the total solution volume constant. However it does not guarantee that the number of QDs in each sample is the same. Also it requires the use of significantly more solvent.

Many of our first steady-state experiments were conducted using the second sample preparation method to allow for the total solution volume to remain unchanged. Realizing the potential problems with this method, we wanted to switch to the first sample preparation method for further studies. However, after conducting the experiments, which led us to re-examine the changes in surface coverage of the QDs (explained in Chapter 5) we were concerned that not having time for the Pd NPs and QDs to achieve equilibrium would alter the measured dynamics.

To see if this would be a problem, a solution of QDs was prepared and consecutive lifetimes were collected as described in Chapter 5. After 12 hours we injected 100 µL of Pd NPs into the cuvette and continued collecting lifetimes for an additional 4 hours. We observed the lifetimes of the QDs stabilize as before and then immediately drop upon the addition of the Pd NPs. There does not appear to be any appreciable equilibration time between the QDs and Pd NPs. We conducted the same experiment with QDs diluted in toluene (which the QDs alone appeared to stabilize at a slower rate). After injection of the Pd NPs, even though the QD lifetimes had not yet completely stabilized, the lifetimes dropped (due to Pd addition) and then continued on the same stabilization trend as before, without being further affected by the Pd NPs. Therefore as long as we prepared the QD dilution in advance and allowed that to equilibrate, there was no harm in running experiments with Pd NPs added without allowing long equilibration time between the titrations.

It should be noted that even though we observed some (deemed inconsequential) differences between the different sample preparation/equilibration methods, the overall trends remained constant. Therefore the sample preparation chosen was considered mostly based on convenience and should not have any measureable effects on the data collected.

6.3 Results

6.3.1 Steady-state PL

Since we were introducing a metal particle to a solution of semiconducting QDs, we expected to observe quenching of the QD PL. Steady-state PL was used to observe any changes in the PL of the QDs upon addition of the Pd NPs. Initial experiments were

conducted adding continuous volumes of Pd NPs until total quenching of the CdSe PL was observed. Using the data gathered from these experiments we then focused to a specific range of Pd and added precise aliquots of Pd NPs within this range.

Upon examining this data (given in Figure 6.2) we found some interesting results. The first few aliquots of Pd NPs (up to 10 or 20 µL) showed a higher PL than the QD sample without any Pd added. Further Pd NP aliquots quenched the QD PL. With 300µL+ of Pd NPs added we effectively quenched most of the measureable QD PL. To confirm that the PL increase at low Pd NPs concentrations was indeed a real effect we ran additional experiments with smaller amounts of Pd NPs added, which once again showed the increase in PL at low concentrations.

Excitation spectra was also collected using the same concentration of QDs and Pd NPs. The only observed change from this experiment was a quenching of the QD fluorescence across all excitation wavelengths with no other apparent spectral changes.

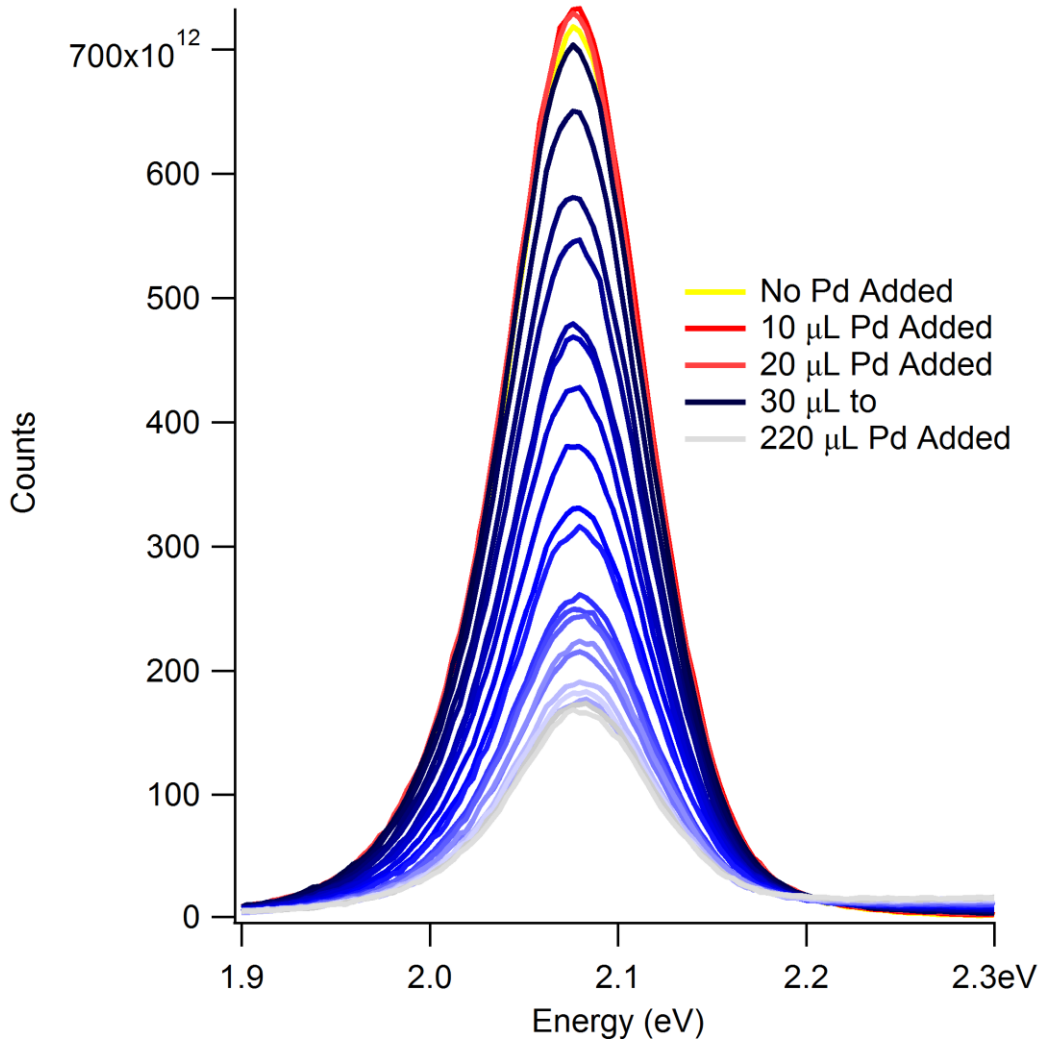

Figure 6.2: PL spectra for a sample of CdSe QDs with increasing aliquots of Pd NPs added. The yellow trace illustrates the PL spectra of the CdSe QDs alone. The two red shaded spectra are for the samples with 10 µL and 20 µL Pd NPs added. The spectra for 30 µL to 220 µL Pd NPs added are given in progressively lighter shades of blue.

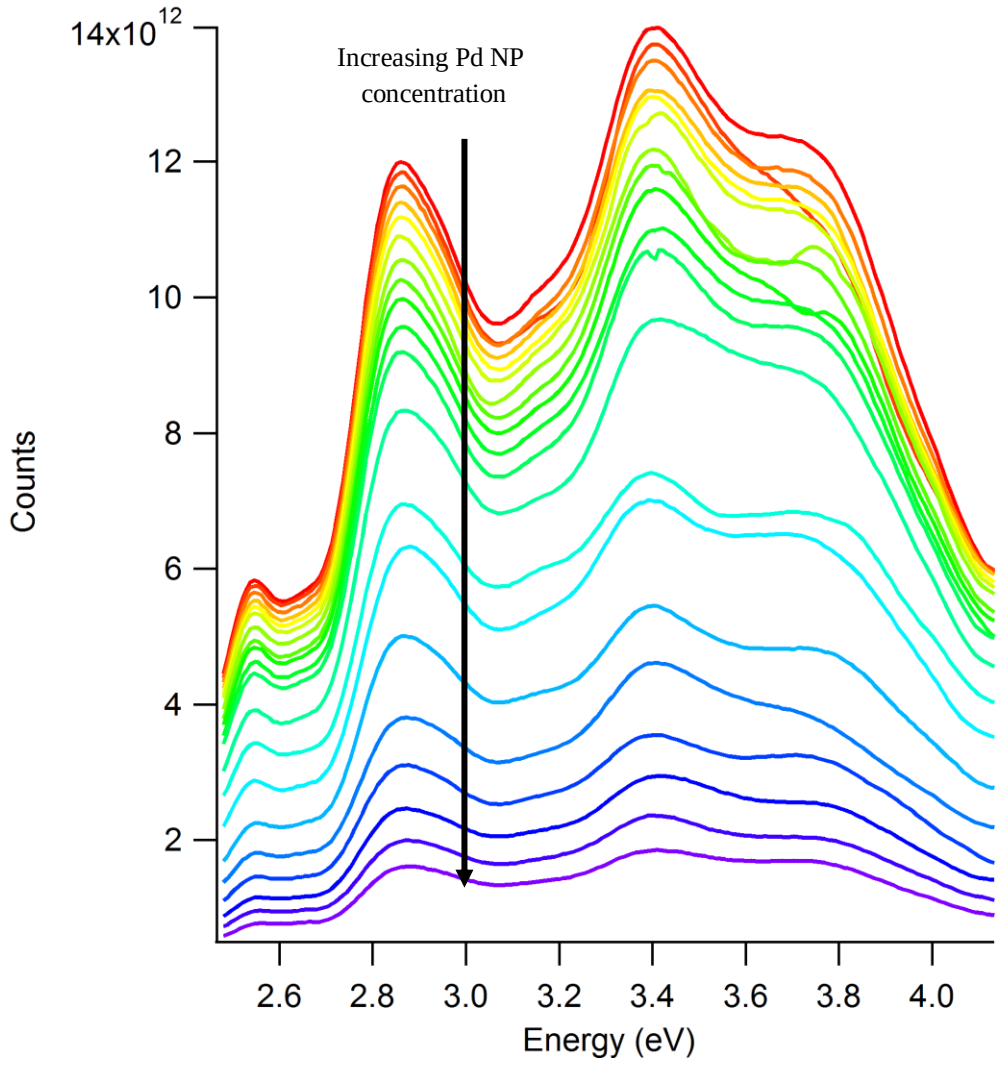

Figure 6.3: Excitation PL spectra for a sample of CdSe QDs with increasing aliquots (0 to 190 µL in 10 µL increments) of Pd NPs added.

6.3.2 Fluorescence lifetimes of CdSe QDs with Pd NPs

Lifetime measurements were conducted on the same samples discussed in the previous section. We found that an increase in fluorescence lifetime accompanied the samples, which demonstrated increased PL. As more Pd was added, the lifetimes began decreasing and with the most Pd added they were shortened by up to 20 ns from the QDs alone. The decreased lifetime upon Pd addition was expected as we presumed that the presence of Pd NPs added an additional non-radiative pathway for exciton recombination. After approximately 140 µL Pd added with this sample it appears that the QD lifetimes demonstrate little change. A variety of QD core samples were studied and demonstrated similar results. With very low Pd NP concentrations (usually just a few µL of Pd NPs added) we tended to observe a slight increase in PL lifetime of a few ns. Further addition of Pd always resulted in a decreased lifetime, which tended to stabilize after a certain point.

These results, coupled with the steady-state results indicated that either energy or charge transfer was occurring from the QDs to the Pd, leading to the shortened lifetimes and quenched PL. However we were not confident which mechanism was occurring, or what was causing the PL and lifetime enhancement at low Pd NP concentrations.

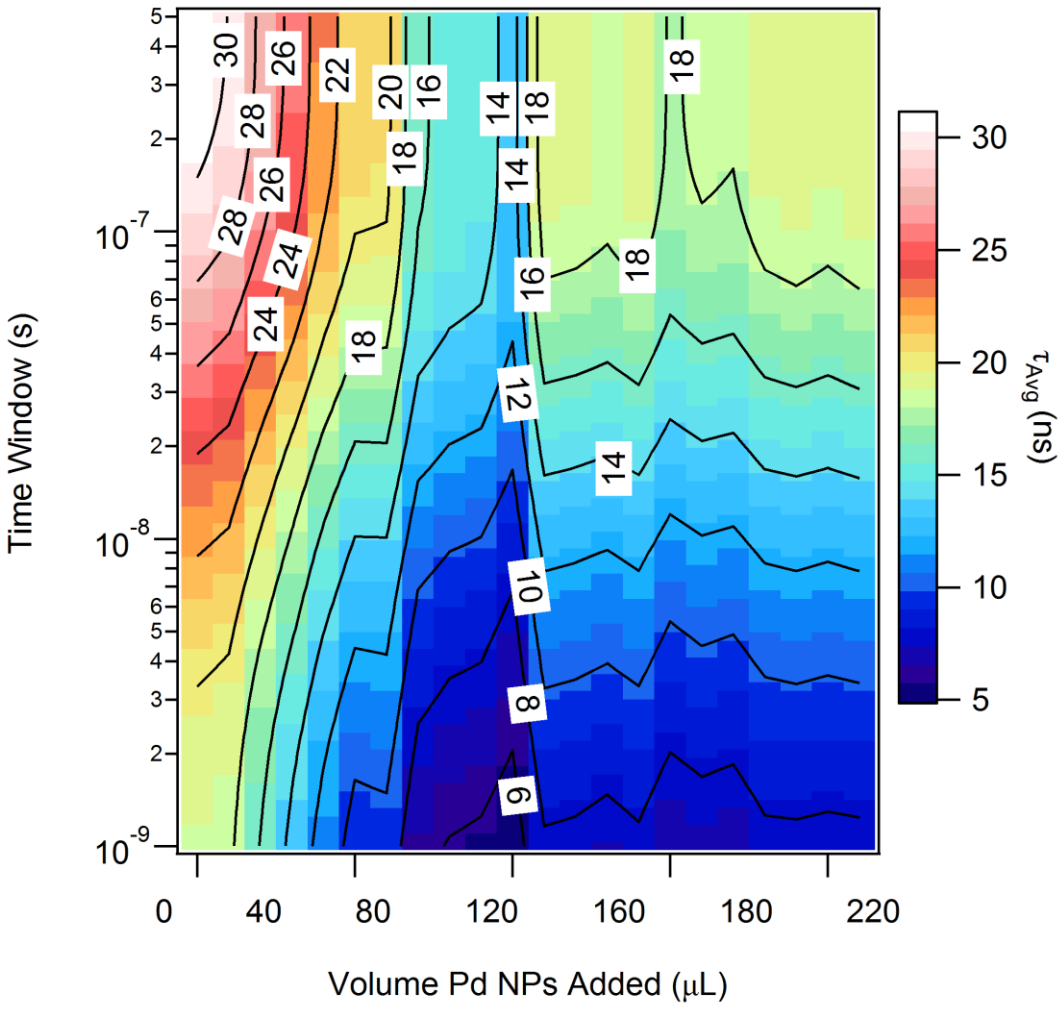

Figure 6.4: Lifetime image plot for a sample of CdSe QDs with increasing aliquots of Pd NPs added.

6.3.3 Changing solvents

As an attempt to determine the mechanism for the above changes, we conducted similar experiments in 4 different organic solvents. We hypothesized that energy transfer was the most likely mechanism of interaction and therefore chose to explore whether the observed effects followed FRET trends. Since FRET depends directly on the refractive index of the solution, by changing the solvent we expected to witness different interaction strengths between the QDs and Pd NPs.

The 4 chosen solvents were: hexanes (refractive index = 1.37), cyclohexane (refractive index = 1.43), toluene (refractive index = 1.496) and benzene (refractive index = 1.501). All of the solvents used were either purchased anhydrous or distilled so impurities would not affect the results. 4 µL of 6.9×10^{-4} mM CdSe QDs was diluted in 10 mL of each of the 4 solvents. 2 mL of these stock solutions were added to vials with either 500 µL blank solvent or blank solvent + 10 µL, 20 µL, or 30 µL of a 7×10^{-4} mM Pd NP solution. Steady-state and time-resolved measurements were run on all samples.

The PL spectrum in Figure 6.5 for the four different solvents show noticeable differences. Ignoring small fluctuations, it is observed that both the toluene and benzene samples show relatively small changes for all three volumes of Pd NPs added. The cyclohexane, and especially the hexanes samples however show a significant quenching effect for both the 20 µL and 30 µL Pd NP samples.

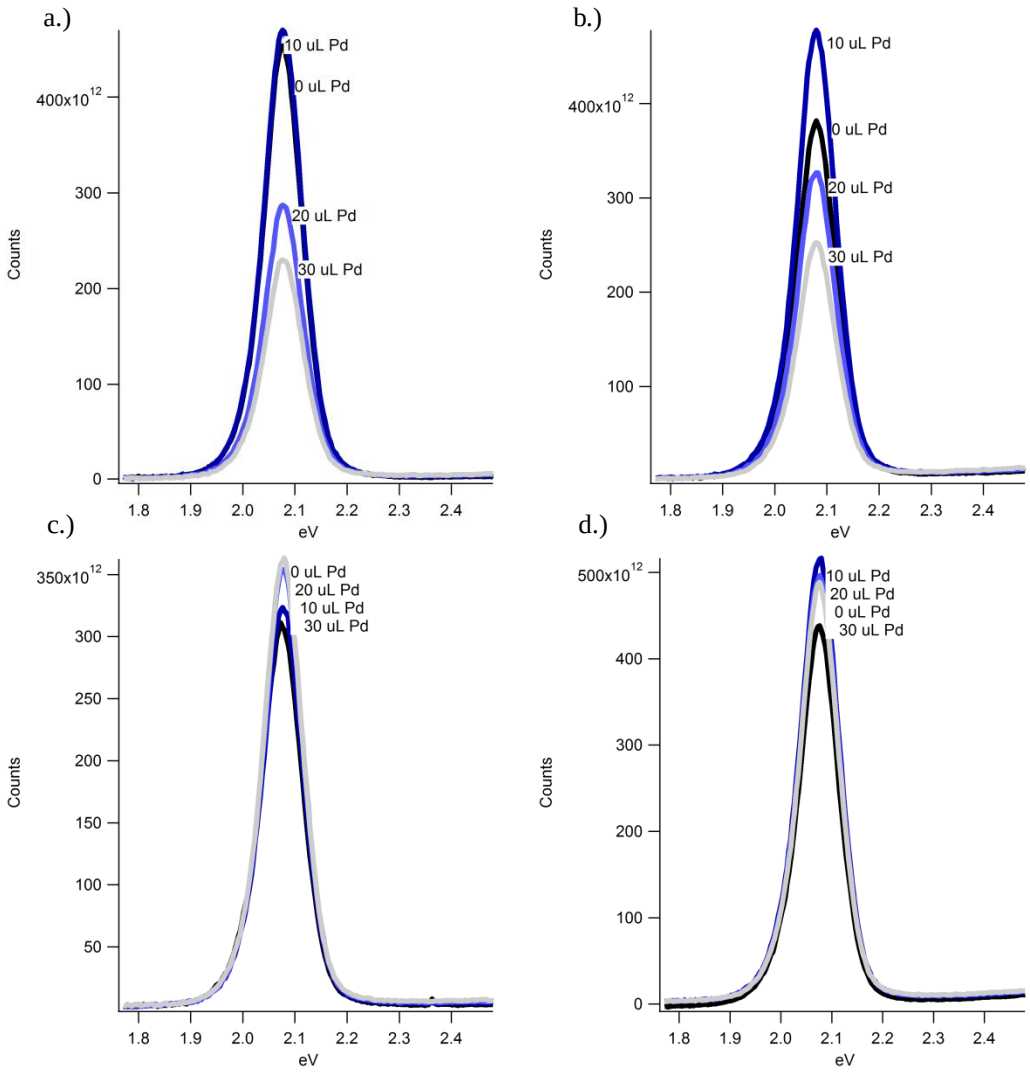

Figure 6.5: PL spectra for CdSe QDs with no Pd added and aliquots of 10 µL, 20 µL, and 30 µL Pd NPs added for samples diluted in a.) hexanes, b.) cyclohexane, c.) toluene, and d.) benzene respectively

Differences in the changes in lifetimes between the various samples is even more telling. When dispersed in hexanes, the lifetimes of the QDs become significantly shorter with each addition of Pd NPs. A similar trend is also observed for the QDs in cyclohexane, however the overall decreases between different Pd NPs additions are less pronounced. In toluene it is observed that the lifetimes, though they still decrease with addition of Pd NPs, show significantly less changes than with either the hexanes or cyclohexanes. After an initial decrease of about 2 ns upon addition of 10 µL Pd, there is less than a nanosecond further decrease with 20 µL and 30 µL Pd NPs added. For the QDs in benzene, the effects actually begin to reverse with increased fluorescence lifetimes with the addition of 10 µL Pd NPs. With 20 µL Pd added, the lifetimes increase further. Finally with 30 µL Pd added the lifetimes begin to decrease, however they still remain longer than their initial starting value with no Pd added.

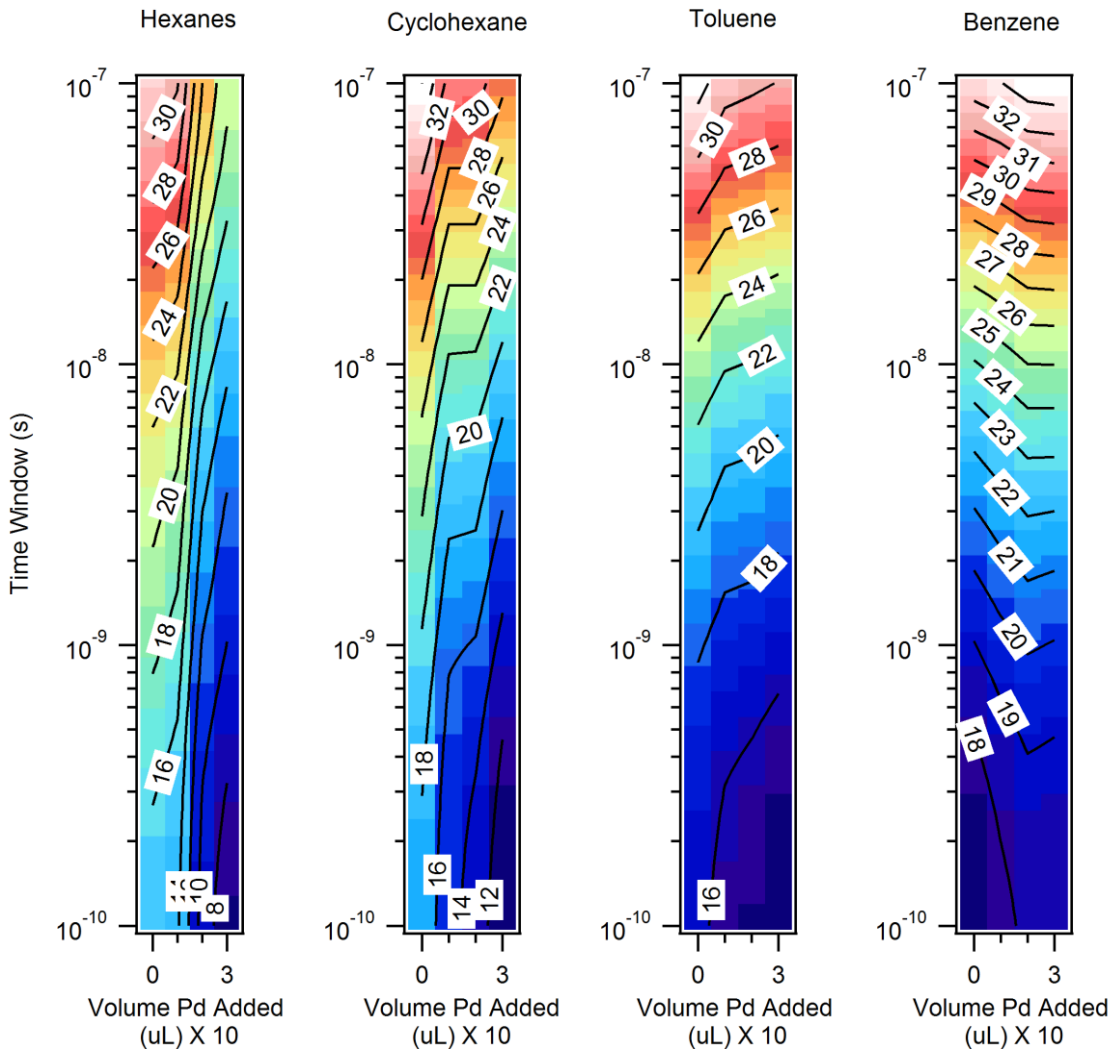

Figure 6.6: Lifetime plots for QDs diluted into hexanes, cyclohexane, toluene, and benzene with the addition of 0, 10 µL, 20µL, and 30 µL of Pd NPs.

These results appear to indicate that at least two different mechanisms are occurring with the addition of Pd. At least one that shortens the lifetime of the QDs, and one that increases the lifetimes. Since we originally hypothesized that FRET would be the most likely mechanism of interaction, we examined how the data changed with refractive index. The Förster rate of energy transfer is proportional to $1/n^4$ where n = refractive index of the surrounding medium, as seen in the derived equation for FRET.

$$k_{Forster} = \frac{1}{\tau_D}\frac{9000(\ln 10)\kappa^2\phi_D I}{128\pi^5 N n^4}\frac{1}{r^6}$$

As refractive index follows hexanes < cyclohexane < toluene < benzene, we would expect that the Förster rate would follow a similar trend and thus energy transfer would be most preferred in the hexanes and least preferred in benzene. For instance, when comparing $1/n^4$ between hexanes (0.28) and benzene (0.20) it is apparent that energy transfer would be preferred in the hexanes and thus the effect from adding Pd is more easily observed. This trend does appear to coincide with our data as PL and lifetime quenching upon addition of Pd is most observed for the samples in hexanes.

To further examine these changes we plotted the changes in the energy transfer rate k_{ET} from the hexanes samples for the 30 µL Pd NP samples of the other three solvents. We also plotted the expected changes in k_{ET} assuming a Förster interaction. This is shown in Figure 6.7. Though the trend of a decreasing k_{ET} with increasing refractive index is observed as expected, the changes appear to be significantly more dramatic in our measured data than found by calculation.

Since we do see the correct trend across the different solvent systems for Förster energy transfer, we expect that FRET is at least partially responsible for the observed effects. The changes appear to be too drastic for the range of solvent refractive indices we

are exploring (for instance the increase in refractive index from toluene to benzene is quite small and yet the lifetime data is noticeably different). Additionally FRET cannot explain the increase in lifetimes observed for the QDs in benzene, when low concentrations of Pd NPs are added, or the fluorescence enhancement observed in the steady state PL.

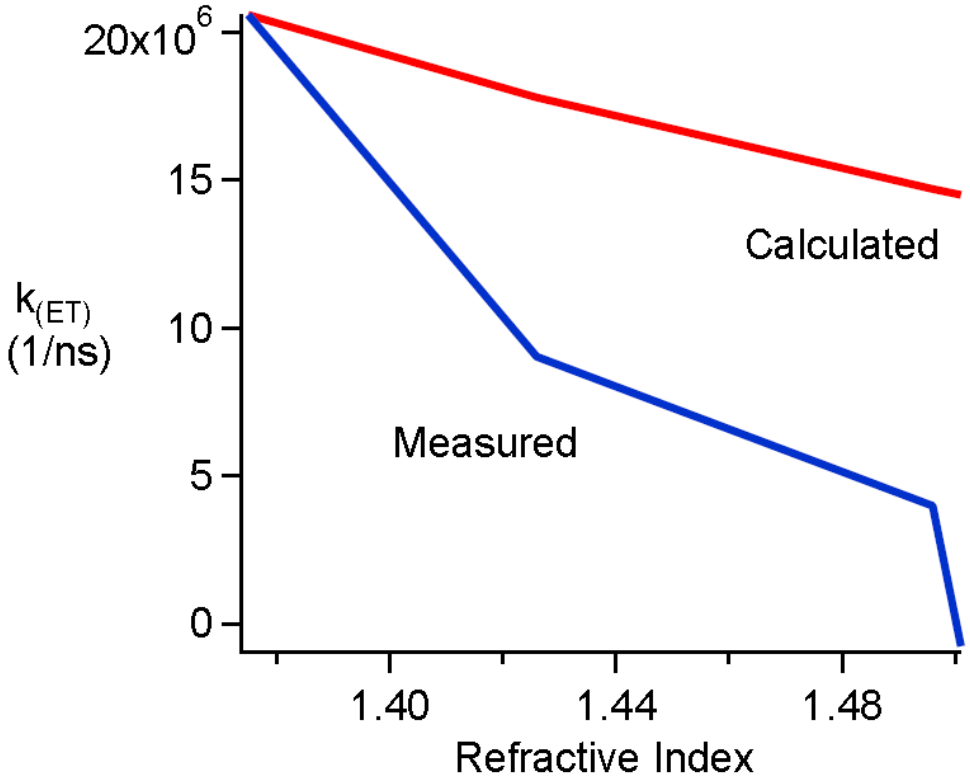

Figure 6.7: Plot for the measured and calculated FRET energy transfer rate ($k_{(ET)}$) for various refractive indices.

We also conducted experiments in solvent mixtures of both hexanes:benzene and hexanes:toluene. For the hexanes:benzene samples (lifetimes shown in Figure 6.8), two stock solutions were prepared with 8 µL of a CdSe QD solution diluted in either 10 mL of hexanes or 10 mL of benzene. So that the percent hexanes could be increased from 0 to 100 in increments of 20, the proper ratios of the two stock solutions were added together with blank hexanes or toluene so that 2.5 mL samples were prepared. The volumes used for each sample are given in Table 6.1.

For the samples without any Pd added, the lifetimes show very little differences up to 50% hexanes. After 60% hexanes, the lifetimes continually increase, so that the 100% hexanes sample has a lifetime about 4 ns longer than the 100% benzene sample. This is what we found in previous experiments. Upon addition of 10 µL Pd NPs, the lifetimes appear to very slightly decrease. Additionally there appear to be more measureable differences between the low percent hexanes samples. With 20 µL Pd added a more dramatic effect is observed. An overall decrease in lifetimes is observed, however the higher percentage hexanes samples exhibit a much larger decrease with the 100% hexanes sample showing a dramatic decrease in lifetime, and is actually now 5 ns shorter than the 100% benzene sample.

We then prepared a smaller range of samples in a mixture of hexanes and toluene. Since toluene and benzene have such similar refractive indices, if drastic differences in QD dynamics between the mixtures with hexanes were observed, they would be due to the chemical effects of the solvent. Additionally, since little change between the 0-60% hexanes samples were observed previously, a smaller range (from 70% hexanes to 100%

hexanes) was studied. The sample preparation volumes for this study are given in Table 6.2.

Similar trends are observed between the lifetimes of these samples (shown in Figure 6.9) and the benzene:hexanes samples for similar hexane percentages. Additionally noticeable changes in the lifetime of the QDs is witnessed for small (approximately 5%) changes in the percent hexanes. These results indicate that even a very small change in the solvent environment surrounding the QDs can have a measureable impact on its fluorescence dynamics and interaction with Pd NPs. Again, these findings point to additional mechanisms occurring as well as FRET, even though the general trends themselves do follow FRET statistics.

Table 6.1: Sample volumes used in preparation of hexanes:benzene mix samples

Hexanes:Benzene Ratio	Hexanes QD Stock (µL)	Benzene QD Stock (µL)	Hexanes (µL)	Benzene (µL)
100:0	1000	0	1500	0
80:20	1000	0	1000	500
60:40	1000	0	500	1000
40:60	0	1000	1000	500
20:80	0	1000	500	1000
0:100	0	1000	0	1500

Table 6.2: Sample volumes used in preparation of hexanes:toluene mix samples

Hexanes:Toluene Ratio	Hexanes QD Stock (µL)	Hexanes (µL)	Toluene (µL)
70:30	1000	750	750
75:25	1000	875	625
80:20	1000	1000	500
85:15	1000	1125	375
90:10	1000	1250	250
95:5	1000	1375	125
100:0	1000	1500	0

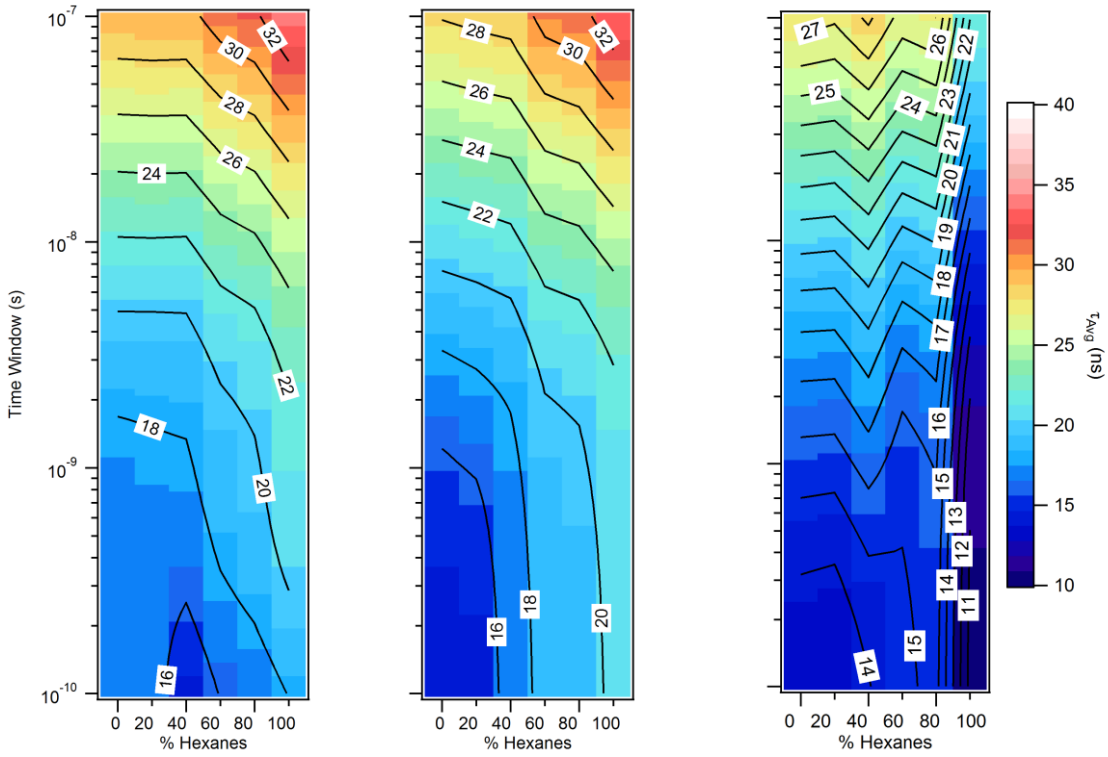

Figure 6.8: Lifetime plots for CdSe QDs in hexane:benzene mix with 0 µL Pd NPs added, 10 µL Pd NPs added, and 20 µL Pd NPs added.

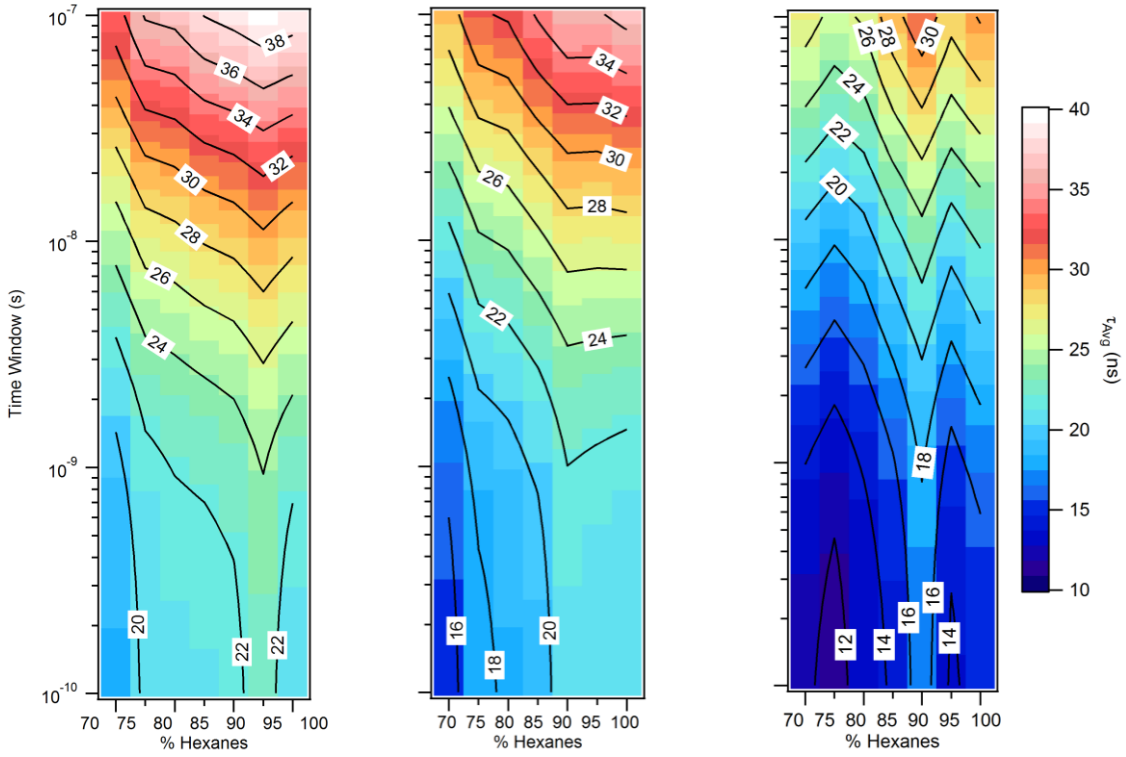

Figure 6.9: Lifetime plots for CdSe QDs in hexane:toluene mix with 0 µL Pd NPs added, 10 µL Pd NPs added, and 20 µL Pd NPs added.

6.4. Interaction of shelled CdSe QDs with Pd NPs

A common practice with CdSe QDs is to add an inorganic "shell" layer to the surface of the particles after synthesis. The purpose of this shell is varied depending on the material added, but is usually added to either increase electron-hole confinement (by adding a material with a wider band gap) or to allow for charge separation (by adding a material, which allows for the wavefunction of either the electron or hole only to spread to the shell, while confining the other charge carrier). The other benefit of either shell type is that it reduces surface trapping of charges due to dangling bonds from incomplete ligand coverage (such as the effects discussed in Chapter 5 of this dissertation).

6.4.1. CdSe/ZnS QDs interaction with Pd NPs

ZnS shelled CdSe QDs were the first shelled dots studied. Due to the fact that ZnS is a wider bandgap material than CdSe, we expect that both the electron and hole will be confined to the CdSe core.[118] This type of band alignment is deemed type-I, as opposed to a type-II band alignment where either the shell valence band or conduction band lies within the bandgap of the core, thus encouraging electron or hole transfer. Because of this confinement, we expect that any charge transfer (whether it be electron or hole) from the QD to the Pd NP would be greatly inhibited. Also a thicker shell, which should lead to more confinement, should further inhibit any charge transfer between the particles.

6.4.2 CdSe/CdS QDs interaction with Pd NPs

The other shelled dots we examined with Pd NPs were CdS capped CdSe QDs. These QDs have a slightly different band structure than the ZnS shelled dots.[177] Though the bandgap of the CdS is also larger than CdSe, and as such is still thus considered to be a type-I band alignment, it is not as wide as ZnS. Additionally the conduction band level

of the CdS is only very slightly higher in energy than the CdSe conduction band energy. This allows for the slight potential (especially for small CdSe cores where the conduction band energy will be highest) of charge separation to occur with the electron transferring from the QD core to its shell. Recent work has demonstrated in detail the potential for CdS shelled CdSe particles to exhibit quasi-type II band-alignment properties with measureable charge separation[108]. Therefore, we expected that if any measureable charge transfer between the CdSe QDs and Pd NPs in solution was occurring we would witness the effects more with CdS shells than their ZnS counterparts.

In fact we observed an opposite trend. Using similar concentrations of shelled QDs and Pd NPs we observed less quenching of PL fluorescence with the CdS capped dots than those capped with ZnS. This assisted in confirming that we were in fact witnessing energy transfer to the Pd NPs and not electron transfer, since the exciton is much more strongly confined in CdSe/ZnS QDs.

These shelled QD studies presented in this dissertation are simply the tip of the iceberg for potential shelled-QD – Pd NP systems and were never meant to be an exhaustive study. We chose these specific experiments to further confirm our hypothesis that energy and not charge transfer was responsible for the observed quenching at these relatively long particle distances.

6.5 Modeling CdSe QD-Pd NP interaction

To gain a complete understanding of the interaction between CdSe QDs and Pd NPs we developed a model. Since these particles were dispersed in solution, and thus had no fixed distance between them, we needed to first determine the distribution of CdSe-Pd distances based on the amount of Pd NPs added.

First we assumed that there was one QD at a point. Then the average volume of a sphere centered on this point in which 1 Pd NP resides is

$$V_R = \frac{4}{3}\pi R^3$$

Where R is the radius of this sphere from the center of the quantum dot.

Since the Pd NP cannot occupy the space of the quantum dot we must subtract the volume of a sphere enclosed by the sum of the radii of the QD and Pd NP (r_o), which has a volume of

$$V_{r_o} = \frac{4}{3}\pi {r_o}^3$$

The average volume in which 1 Pd NP lies is then given by the difference of V_R and V_{ro}

$$V = \frac{4}{3}\pi(R + r_o)^3 - \frac{4}{3}\pi {r_o}^3$$

To determine the probability of finding a Pd NP at a given distance r, from the QD we examine infinitesimally small shells with volume equal to the surface area of a sphere that is given by

$$4\pi r^2$$

Adding these shells together from r_o to $R+r_o$ must equal the average volume in which 1 Pd NP lies

$$\int_{r_o}^{R+r_o} 4\pi r^2 = V$$

Let

$$\alpha = \frac{1}{V}$$

Then the probability of finding 1 Pd NP in V, given by P(V) is

$$P(V) = \alpha \int_{r_o}^{R+r_o} 4\pi r^2 dr = 1$$

And the probability of finding a Pd NP in one shell, or between r and r + dr is given by

$$P(r) = \alpha 4\pi r^2 dr - \alpha 4\pi {r_o}^2 dr$$

Using this formulation we are able to find the probability of finding a Pd NP at a radius r from a CdSe QD. With a Pd NP particle concentration of 7×10^{-7} M we determine probability curves based off the above formulation as shown in Figure 6.9 for varying volumes of Pd NP solution added. Though these curves show the absolute probability of finding 1 Pd NP at a certain distance from a QD, the more useful values for comparison is the integral of these curves. By integrating, we find the probability of finding a Pd NP within a volume of radius R from a QD. This can be thought of as the average distance at which one Pd NP will be found from a given QD. The integrated curves for select Pd NP volumes added are given in Figure 6.11.

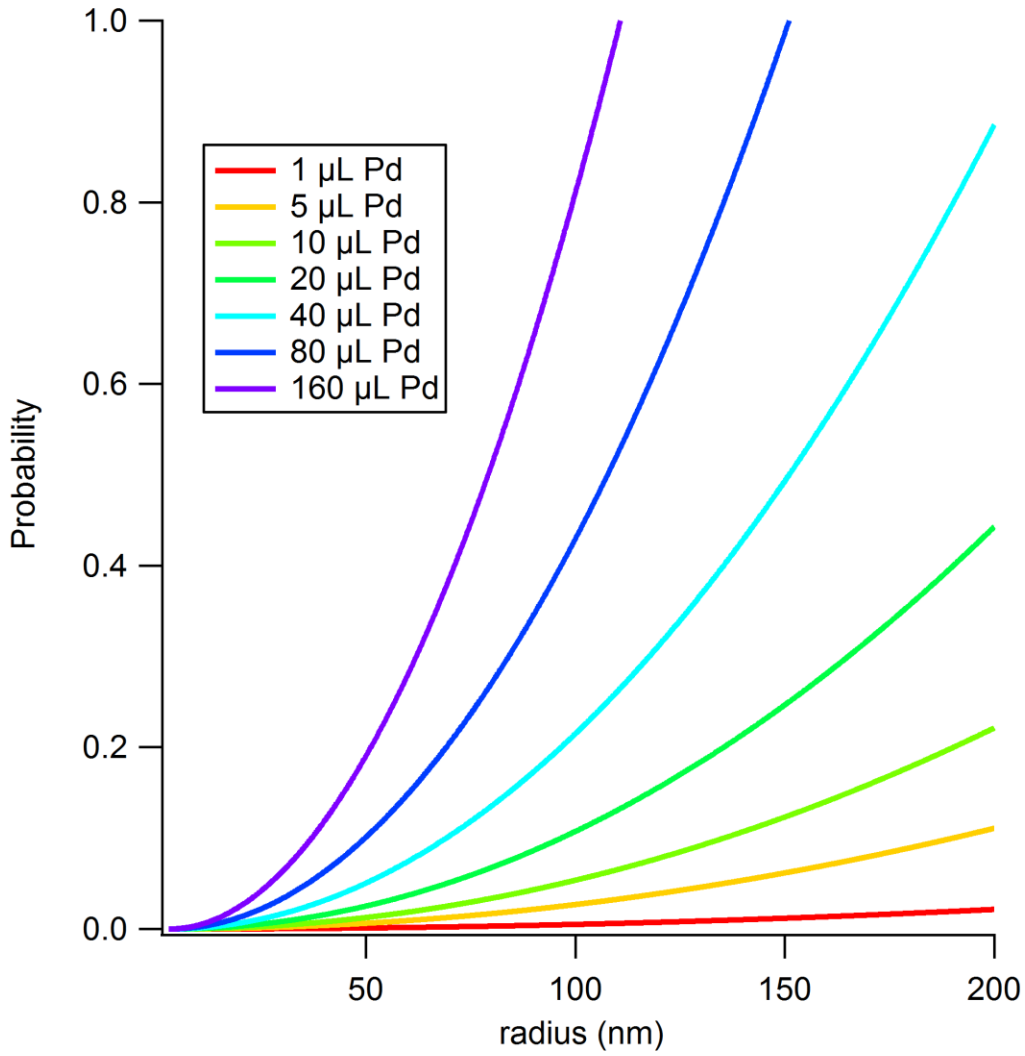

Figure 6.10: Probability curves for finding a Pd NP at a radius from a QD for selected Pd NP volumes.

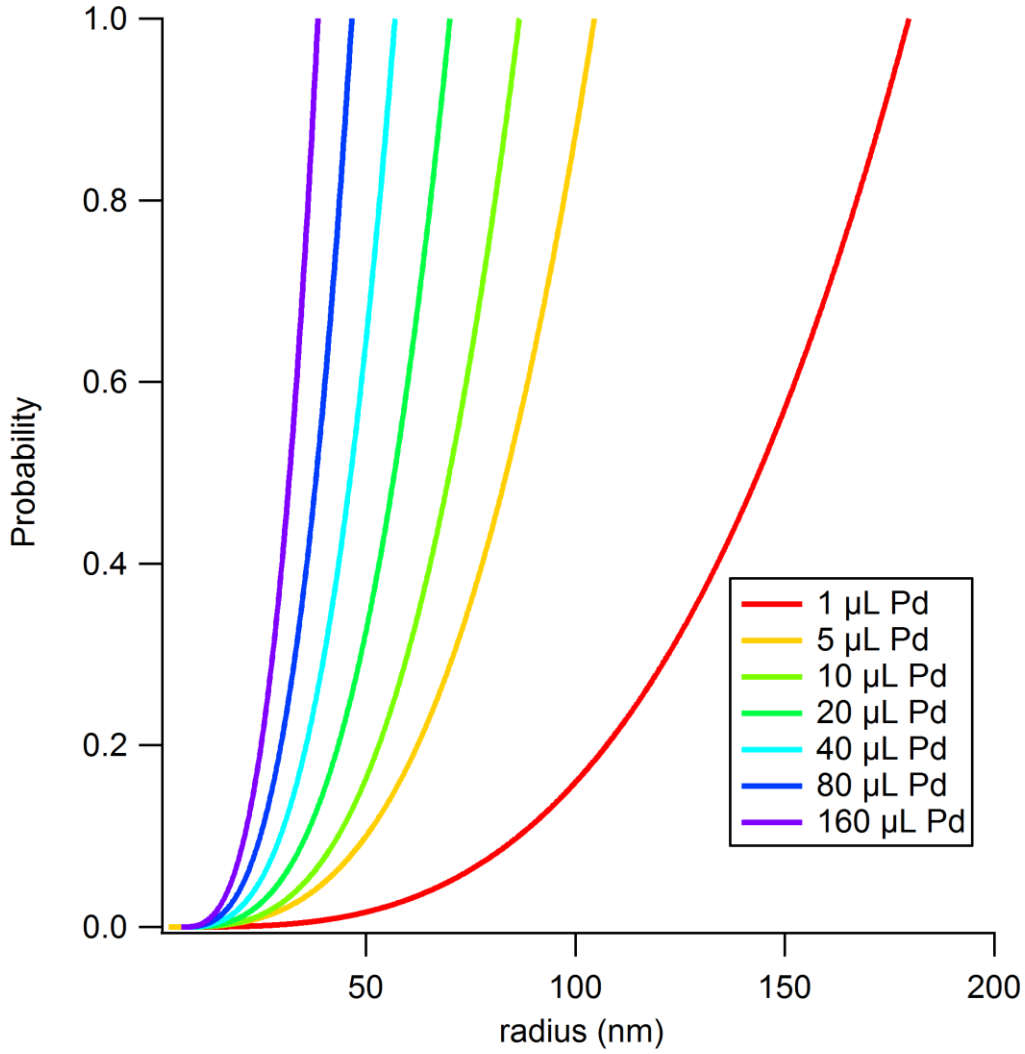

Figure 6.11: Probability curves for finding a Pd NP within a radius from a QD for selected Pd NP volumes. Found by integrating the curves in Figure 6.10.

As a starting point, if we assume that only FRET is occurring, then the rate of EET from donor D, to acceptor A is given as

$$k^{Forster} = \frac{1}{\tau_D}\frac{9000(\ln 10)\kappa^2\phi_D I}{128\pi^5 N n^4}\frac{1}{r^6}$$

Where κ is the orientation factor associated with the dipole-dipole interaction between donor and acceptor and is assumed to be 2/3 for freely rotating dipoles,[178] ϕ_D is the quantum yield of the donor (the QD in this system), τ_D is the donor lifetime, *N* is Avogadros number, *n* is the refractive index of the surrounding medium, *r* is the distance between donor and acceptor, and *I* is the spectral overlap integral obtained from an experimentally measured absorption spectrum for the acceptor ($a_A(\lambda)$) (on a wavelength scale) and an area-normalized emission spectrum $f_D(\lambda)$ of the donor.

$$I = \int_0^\infty a_A(\lambda) f_D(\lambda)\lambda^4 d\lambda$$

If we let

$$\frac{1}{\tau_D}\frac{9000(\ln 10)\kappa^2\phi_D I}{128\pi^5 N n^4} = \beta$$

Thus

$$P(r) \times k^{Forster} = \frac{4\pi\alpha\beta r^2 dr}{r^6} = \frac{4\pi\alpha\beta dr}{r^4}$$

Integrating over all space ($r_o \rightarrow \infty$) gives

$$\int_{r_o}^\infty 4\pi\alpha\beta^{-1} r^{-4} dr = -\frac{4}{3}\pi\alpha\beta {r_o}^{-3}$$

Using this formulation we are able to plot a curve for a Förster interaction between CdSe QDs and Pd NPs. The addition of a Förster rate acts as an additional non-radiative decay pathway.

Thus based off of the starting lifetime of the dots, we are able to plot how the lifetimes should decrease with added Pd assuming only a Förster interaction. Figure 6.12 shows this curve plotted versus the average lifetimes for the collected average lifetimes shown in Figure 6.4.

Though the data follows the fitted Förster curve fairly well for low concentrations of Pd NPs added, a few differences are observed. First, as previously mentioned, a Förster interaction cannot account for an increase in fluorescence lifetimes and at very low amounts of Pd added the lifetimes are higher than expected. From 10-50 µL Pd added the curve follows the raw data quite well. This is encouraging because based off of our particle distance curves we are within less than 50 nm maximum distance between a QD and its nearest Pd neighbor. FRET typically occurs within a few tens of nm distance so this follows quite well as at these concentrations a measureable amount of the QDs will experience a quenching FRET interaction. Eventually the collected average lifetimes begin to flatten out with a value of approximately17 ns for this select data. This is due to the fact that we are only collecting data for QDs that are not quenched. In an ensemble measurement such as this, as more and more dots are fully quenched, the data eventually is weighted such that it will flatten out.

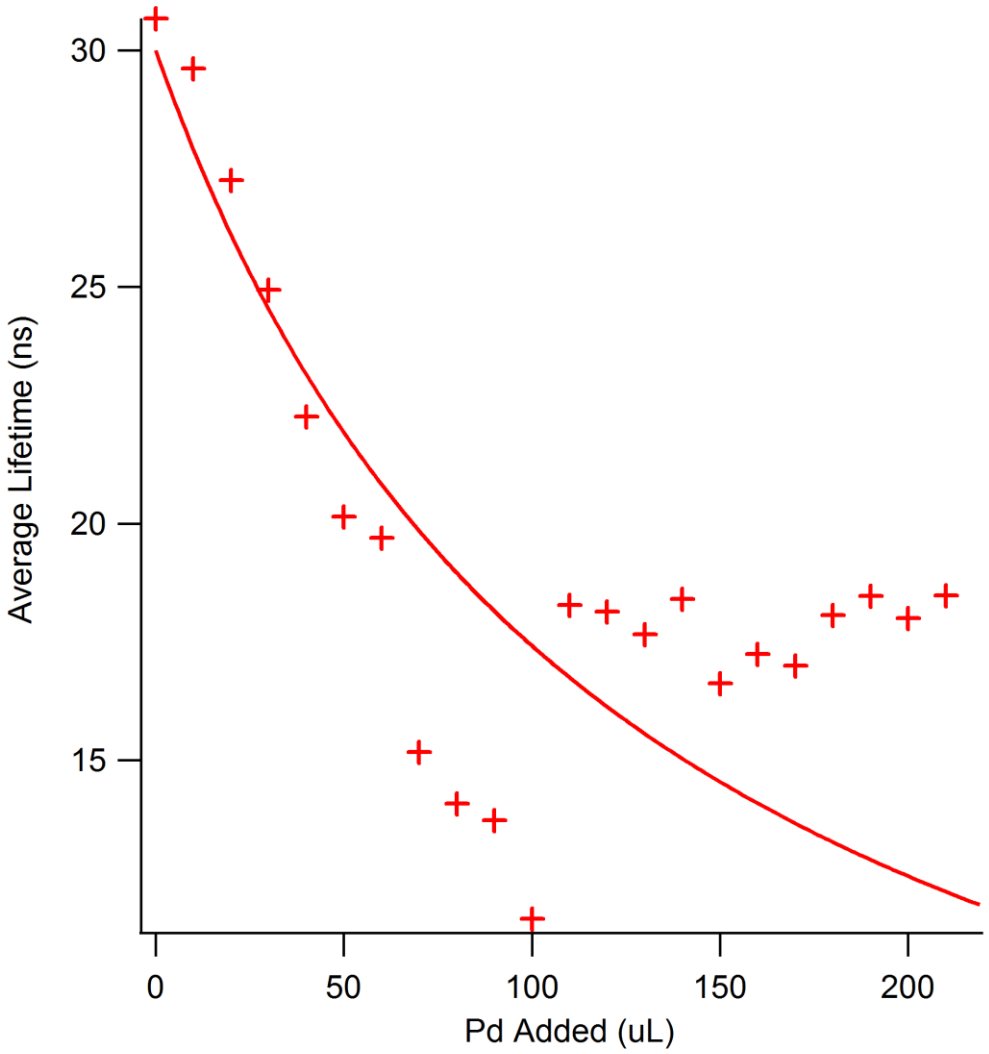

Figure 6.12: Forster fit (solid line) for the average lifetimes (crosses) with increasing Pd NP concentration from Figure 6.4.

After further examination of the literature we found some references that suggest enhanced absorption from the Pd NPs may be responsible for the slight enhancement effect we were witnessing. As mentioned in the introduction to this chapter, the majority of QD-metal NP systems that have been explored use Au NPs due to their visible plasmon absorption band. Pd NPs have no such plasmon band in the visible range, and thus we did not expect to observe any similar effects. Some recent work with Au NP-QD systems however has demonstrated a plasmonic effect even for samples where the plasmon band of the Au and QD emission peak do not directly coincide.[179]

It was proposed that the enhancement observed with these systems, though significantly less pronounced than when the plasmon and QD peaks align, is due to a similar process, through enhanced absorption. Observing that the plasmon "tail"/QD emission peak alignment from this system looked similar to our Pd absorption/QD emission spectral overlap , we proposed that a similar effect was occurring in our system. Since there is no visible plasmon resonance for Pd, and thus the coupling interaction would be even less than the off-resonance Au system, we expected that the enhancement effect would tend to be smaller with Pd NPs.

6.6 Single particle studies of CdSe QD – Pd NP interactions

To confirm that these enhancement effects were occurring with single quantum dots we performed single particle studies on QD/Pd samples. The benefit of studying single particles, is that we are able to observe any effects that Pd NPs have on QD fluorescence intermittency, also described as blinking. Blinking is a well known phenomenon, which occurs in nearly all QDs. Similar to molecular fluorophores, QDs are found to "turn off" by entering non-emissive states. This is observed by recording the

fluorescence emitted by a single QD over time, and most QDs that blink are found to cycle on and off 1 to many times over a 60 second cycle. Though the exact mechanism for blinking is still debated, the general consensus is that it is caused by charging/discharging of the QDs.

When a charge (or more likely multiple charges) is trapped on a QD it has the potential to reside in a trapped state for a measurable amount of time. If, within this time frame, a second exciton is formed via additional excitation, a 3-particle state (consisting of the electron, hole, and trapped charge), known as a trion, is formed. A trion state in a QD is a non-emissive state, and therefore the QD will switch off. When the excess charge is removed (via some recombination process such as Auger recombination) the QD no longer resides in a non-emissive state and therefore will turn back on, as evidenced by single particle studies.

6.6.1 Sample preparation for single particle studies

For the first set of single QD experiments, we simply utilized previously prepared CdSe core samples, which were used for ensemble studies. These samples proved to be ill-suited for single particle studies as the QDs would quickly bleach once we began zooming in on a specific dot. This is a relatively common phenomenon observed with unshelled QDs.

Because of this effect we chose to use commercial shelled CdSe QDs purchased from Evident Technologies. The 4 nm QDs consisted of a CdSe core with a CdS shell, capped with an additional ZnS shell, and demonstrated a maximum fluorescence at 600 nm. Therefore we expect that the exciton should be well-confined to the CdSe core and the effects of surface trapping due to dangling bonds would be reduced. These QDs were

shown to be successful in a variety of single-particle studies conducted by the Moyer group in the department of physics at UNC Charlotte, without noticeable quenching under normal laser power for typical experimental collection times.

To further assist in single particle data acquisition (by preventing particle aggregation) the QDs and Pd NPs were embedded in a poly(methyl methacrylate) (PMMA) thin film by spin coating with a 5 wt% PMMA toluene solution onto a glass cover slip. The stock concentration of QDs was 10^{-6} M and the stock Pd solution was 10^{-7} M. Samples were prepared by adding either 0, 3 µL, 5 µL, 7µL or 9 µL Pd NPs to 5 µL of QD stock solution and then diluting in the 5 wt% PMMA/toluene solution. 25 µL of the resulting solution was then spin coated onto a glass cover slip for analysis.

Samples were studied on a homebuilt scanning confocal microscope in the Moyer lab, which allowed for single particle studies. Blinking traces were built by the time tagged time-resolved method (TTTR), and TCSPC was used to construct fluorescence lifetime decays.

6.6.2 Changes in QD blinking with added Pd NPs

The main piece of data, which these single particle studies allowed us to examine was how the addition of Pd NPs affected CdSe QD blinking. We collected blinking traces for approximately 20 QDs for each sample. The QD samples with no Pd added demonstrated typical blinking with relatively well-defined on and off states of varying lengths of time across the different dots. For the samples with higher concentrations of Pd added (most prominent in the 7 µL and 9 µL samples) some of the dots exhibited nearly completely “off” behavior and only showed one or two very short lived on states. This is

attributed to the quenching behavior due to FRET, that we witnessed in our ensemble measurements.

Samples at lower concentrations of Pd exhibited some interesting results. First, for many of the QDs, we observed an increased PL intensity, similar to that seen in the steady-state PL ensemble measurements. The single QDs, which showed a noticeable increase in PL intensity also again had longer fluorescence lifetimes. Examination of the blinking traces for these QDs showed that none of the samples appeared to have any long off times (as observed in many of the QDs without any Pd present, or with 10+ μL Pd present). In fact it appeared that the blinking overall was suppressed, and whenever a dot would happen to "switch off," it would very quickly turn back on.

These changes in blinking follow the same trend, which was observed in the QD-Au samples in the literature, which demonstrated enhancement effects. Therefore these single-particle experiments confirm that a similar mechanism is occurring with the Pd NPs.

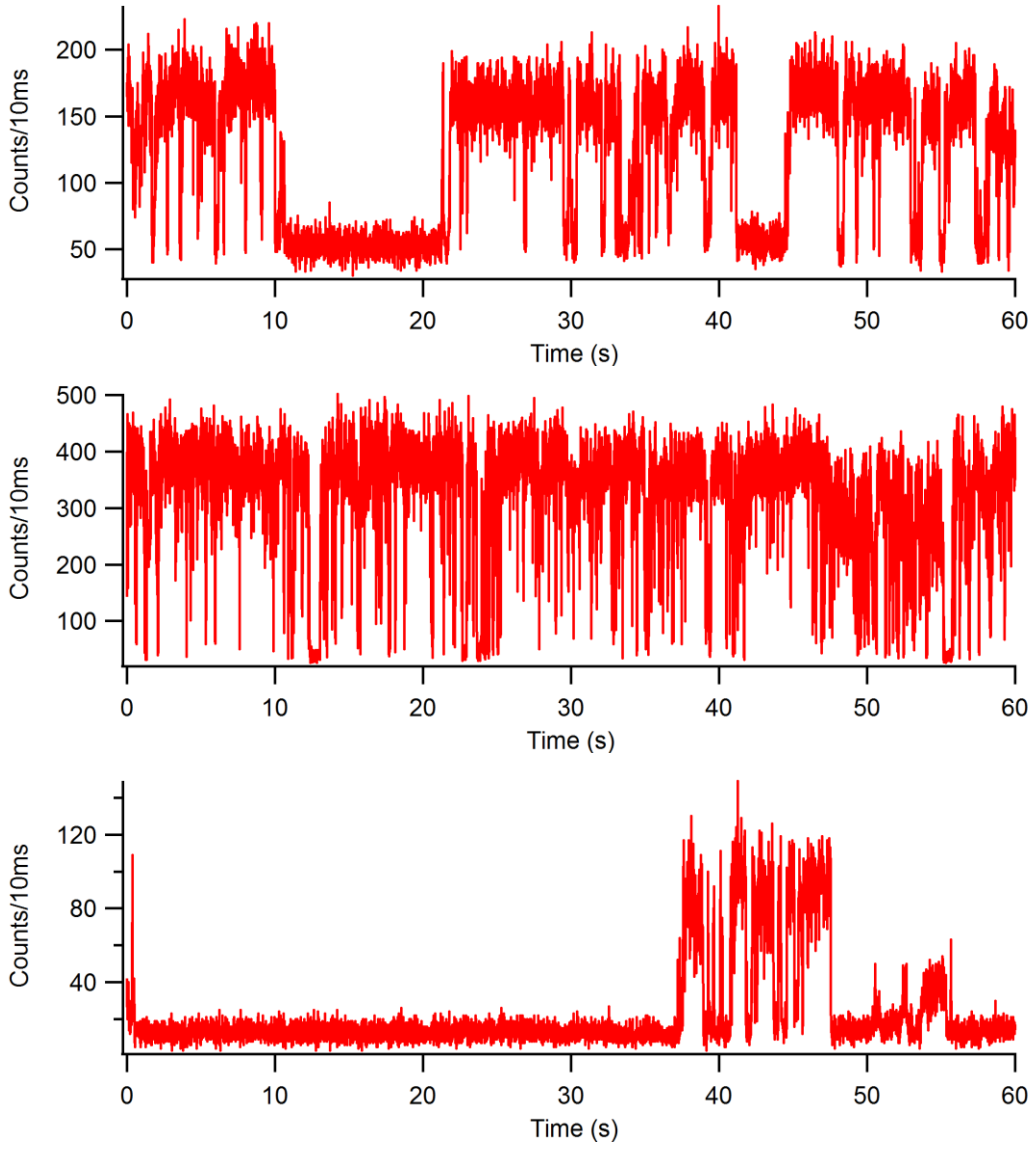

Figure 6.13: Blinking traces collected over 60 seconds for CdSe QDs with 0 µL, 5 µL, and 7 µL Pd NPs added respectively.

6.7 Conclusions

We have explored the effects of well-defined 2.5 nm Pd NPs on CdSe QDs in solution. At higher concentrations of Pd NPs, we observed an expected quenching of the QD PL, which we attributed to energy transfer from the QDs to the Pd NPs. PL quenching was accompanied by a decrease in the QD fluorescence lifetime. This also was expected as energy transfer pathway from the QD to the Pd NPs would allow for an additional non-radiative decay process.

At low Pd concentrations we found that the QDs actually exhibited enhancement of the steady-state PL intensity and longer lifetimes. After performing single-particle studies of the QDs in presence of Pd NPs we found blinking suppression of the QDs which exhibited these enhancement effects. By comparing to results in the literature, we concluded that this enhancement was due to enhanced absorption due to the Pd NPs, which is similar to that observed with Au NPs even with particles whose plasmons are off-resonance from the QDs.

It should be noted that preliminary studies (using steady state PL) were also conducted with 2.5 nm Pt NPs. These experiments yielded almost identical results to those with Pd NPs. We therefore expected that the Pt NPs would behave similarly in further studies and thus we chose to focus our efforts on the Pd NPs as presented in this chapter.

CHAPTER 7: CONCLUSION

The work presented in this dissertation described the synthesis, characterization, and basic development of Pd and Pt NPs as photocatalysts. We developed a facile method for producing monodisperse Pt and Pd NPs with diameters of less than 5 nm using n-dodecyl sulfide as a stabilizing agent. This is one of the first methods available for a one-pot synthesis of stable, monodisperse Pt and Pd NPs of such small size. The benefits of this straightforward synthesis method should not be overlooked. The fact that is it one-pot, and only uses 3 reagents (the metal salt, stabilizing ligand, and solvent) both allow for high reproducibility. Additionally it is difficult to produce monodisperse NPs of such a small size, since particle growth tends to be less uniform when aiming for small particles. The more that these types of reproducible, facile synthesis methods are developed, the more the future nanoscience community will benefit. These methods allow for the production of specific particles for specific needs, even by scientists with lesser synthetic backgrounds.

Like their bulk counterparts, these NPs were found to be efficient catalysts for hydrogenation across a C-C double bond. We further improved the reusability of these particles as catalysts by linking them to magnetic $CoFe_2O_4$ NPs, which allowed for the recovery and reuse of the NPs over 5 times. By using this magnetic recovery method, we were able to exploit the benefits of NP catalysts (mainly the high surface area to volume ratio) while minimizing their largest pitfall of difficult recovery and reuse.

We then began studying new potential photocatalytic uses of these NPs. The first system we explored utilized Pt NPs as effective charge capture and storage particles from nanocrystalline TiO_2. The charged Pt NPs were found to be capable of reducing methyl viologen as well as in the production of hydrogen from water splitting. The greatest benefit of this system over those previously developed is the potential for "dark" water splitting or dye reduction, as previously developed systems required continuous irradiation of the particles, which promotes degradation.

This realization of water splitting in the dark is a significant step forward for such TiO_2-Pt systems. One could envision a potential system where a large solar array containing TiO_2 (most likely doped) or other semiconducting materials is directly exposed to sunlight. Then, a limited number of Pt NPs could be used to harvest the electrons from the semiconducting array before discharging them in the production of hydrogen. This would greatly reduce the amount of Pt necessary over traditional linked TiO_2-Pt systems, since each Pt NP could harvest over a semiconducting area after it has been exposed to sunlight for an amount of time, rather than having the Pt in stationary positions. Such a system (once optimized) would have the potential for large quantities of hydrogen production with a large amount of relatively inexpensive semiconductor material, while limiting the need for the significantly more expensive Pt.

The final system we chose to explore utilized Pd NPs in conjunction with CdSe QDs, which are one of the most studied particles in nanoscience research. Though a variety of Au and Ag NP – QD systems have been studied, no work using Pd NPs was found in the literature. Before we could fully explore this system however we realized

that we needed to more fully understand the photophysics of the CdSe QDs alone. This realization led to a complete research project studying the effects of stabilizing ligands on the QD fluorescence.

We found that the photophysical properties of CdSe QDs were drastically affected by changes in their surface ligand coverage and surrounding environment. We demonstrated the importance of using pristine solvents for QD sample preparation as well as the effects that different solvents have on stored QDs over time. Addition of excess stabilizing ligands to prepared QD samples altered both the steady-state fluorescence and lifetimes of the QDs.

This work demonstrates potential pitfalls in commonly utilized QD sample preparation as the surface ligand coverage and subsequent surface dynamics of the QDs could be altered without control. If these changes are not accounted for, one may attribute them as due to the system being explored (for instance, as an effect of the addition of Pd NPs for our studies) where they in fact are solely due to the changing surface ligand coverage. To minimize the change in surface coverage, we advise that a careful, systematic method from QD synthesis to experiment be adhered to as follows. First, the QDs should be stored in their raw, unpurified solution whenever possible. Since the QDs are synthesized in an excess of stabilizing ligands, storing them in this solution helps prevent surface ligand loss and subsequent aggregation overtime. When a sample needs prepared for experimental study, an aliquot of this raw solution should be purified in the least aggressive means possible and as close to experimental data collection.

If orders of magnitude dilution is required, as is the case for most fluorescence studies, the QDs can be diluted into solutions containing excess surface ligands to combat

ligand-loss effects. Of course this will only work if the stabilizing ligands will not have any adverse effects on data collection. Once the QDs are diluted, the samples should be allowed to equilibrate (preferably on a shaker table) before use. It is advised that for the first time a new sample is prepared, one should study the dynamics of the QDs throughout this equilibration time to determine how long the samples need to equilibrate before experimental study. This process opens up the potential for a multitude of studies exploring the changes in charge trapping on the QD surface.

One final and important note learned from these experiments is the effects of the solvent environment on the surface ligand coverage of the QDs. We recommend that whenever possible pristine anhydrous hexanes be utilized as the solvent for TOPO/HDA/TOP stabilized CdSe QDs. Since TOPO is less soluble in hexanes than either toluene or chloroform, less surface ligand removal will occur. If a different solvent needs to be used we recommend toluene over chloroform as these QDs diluted in chloroform exhibited drastic dynamics changes attributed to ligand loss. Many prominent research groups conduct their experiments in chloroform which leads us to believe that surface traps play a key role in their reported QD dynamics. It should be noted that while these findings are specific to this QD-ligand systems these types of experiments (examining the changes in surface ligand coverage) should be conducted for any QD-ligand system one wishes to explore. For instance we found drastic differences in the changes in QD dynamics with the addition of excess HDA, which is also a native ligand for these QDs. With diligent sample storage and preparation, and by accounting for changes in surface ligand coverage, an understanding of how to control for changes in the trapping dynamics can be obtained.

In addition to demonstrating the importance of diligent sample preparation to prevent surface changes, this work also illustrates the vast potential for controlled surface modification of QDs. If a large amount of surface trapping is desired (either for experimental study or an application where controlled charge separation is preferred, such as for a solar cell) one could use the experimental designs described in this dissertation to increase surface traps. By selecting a solvent in which the native ligands are highly soluble or employing a harsh purification method, it is possible to open a large amount of surface sides for either modification with a non-native ligand or to leave as bare trap sites, depending on the desired application. By carefully examining the dynamics of the QDs with various surface modifications, valuable insights into the best means for charge trapping in the QDs themselves could be determined.

An extensive study was conducted on the effects of TOPO on CdSe QD lifetimes, which allowed us to fully model this system. We found equilibrium constants for QD-TOPO binding that were much smaller than those for other QD-ligand binding systems described in the literature. This realization led us to conclude that TOPO in fact is relatively weakly coordinated to the QD surface and as such the surface coverage and resulting fluorescence of the QDs can be drastically altered.

One of the major developments of this modeling was that we developed a new way to describe the surface ligand coverage on a QD. Instead of previous models which utilized a Langmuir model as a starting point, we developed an equilibrium series from a QD with no ligands bound up to a QD with complete ligand coverage. This type of formulation more accurately describes the distribution of QDs in solution with various numbers of ligands bound. Additionally, our model utilized QD fluorescence lifetimes as

opposed to simply observing changes in the QD PL which provided a more complete understanding of how the bound ligands affected the QD dynamics.

Interestingly, this model illustrated that surface trapping alone could not fully describe the observed QD dynamics changes. We found that a 3-state model (exciton, ground, surface trap) was insufficient and instead utilized a 4-state model which incorporated a TOPO σ* state. This model demonstrates the inherent complexity in QD trapping dynamics. The model developed will serve as the groundwork for additional QD-native ligand studies as well as novel ligand systems currently being explored further by our research group.

Such findings may even call into question the typical synthetic methods employed for these particles. The majority of synthetic methods currently employed for QDs require the use of multiple stabilizing ligands. Having various ligands present on the surface of the QDs could lead to potential issues upon experimental sample preparation. Since different ligand will have its own effects on QD dynamics, as well as varying degrees of solubility in different solvents, each additional type of ligand adds another layer of complexity to being able to understand all of the potential decay pathways present in a QD. Therefore it may prove to be prudent to develop new synthetic methods which employ only one native stabilizing ligand for QDs, so that once a full complement of experiments has been conducted, one can develop a model (such as we have for CdSe QDs-TOPO) that will fully explain what role the ligands themselves are playing in the observed QD dynamics. Simplifying the surface composition of the QDs such that a complete dynamic model of possible decay pathways can be obtained would be a vital step forward in improving the potential for QD applications.

Armed with this knowledge about QD-ligand equilibration, we then returned to study the effects of Pd NPs in solution on CdSe QD fluorescence dynamics. We observed that at high Pd concentrations (relating to shorter QD-Pd NP distances) a significant quenching mechanism dominates the QD dynamics. Through a series of solvent studies we attributed this quenching to FRET. With low Pd concentrations however we observed a slight enhancement in both the steady-state PL and fluorescence lifetimes of the QDs. Single particle studies of the QD-Pd NP interaction confirmed these findings and additionally showed blinking suppression of the QDs. We attributed these enhancement effects to an increased absorption due to the Pd NPs, similar to that witnessed in off-resonance Au NP-QD systems.

The enhancement of QD fluorescence in the presence of Pd NPs was completely unexpected. Since Pd has no visible plasmon mode we expected that only quenching would be observed. Therefore this work demonstrates that the currently accepted plasmon induced enhancement mechanism may not tell the whole story for QD-metal NP systems, even when those metals have visible plasmon modes (such as the case for Au and Ag). Therefore some of the work previously conducted with these experiments perhaps warrants a second look to fully understand this complex interaction. The ramifications of these experimental results could have far-reaching consequences for the many researchers studying precisely how to manipulate QD dynamics with metal nanoparticles and surfaces.

A variety of future projects (in addition to those already mentioned) could be developed based off of any of the three proposed applications for Pt and Pd NPs presented in this dissertation. Since catalysis and photocatalysis are extremely important

fields, one could envision a multitude of systems utilizing the basic science developed through these studies, especially in the fields of alternative energy and environmental remediation. The QD-ligand studies are also important as the surface dynamics of QDs are not yet fully understood, and any future development will require precise knowledge and control over all possible electronic pathways in the particles.

One final point about the research presented in this dissertation is that it presents an all-encompassing approach to nanoscience research which was found to have distinct benefits. Rather than focusing solely on particle synthesis or characterization or application, we instead completely developed our Pt and Pd NPs throughout the entire process. This allowed for the formulation of a more complete picture of the possibilities and challenges of utilizing these particles for our proposed applications. Being involved in the synthesis and characterization of the particles allowed us to understand the limitations of what particles could and could not be produced. Likewise, being focused on examining the properties of the NPs for a variety of applications gave a direct rationale for the development of the particles themselves. This development of a symbiotic relationship between particle production and application prevented us from becoming too locked into one aspect of the research, while not accounting for the second half of the research picture. Such an approach is a little-used, but extremely valuable way to tackle the fundamental problems and discover the future potential for these, and other new materials.

REFERENCES

1. Albrecht, M.; van Koten, G., Platinum group organometallics based on "Pincer" complexes: Sensors, switches, and catalysts. *Angew. Chem.-Int. Edit.* **2001,** *40* (20), 3750-3781.

2. Behar, D.; Rabani, J., Kinetics of hydrogen production upon reduction of aqueous TiO2 nanoparticles catalyzed by Pd-0, Pt-0, or Au-0 coatings and an unusual hydrogen abstraction; Steady state and pulse radiolysis study. *Journal of Physical Chemistry B* **2006,** *110* (17), 8750-8755.

3. Bell, A. T., The impact of nanoscience on heterogeneous catalysis. *Science* **2003,** *299* (5613), 1688-1691.

4. Besenbacher, F.; Chorkendorff, I.; Clausen, B. S.; Hammer, B.; Molenbroek, A. M.; Norskov, J. K.; Stensgaard, I., Design of a surface alloy catalyst for steam reforming. *Science* **1998,** *279* (5358), 1913-1915.

5. Duckett, S. B.; Newell, C. L.; Eisenberg, R., OBSERVATION OF NEW INTERMEDIATES IN HYDROGENATION CATALYZED BY WILKINSONS CATALYST, RHCL(PPH(3))(3), USING PARAHYDROGEN-INDUCED POLARIZATION. *Journal of the American Chemical Society* **1994,** *116* (23), 10548-10556.

6. Fu, Q.; Saltsburg, H.; Flytzani-Stephanopoulos, M., Active nonmetallic Au and Pt species on ceria-based water-gas shift catalysts. *Science* **2003,** *301* (5635), 935-938.

7. Ganesan, M.; Freemantle, R. G.; Obare, S. O., Monodisperse thioether-stabilized palladium nanoparticles: Synthesis, characterization, and reactivity. *Chemistry of Materials* **2007,** *19* (14), 3464-3471.

8. Gasteiger, H. A.; Kocha, S. S.; Sompalli, B.; Wagner, F. T., Activity benchmarks and requirements for Pt, Pt-alloy, and non-Pt oxygen reduction catalysts for PEMFCs. *Applied Catalysis B-Environmental* **2005,** *56* (1-2), 9-35.

9. Hayashi, T.; Konishi, M.; Kobori, Y.; Kumada, M.; Higuchi, T.; Hirotsu, K., DICHLORO 1,1'-BIS(DIPHENYLPHOSPHINO)FERROCENE PALLADIUM-(II) - AN EFFECTIVE CATALYST FOR CROSS-COUPLING OF SECONDARY AND PRIMARY ALKYL GRIGNARD AND ALKYLZINC REAGENTS WITH ORGANIC HALIDES. *Journal of the American Chemical Society* **1984,** *106* (1), 158-163.

10. Littke, A. F.; Dai, C. Y.; Fu, G. C., Versatile catalysts for the Suzuki cross-coupling of arylboronic acids with aryl and vinyl halides and triflates under mild conditions. *Journal of the American Chemical Society* **2000,** *122* (17), 4020-4028.

11. Muci, A. R.; Buchwald, S. L., Practical palladium catalysts for C-N and C-O bond formation. *Cross-Coupling Reactions* **2002,** *219*, 131-209.

12. Old, D. W.; Wolfe, J. P.; Buchwald, S. L., A highly active catalyst for palladium-catalyzed cross-coupling reactions: Room-temperature Suzuki couplings and amination of unactivated aryl chlorides. *Journal of the American Chemical Society* **1998,** *120* (37), 9722-9723.

13. Periana, R. A.; Taube, D. J.; Gamble, S.; Taube, H.; Satoh, T.; Fujii, H., Platinum catalysts for the high-yield oxidation of methane to a methanol derivative. *Science* **1998,** *280* (5363), 560-564.

14. Silvestre-Albero, J.; Rupprechter, G.; Freund, H.-J., From Pd nanoparticles to single crystals: 1,3-butadiene hydrogenation on well-defined model catalysts. *Chem. Commun.* **2006,** (1), 80-82.

15. Wolfe, J. P.; Singer, R. A.; Yang, B. H.; Buchwald, S. L., Highly active palladium catalysts for Suzuki coupling reactions. *Journal of the American Chemical Society* **1999,** *121* (41), 9550-9561.

16. Freestone, I.; Meeks, N.; Sax, M.; Higgitt, C., The Lycurgus Cup - A Roman nanotechnology. *Gold Bulletin* **2007,** *40* (4), 270-277.

17. Scott, G. D., A STUDY OF THE LYCURGUS-CUP. *Journal of Glass Studies* **1995,** *37*, 51-64.

18. Colomban, P., The Use of Metal Nanoparticles to Produce Yellow, Red and Iridescent Colour, from Bronze Age to Present Times in Lustre Pottery and Glass: Solid State Chemistry, Spectroscopy and Nanostructure. *Journal of Nano Research* **2009,** *8*, 109-132.

19. Schalm, O.; Van der Linden, V.; Frederickx, P.; Luyten, S.; Van der Snickt, G.; Caen, J.; Schryvers, D.; Janssens, K.; Cornelis, E.; Van Dyck, D.; Schreiner, M., Enamels in stained glass windows: Preparation, chemical composition, microstructure and causes of deterioration. *Spectrochimica Acta Part B-Atomic Spectroscopy* **2009,** *64* (8), 812-820.

20. Haynes, C. L.; McFarland, A. D.; Zhao, L. L.; Van Duyne, R. P.; Schatz, G. C.; Gunnarsson, L.; Prikulis, J.; Kasemo, B.; Kall, M., Nanoparticle optics: The importance of radiative dipole coupling in two-dimensional nanoparticle arrays. *Journal of Physical Chemistry B* **2003,** *107* (30), 7337-7342.

21. Haynes, C. L.; Van Duyne, R. P., Nanosphere lithography: A versatile nanofabrication tool for studies of size-dependent nanoparticle optics. *Journal of Physical Chemistry B* **2001,** *105* (24), 5599-5611.

22. Zou, S. L.; Schatz, G. C., Silver nanoparticle array structures that produce giant enhancements in electromagnetic fields. *Chemical Physics Letters* **2005,** *403* (1-3), 62-67.

23. Bonnemann, H.; Richards, R. M., Nanoscopic metal particles - Synthetic methods and potential applications. *European Journal of Inorganic Chemistry* **2001,** (10), 2455-2480.

24. Shipway, A. N.; Katz, E.; Willner, I., Nanoparticle arrays on surfaces for electronic, optical, and sensor applications. *Chemphyschem* **2000,** *1* (1), 18-52.

25. Tang, Z. Y.; Kotov, N. A., One-dimensional assemblies of nanoparticles: Preparation, properties, and promise. *Adv. Mater.* **2005,** *17* (8), 951-962.

26. Guo, S. J.; Dong, S. J., Biomolecule-nanoparticle hybrids for electrochemical biosensors. *Trac-Trends in Analytical Chemistry* **2009,** *28* (1), 96-109.

27. Murphy, C. J.; Gole, A. M.; Stone, J. W.; Sisco, P. N.; Alkilany, A. M.; Goldsmith, E. C.; Baxter, S. C., Gold Nanoparticles in Biology: Beyond Toxicity to Cellular Imaging. *Accounts of Chemical Research* **2008,** *41* (12), 1721-1730.

28. Santra, S.; Xu, J. S.; Wang, K. M.; Tan, W. H., Luminescent nanoparticle probes for bioimaging. *Journal of Nanoscience and Nanotechnology* **2004,** *4* (6), 590-599.

29. Turkevich, J. S., PC; Hillier J, A study of the nucleation and growth processes in the synthesis of colloidal gold. *Discussions of the Faraday Society* **1951,** *11*, 55-75.

30. Tao, A. R.; Habas, S.; Yang, P. D., Shape control of colloidal metal nanocrystals. *Small* **2008,** *4* (3), 310-325.

31. Carl, H.; Michael, Z.; Bengt, K., Enhanced charge carrier generation in dye sensitized solar cells by nanoparticle plasmons. *Applied Physics Letters* **2008,** *92* (1), 013113.

32. Carsten, R.; Falk, L., Photon management by metallic nanodiscs in thin film solar cells. *Applied Physics Letters* **2009,** *94* (21), 213102.

33. Catchpole, K. R.; Polman, A., Design principles for particle plasmon enhanced solar cells. *Applied Physics Letters* **2008,** *93* (19), 191113.

34. Chen, X. H.; Zhao, C. C.; Rothberg, L.; Ng, M. K., Plasmon enhancement of bulk heterojunction organic photovoltaic devices by electrode modification. *Applied Physics Letters* **2008,** *93* (12).

35. Kim, S. S.; Na, S. I.; Jo, J.; Kim, D. Y.; Nah, Y. C., Plasmon enhanced performance of organic solar cells using electrodeposited Ag nanoparticles. *Applied Physics Letters* **2008,** *93* (7).

36. Konda, R. B.; Mundle, R.; Mustafa, H.; Bamiduro, O.; Pradhana, A. K.; Roy, U. N.; Cui, Y.; Burger, A., Surface plasmon excitation via Au nanoparticles in n-CdSe/p-Si heterojunction diodes. *Applied Physics Letters* **2007,** *91*.

37. Lee, J. S.; Shevchenko, E. V.; Talapin, D. V., Au-PbS core-shell nanocrystals: Plasmonic absorption enhancement and electrical doping via intra-particle charge transfer. *Journal of the American Chemical Society* **2008,** *130* (30), 9673-+.

38. Major, K. J.; De, C.; Obare, S. O., Recent Advances in the Synthesis of Plasmonic Bimetallic Nanoparticles. *Plasmonics* **2009,** *4* (1), 61-78.

39. Derkacs, D.; Lim, S. H.; Matheu, P.; Mar, W.; Yu, E. T., Improved performance of amorphous silicon solar cells via scattering from surface plasmon polaritons in nearby metallic nanoparticles. *Applied Physics Letters* **2006,** *89* (9).

40. Derkacs, D.; Chen, W. V.; Matheu, P. M.; Lim, S. H.; Yu, P. K. L.; Yu, E. T., Nanoparticle-induced light scattering for improved performance of quantum-well solar cells. *Applied Physics Letters* **2008,** *93* (9).

41. Chang, Y. C.; Chou, F. Y.; Yeh, P. H.; Chen, H. W.; Chang, S. H.; Lan, Y. C.; Guo, T. F.; Tsai, T. C.; Lee, C. T., Effects of surface plasmon resonant scattering on the power conversion efficiency of organic thin-film solar cells. *Journal of Vacuum Science & Technology B* **2007,** *25* (6), 1899-1902.

42. Ahmadi, T. S.; Wang, Z. L.; Green, T. C.; Henglein, A.; ElSayed, M. A., Shape-controlled synthesis of colloidal platinum nanoparticles. *Science* **1996,** *272* (5270), 1924-1926.

43. Herrmann, W. A., N-heterocyclic carbenes: A new concept in organometallic catalysis. *Angew. Chem.-Int. Edit.* **2002,** *41* (8), 1290-1309.

44. Huber, G. W.; Iborra, S.; Corma, A., Synthesis of transportation fuels from biomass: Chemistry, catalysts, and engineering. *Chemical Reviews* **2006,** *106* (9), 4044-4098.

45. Johnson, L. K.; Mecking, S.; Brookhart, M., Copolymerization of ethylene and propylene with functionalized vinyl monomers by palladium(II) catalysts. *Journal of the American Chemical Society* **1996,** *118* (1), 267-268.

46. Kotha, S.; Lahiri, K.; Kashinath, D., Recent applications of the Suzuki-Miyaura cross-coupling reaction in organic synthesis. *Tetrahedron* **2002,** *58* (48), 9633-9695.

47. Mallat, T.; Baiker, A., Oxidation of alcohols with molecular oxygen on solid catalysts. *Chemical Reviews* **2004,** *104* (6), 3037-3058.

48. Roucoux, A.; Schulz, J.; Patin, H., Reduced transition metal colloids: A novel family of reusable catalysts? *Chemical Reviews* **2002,** *102* (10), 3757-3778.

49. Wasmus, S.; Kuver, A., Methanol oxidation and direct methanol fuel cells: a selective review. *J. Electroanal. Chem.* **1999,** *461* (1-2), 14-31.

50. Yang, B. H.; Buchwald, S. L., Palladium-catalyzed amination of aryl halides and sulfonates. *Journal of Organometallic Chemistry* **1999,** *576* (1-2), 125-146.

51. Suzuki, A., Organoboron Compounds in New Synthetic Reactions. *Pure and Applied Chemistry* **1985,** *57* (12), 1749-1758.

52. Fujishima, A.; Honda, K., Electrochemical Photolysis of Water at a Semiconductor Electrode. *Nature* **1972,** *238* (5358), 37-+.

53. Guo, S. J.; Wang, E. K., Synthesis and electrochemical applications of gold nanoparticles. *Anal. Chim. Acta* **2007,** *598* (2), 181-192.

54. Murray, C. B.; Kagan, C. R.; Bawendi, M. G., Synthesis and characterization of monodisperse nanocrystals and close-packed nanocrystal assemblies. *Annu. Rev. Mater. Sci.* **2000,** *30*, 545-610.

55. Ofir, Y.; Samanta, B.; Rotello, V. M., Polymer and biopolymer mediated self-assembly of gold nanoparticles. *Chem. Soc. Rev.* **2008,** *37* (9), 1814-1823.

56. Pachon, L. D.; Rothenberg, G., Transition-metal nanoparticles: synthesis, stability and the leaching issue. *Appl. Organomet. Chem.* **2008,** *22* (6), 288-299.

57. Schmid, G., Large Clusters and Colloids - Metals in the Embryonic State. *Chemical Reviews* **1992,** *92* (8), 1709-1727.

58. Leff, D. V.; Brandt, L.; Heath, J. R., Synthesis and characterization of hydrophobic, organically-soluble gold nanocrystals functionalized with primary amines. *Langmuir* **1996,** *12* (20), 4723-4730.

59. Murthy, S.; Bigioni, T. P.; Wang, Z. L.; Khoury, J. T.; Whetten, R. L., Liquid-phase synthesis of thiol-derivatized silver nanocrystals. *Materials Letters* **1997,** *30* (4), 321-325.

60. Ding, Y.; Gao, Y.; Wang, Z. L.; Tian, N.; Zhou, Z.-Y.; Sun, S.-G., Facets and surface relaxation of tetrahexahedral platinum nanocrystals. *Applied Physics Letters* **2007,** *91* (12), 121901-3.

61. Jintian, R.; Richard , D. T., Shape-Controlled Growth of Platinum Nanoparticles13. *Small* **2007,** *3* (9), 1508-1512.

62. LaMer, V. K.; Dinegar, R. H., Theory, Production and Mechanism of Formation of Monodispersed Hydrosols. *Journal of the American Chemical Society* **1950,** *72* (11), 4847-4854.

63. Murray, C. B.; Norris, D. J.; Bawendi, M. G., Synthesis and Characterization of Nearly Monodisperse Cde (E = S, Se, Te) Semiconductor Nanocrystallites. *Journal of the American Chemical Society* **1993,** *115* (19), 8706-8715.

64. Song, Q.; Zhang, Z. J., Shape Control and Associated Magnetic Properties of Spinel Cobalt Ferrite Nanocrystals. *Journal of the American Chemical Society* **2004,** *126* (19), 6164-6168.

65. Bagaria, H. G.; Johnson, D. T.; Srivastava, C.; Thompson, G. B.; Shamsuzzoha, M.; Nikles, D. E., Formation of FePt nanoparticles by organometallic synthesis. *Journal of Applied Physics* **2007,** *101* (10), 104313-5.

66. Chen, S. W., Chemical manipulations of nanoscale electron transfers. *J. Electroanal. Chem.* **2004,** *574* (1), 153-165.

67. Chen, S. W.; Ingram, R. S.; Hostetler, M. J.; Pietron, J. J.; Murray, R. W.; Schaaff, T. G.; Khoury, J. T.; Alvarez, M. M.; Whetten, R. L., Gold nanoelectrodes of varied size: Transition to molecule-like charging. *Science* **1998,** *280* (5372), 2098-2101.

68. Murray, R. W., Nanoelectrochemistry: Metal nanoparticles, nanoelectrodes, and nanopores. *Chemical Reviews* **2008,** *108* (7), 2688-2720.

69. Weaver, M. J.; Gao, X. P., Molecular Capacitance - Sequential Electron-Transfer Energetics for Solution-Phase Metallic Clusters in Relation to Gas-Phase Clusters and Analogous Interfaces. *J. Phys. Chem.* **1993,** *97* (2), 332-338.

70. Subramanian, V.; Wolf, E.; Kamat, P. V., Semiconductor-metal composite nanostructures. To what extent do metal nanoparticles improve the photocatalytic activity of TiO2 films? *Journal of Physical Chemistry B* **2001,** *105* (46), 11439-11446.

71. Dawson, A.; Kamat, P. V., Semiconductor-metal nanocomposites. Photoinduced fusion and photocatalysis of gold-capped TiO2 (TiO2/Gold) nanoparticles. *Journal of Physical Chemistry B* **2001,** *105* (5), 960-966.

72. Subramanian, V.; Wolf, E. E.; Kamat, P. V., Catalysis with TiO2/gold nanocomposites. Effect of metal particle size on the Fermi level equilibration. *Journal of the American Chemical Society* **2004,** *126* (15), 4943-4950.

73. Subramanian, V.; Wolf, E. E.; Kamat, P. V., Green emission to probe photoinduced charging events in ZnO-Au nanoparticles. Charge distribution and

fermi-level equilibration. *Journal of Physical Chemistry B* **2003,** *107* (30), 7479-7485.

74. Okazawa, T.; Fujiwara, M.; Nishimura, T.; Akita, T.; Kohyama, M.; Kido, Y., Growth mode and electronic structure of Au nano-clusters on NiO(001) and TiO2(110). *Surface Science* **2006,** *600* (6), 1331-1338.

75. Okazawa, T.; Kohyama, M.; Kido, Y., Electronic properties of Au nano-particles supported on stoichiometric and reduced TiO2 (110) substrates. *Surface Science* **2006,** *600* (19), 4430-4437.

76. Cozzoli, P. D.; Fanizza, E.; Comparelli, R.; Curri, M. L.; Agostiano, A.; Laub, D., Role of metal nanoparticles in TiO2/Ag nanocomposite-based microheterogeneous photocatalysis. *Journal of Physical Chemistry B* **2004,** *108* (28), 9623-9630.

77. Naoi, K.; Ohko, Y.; Tatsuma, T., TiO2 films loaded with silver nanoparticles: Control of multicolor photochromic behavior. *Journal of the American Chemical Society* **2004,** *126* (11), 3664-3668.

78. Yu, J. G.; Xiong, J. F.; Cheng, B.; Liu, S. W., Fabrication and characterization of Ag-TiO2 multiphase nanocomposite thin films with enhanced photocatalytic activity. *Applied Catalysis B-Environmental* **2005,** *60* (3-4), 211-221.

79. Zhang, L. Z.; Yu, J. C.; Yip, H. Y.; Li, Q.; Kwong, K. W.; Xu, A. W.; Wong, P. K., Ambient light reduction strategy to synthesize silver nanoparticles and silver-coated TiO2 with enhanced photocatalytic and bactericidal activities. *Langmuir* **2003,** *19* (24), 10372-10380.

80. Yao, Y.; Ohko, Y.; Sekiguchi, Y.; Fujishima, A.; Kubota, Y., Self-sterilization using silicone catheters coated with Ag and TiO2 nanocomposite thin film. *J. Biomed. Mater. Res. Part B* **2008,** *85B* (2), 453-460.

81. Zhang, H. J.; Chen, G. H., Potent Antibacterial Activities of Ag/TiO2 Nanocomposite Powders Synthesized by a One-Pot Sol-Gel Method. *Environ. Sci. Technol.* **2009,** *43* (8), 2905-2910.

82. Hirakawa, T.; Kamat, P. V., Charge separation and catalytic activity of Ag@TiO2 core-shell composite clusters under UV-irradiation. *Journal of the American Chemical Society* **2005,** *127* (11), 3928-3934.

83. Wood, A.; Giersig, M.; Mulvaney, P., Fermi level equilibration in quantum dot-metal nanojunctions. *Journal of Physical Chemistry B* **2001,** *105* (37), 8810-8815.

84. Bamwenda, G. R.; Tsubota, S.; Nakamura, T.; Haruta, M., Photoassisted Hydrogen-Production from a Water-Ethanol Solution - a Comparison of

Activities of Au-Tio2 and Pt-Tio2. *Journal of Photochemistry and Photobiology a-Chemistry* **1995,** *89* (2), 177-189.

85. Kitano, M.; Takeuchi, M.; Matsuoka, M.; Thomas, J. A.; Anpo, M., Photocatalytic water splitting using Pt-loaded visible light-responsive TiO2 thin film photocatalysts. *Catal. Today* **2007,** *120* (2), 133-138.

86. Chen, T.; Feng, Z. H.; Wu, G. P.; Shi, J. Y.; Ma, G. J.; Ying, P. L.; Li, C., Mechanistic studies of photocatalytic reaction of methanol for hydrogen production on Pt/TiO2 by in situ Fourier transform IR and time-resolved IR spectroscopy. *Journal of Physical Chemistry C* **2007,** *111*, 8005-8014.

87. Gratzel, M.; Moser, J., Multielectron Storage and Hydrogen Generation with Colloidal Semiconductors. *Proceedings of the National Academy of Sciences of the United States of America-Physical Sciences* **1983,** *80* (10), 3129-3132.

88. Abe, R.; Sayama, K.; Arakawa, H., Significant effect of iodide addition on water splitting into H-2 and O-2 over Pt-loaded TiO2 photocatalyst: suppression of backward reaction. *Chemical Physics Letters* **2003,** *371* (3-4), 360-364.

89. Galinska, A.; Walendziewski, J., Photocatalytic water splitting over Pt-TiO2 in the presence of sacrificial reagents. *Energy Fuels* **2005,** *19* (3), 1143-1147.

90. Malinka, E. A.; Kamalov, G. L.; Vodzinskii, S. V.; Melnik, V. I.; Zhilina, Z. I., Hydrogen-Production from Water by Visible-Light Using Zinc Porphyrin-Sensitized Platinized Titanium-Dioxide. *Journal of Photochemistry and Photobiology a-Chemistry* **1995,** *90* (2-3), 153-158.

91. Petkovic, L. M.; Ginosar, D. M.; Rollins, H. W.; Burch, K. C.; Pinhero, P. J.; Farrell, H. H., Pt/TiO2 (rutile) catalysts for sulfuric acid decomposition in sulfur-based thermochemical water-splitting cycles. *Applied Catalysis a-General* **2008,** *338* (1-2), 27-36.

92. Yin, R. H.; Ji, X. B.; Zhang, L.; Lu, S. Y.; Cao, W. G.; Fan, Q. B., Multilayer nano Ti/TiO2-Pt electrode for coal-hydrogen production. *Journal of the Electrochemical Society* **2007,** *154* (12), D637-D641.

93. Bae, E. Y.; Choi, W. Y.; Park, J. W.; Shin, H. S.; Kim, S. B.; Lee, J. S., Effects of surface anchoring groups (Carboxylate vs phosphonate) in ruthenium-complex-sensitized TiO2 on visible light reactivity in aqueous suspensions. *Journal of Physical Chemistry B* **2004,** *108* (37), 14093-14101.

94. Patsoura, A.; Kondarides, D. I.; Verykios, X. E., Enhancement of photoinduced hydrogen production from irradiated Pt/TiO2 suspensions with simultaneous degradation of azo-dyes. *Applied Catalysis B-Environmental* **2006,** *64* (3-4), 171-179.

95. Lakshminarasimhan, N.; Bae, E.; Choi, W., Enhanced photocatalytic production of H-2 on mesoporous TiO2 prepared by template-free method: Role of interparticle charge transfer. *Journal of Physical Chemistry C* **2007,** *111* (42), 15244-15250.

96. Park, H.; Choi, W.; Hoffmann, M. R., Effects of the preparation method of the ternary CdS/TiO2/Pt hybrid photocatalysts on visible light-induced hydrogen production. *Journal of Materials Chemistry* **2008,** *18* (20), 2379-2385.

97. Smotkin, E.; Bard, A. J.; Campion, A.; Fox, M. A.; Mallouk, T.; Webber, S. E.; White, J. M., Bipolar Tio2/Pt Semiconductor Photoelectrodes and Multielectrode Arrays for Unassisted Photolytic Water Splitting. *J. Phys. Chem.* **1986,** *90* (19), 4604-4607.

98. Yamakata, A.; Ishibashi, T.; Onishi, H., Pressure dependence of electron- and hole-consuming reactions in photocatalytic water splitting on Pt/TiO2 studied by time-resolved IR absorption spectroscopy. *International Journal of Photoenergy* **2003,** *5* (1), 7-9.

99. Yamakata, A.; Ishibashi, T.-a.; Onishi, H., Kinetics of the photocatalytic water-splitting reaction on TiO2 and Pt/TiO2 studied by time-resolved infrared absorption spectroscopy. *Journal of Molecular Catalysis A: Chemical* **2003,** *199* (1-2), 85-94.

100. Yang, H. H.; Guo, L. J.; Yan, W.; Liu, H. T., A novel composite photocatalyst for water splitting hydrogen production. *Journal of Power Sources* **2006,** *159* (2), 1305-1309.

101. Zou, J.-J.; Chen, C.; Liu, C.-J.; Zhang, Y.-P.; Han, Y.; Cui, L., Pt nanoparticles on TiO2 with novel metal-semiconductor interface as highly efficient photocatalyst. *Materials Letters* **2005,** *59* (27), 3437-3440.

102. Du, P.; Schneider, J.; Fan, L.; Zhao, W.; Patel, U.; Castellano, F. N.; Eisenberg, R., Bi- and terpyridyl platinum(II) chloro complexes: Molecular catalysts for the photogeneration of hydrogen from water or simply precursors for colloidal platinum? *Journal of the American Chemical Society* **2008,** *130* (15), 5056-+.

103. Teoh, W. Y.; Madler, L.; Beydoun, D.; Pratsinis, S. E.; Amal, R., Direct (one-step) synthesis of TiO2 and Pt/TiO2 nanoparticles for photocatalytic mineralisation of sucrose. *Chem. Eng. Sci.* **2005,** *60* (21), 5852-5861.

104. Iliev, V.; Tomova, D.; Bilyarska, L.; Eliyas, A.; Petrov, L., Photocatalytic properties of TiO2 modified with platinum and silver nanoparticles in the degradation of oxalic acid in aqueous solution. *Applied Catalysis B-Environmental* **2006,** *63* (3-4), 266-271.

105. Iliev, V.; Tomova, D.; Bilyarska, L.; Petrov, L., Photooxidation of xylenol orange in the presence of palladium-modified TiO2 catalysts. *Catal. Commun.* **2004,** *5* (12), 759-763.

106. Wang, X. C.; Yu, J. C.; Yip, H. Y.; Wu, L.; Wong, P. K.; Lai, S. Y., A mesoporous Pt/TiO2 nanoarchitecture with catalytic and photocatalytic functions. *Chem.-Eur. J.* **2005,** *11* (10), 2997-3004.

107. Heimer, T. A.; Darcangelis, S. T.; Farzad, F.; Stipkala, J. M.; Meyer, G. J., An acetylacetonate-based semiconductor-sensitizer linkage. *Inorganic Chemistry* **1996,** *35* (18), 5319-5324.

108. Burda, C.; Chen, X. B.; Narayanan, R.; El-Sayed, M. A., Chemistry and properties of nanocrystals of different shapes. *Chemical Reviews* **2005,** *105* (4), 1025-1102.

109. Talapin, D. V.; Lee, J. S.; Kovalenko, M. V.; Shevchenko, E. V., Prospects of Colloidal Nanocrystals for Electronic and Optoelectronic Applications. *Chemical Reviews* **2010,** *110* (1), 389-458.

110. Gratzel, M., Solar energy conversion by dye-sensitized photovoltaic cells. *Inorganic Chemistry* **2005,** *44* (20), 6841-6851.

111. Harman, T. C.; Taylor, P. J.; Walsh, M. P.; LaForge, B. E., Quantum dot superlattice thermoelectric materials and devices. *Science* **2002,** *297* (5590), 2229-2232.

112. Reithmaier, J. P.; Sek, G.; Loffler, A.; Hofmann, C.; Kuhn, S.; Reitzenstein, S.; Keldysh, L. V.; Kulakovskii, V. D.; Reinecke, T. L.; Forchel, A., Strong coupling in a single quantum dot-semiconductor microcavity system. *Nature* **2004,** *432* (7014), 197-200.

113. Chan, W. C. W.; Maxwell, D. J.; Gao, X. H.; Bailey, R. E.; Han, M. Y.; Nie, S. M., Luminescent quantum dots for multiplexed biological detection and imaging. *Current Opinion in Biotechnology* **2002,** *13* (1), 40-46.

114. Jaiswal, J. K.; Mattoussi, H.; Mauro, J. M.; Simon, S. M., Long-term multiple color imaging of live cells using quantum dot bioconjugates. *Nature Biotechnology* **2003,** *21* (1), 47-51.

115. Medintz, I. L.; Uyeda, H. T.; Goldman, E. R.; Mattoussi, H., Quantum dot bioconjugates for imaging, labelling and sensing. *Nature Materials* **2005,** *4* (6), 435-446.

116. Michalet, X.; Pinaud, F. F.; Bentolila, L. A.; Tsay, J. M.; Doose, S.; Li, J. J.; Sundaresan, G.; Wu, A. M.; Gambhir, S. S.; Weiss, S., Quantum dots for live cells, in vivo imaging, and diagnostics. *Science* **2005,** *307* (5709), 538-544.

117. Pavesi, L.; Dal Negro, L.; Mazzoleni, C.; Franzo, G.; Priolo, F., Optical gain in silicon nanocrystals. *Nature* **2000,** *408* (6811), 440-444.

118. Dabbousi, B. O.; RodriguezViejo, J.; Mikulec, F. V.; Heine, J. R.; Mattoussi, H.; Ober, R.; Jensen, K. F.; Bawendi, M. G., (CdSe)ZnS core-shell quantum dots: Synthesis and characterization of a size series of highly luminescent nanocrystallites. *Journal of Physical Chemistry B* **1997,** *101* (46), 9463-9475.

119. Peng, X. G.; Manna, L.; Yang, W. D.; Wickham, J.; Scher, E.; Kadavanich, A.; Alivisatos, A. P., Shape control of CdSe nanocrystals. *Nature* **2000,** *404* (6773), 59-61.

120. Peng, X. G.; Schlamp, M. C.; Kadavanich, A. V.; Alivisatos, A. P., Epitaxial growth of highly luminescent CdSe/CdS core/shell nanocrystals with photostability and electronic accessibility. *Journal of the American Chemical Society* **1997,** *119* (30), 7019-7029.

121. Clapp, A. R.; Goldman, E. R.; Mattoussi, H., Capping of CdSe-ZnS quantum dots with DHLA and subsequent conjugation with proteins. *Nature Protocols* **2006,** *1* (3), 1258-1266.

122. Battaglia, D.; Li, J. J.; Wang, Y. J.; Peng, X. G., Colloidal two-dimensional systems: CdSe quantum shells and wells. *Angew. Chem.-Int. Edit.* **2003,** *42* (41), 5035-5039.

123. Schill, A. W.; Gaddis, C. S.; Qian, W.; El-Sayed, M. A.; Cai, Y.; Milam, V. T.; Sandhage, K., Ultrafast electronic relaxation and charge-carrier localization in CdS/CdSe/CdS quantum-dot quantum-well heterostructures. *Nano Lett.* **2006,** *6* (9), 1940-1949.

124. Guyot-Sionnest, P.; Wehrenberg, B.; Yu, D., Intraband relaxation in CdSe nanocrystals and the strong influence of the surface ligands. *J. Chem. Phys.* **2005,** *123* (7).

125. Hammer, N. I.; Early, K. T.; Sill, K.; Odoi, M. Y.; Emrick, T.; Barnes, M. D., Coverage-mediated suppression of blinking in solid state quantum dot conjugated organic composite nanostructures. *Journal of Physical Chemistry B* **2006,** *110* (29), 14167-14171.

126. Kalyuzhny, G.; Murray, R. W., Ligand effects on optical properties of CdSe nanocrystals. *Journal of Physical Chemistry B* **2005,** *109* (15), 7012-7021.

127. Majetich, S. A.; Carter, A. C., SURFACE EFFECTS ON THE OPTICAL-PROPERTIES OF CADMIUM SELENIDE QUANTUM DOTS. *J. Phys. Chem.* **1993,** *97* (34), 8727-8731.

128. Pandey, A.; Guyot-Sionnest, P., Slow Electron Cooling in Colloidal Quantum Dots. *Science* **2008,** *322* (5903), 929-932.

129. Baker, D. R.; Kamat, P. V., Tuning the Emission of CdSe Quantum Dots by Controlled Trap Enhancement. *Langmuir* **2010,** *26* (13), 11272-11276.

130. Boldt, K.; Jander, S.; Hoppe, K.; Weller, H., Characterization of the Organic Ligand Shell of Semiconductor Quantum Dots by Fluorescence Quenching Experiments. *ACS Nano* **2011,** *5* (10), 8115-8123.

131. Dorokhin, D.; Tomczak, N.; Velders, A. H.; Reinhoudt, D. N.; Vancso, G. J., Photoluminescence Quenching of CdSe/ZnS Quantum Dots by Molecular Ferrocene and Ferrocenyl Thiol Ligands. *Journal of Physical Chemistry C* **2009,** *113* (43), 18676-18680.

132. Greenham, N. C.; Peng, X. G.; Alivisatos, A. P., Charge separation and transport in conjugated-polymer/semiconductor-nanocrystal composites studied by photoluminescence quenching and photoconductivity. *Physical Review B* **1996,** *54* (24), 17628-17637.

133. Koole, R.; Schapotschnikow, P.; Donega, C. D.; Vlugt, T. J. H.; Meijerink, A., Time-dependent photoluminescence spectroscopy as a tool to measure the ligand exchange kinetics on a quantum dot surface. *ACS Nano* **2008,** *2* (8), 1703-1714.

134. Landes, C. F.; Braun, M.; El-Sayed, M. A., On the nanoparticle to molecular size transition: Fluorescence quenching studies. *Journal of Physical Chemistry B* **2001,** *105* (43), 10554-10558.

135. Liu, I. S.; Lo, H. H.; Chien, C. T.; Lin, Y. Y.; Chen, C. W.; Chen, Y. F.; Su, W. F.; Liou, S. C., Enhancing photoluminescence quenching and photoelectric properties of CdSe quantum dots with hole accepting ligands. *Journal of Materials Chemistry* **2008,** *18* (6), 675-682.

136. Morris-Cohen, A. J.; Frederick, M. T.; Cass, L. C.; Weiss, E. A., Simultaneous Determination of the Adsorption Constant and the Photoinduced Electron Transfer Rate for a Cds Quantum Dot-Viologen Complex. *Journal of the American Chemical Society* **2011,** *133* (26), 10146-10154.

137. Morris-Cohen, A. J.; Vasilenko, V.; Amin, V. A.; Reuter, M. G.; Weiss, E. A., Model for Adsorption of Ligands to Colloidal Quantum Dots with Concentration-Dependent Surface Structure. *ACS Nano* **2012,** *6* (1), 557-565.

138. Munro, A. M.; Jen-La Plante, I.; Ng, M. S.; Ginger, D. S., Quantitative study of the effects of surface ligand concentration on CdSe nanocrystal photoluminescence. *Journal of Physical Chemistry C* **2007,** *111* (17), 6220-6227.

139. Uematsu, T.; Waki, T.; Torimoto, T.; Kuwabata, S., Systematic Studies on Emission Quenching of Cadmium Telluride Nanoparticles. *Journal of Physical Chemistry C* **2009,** *113* (52), 21621-21628.

140. Jones, M.; Scholes, G. D., On the use of time-resolved photoluminescence as a probe of nanocrystal photoexcitation dynamics. *Journal of Materials Chemistry* **2010,** *20* (18), 3533-3538.

141. Evans, C. M.; Evans, M. E.; Krauss, T. D., Mysteries of TOPSe Revealed: Insights into Quantum Dot Nucleation. *Journal of the American Chemical Society* **2010,** *132* (32), 10973-10975.

142. Wang, F. D.; Tang, R.; Buhro, W. E., The Trouble with TOPO; Identification of Adventitious Impurities Beneficial to the Growth of Cadmium Selenide Quantum Dots, Rods, and Wires. *Nano Lett.* **2008,** *8* (10), 3521-3524.

143. Zhao, H. G.; Zhang, T.; Chaker, M.; Ma, D. L., Ligand and Precursor Effects on the Synthesis and Optical Properties of PbS Quantum Dots. *Journal of Nanoscience and Nanotechnology* **2010,** *10* (8), 4897-4905.

144. Crooker, S. A.; Barrick, T.; Hollingsworth, J. A.; Klimov, V. I., Multiple temperature regimes of radiative decay in CdSe nanocrystal quantum dots: Intrinsic limits to the dark-exciton lifetime. *Applied Physics Letters* **2003,** *82* (17), 2793-2795.

145. Langmuir, I., The constitution and fundamental properties of solids and liquids Part I Solids. *Journal of the American Chemical Society* **1916,** *38*, 2221-2295.

146. Bullen, C.; Mulvaney, P., The effects of chemisorption on the luminescence of CdSe quantum dots. *Langmuir* **2006,** *22* (7), 3007-3013.

147. Morris-Cohen, A. J.; Donakowski, M. D.; Knowles, K. E.; Weiss, E. A., The Effect of a Common Purification Procedure on the Chemical Composition of the Surfaces of CdSe Quantum Dots Synthesized with Trioctylphosphine Oxide. *Journal of Physical Chemistry C* **2010,** *114* (2), 897-906.

148. Ji, X.; Copenhaver, D.; Sichmeller, C.; Peng, X., Ligand bonding and dynamics on colloidal nanocrystals at room temperature: The case of alkylamines on CdSe nanocrystals. *Journal of the American Chemical Society* **2008,** *130* (17), 5726-5735.

149. Jones, M.; Lo, S. S.; Scholes, G. D., Signatures of Exciton Dynamics and Carrier Trapping in the Time-Resolved Photoluminescence of Colloidal CdSe Nanocrystals. *Journal of Physical Chemistry C* **2009,** *113* (43), 18632-18642.

150. Jones, M.; Lo, S. S.; Scholes, G. D., Quantitative modeling of the role of surface traps in CdSe/CdS/ZnS nanocrystal photoluminescence decay dynamics.

Proceedings of the National Academy of Sciences of the United States of America **2009,** *106* (9), 3011-3016.

151. Kamat, P. V., Quantum Dot Solar Cells. Semiconductor Nanocrystals as Light Harvesters. *Journal of Physical Chemistry C* **2008,** *112* (48), 18737-18753.

152. Klimov, V. I., Optical nonlinearities and ultrafast carrier dynamics in semiconductor nanocrystals. *Journal of Physical Chemistry B* **2000,** *104* (26), 6112-6123.

153. Klimov, V. I.; McBranch, D. W.; Leatherdale, C. A.; Bawendi, M. G., Electron and hole relaxation pathways in semiconductor quantum dots. *Physical Review B* **1999,** *60* (19), 13740-13749.

154. Leatherdale, C. A.; Kagan, C. R.; Morgan, N. Y.; Empedocles, S. A.; Kastner, M. A.; Bawendi, M. G., Photoconductivity in CdSe quantum dot solids. *Physical Review B* **2000,** *62* (4), 2669-2680.

155. Plass, R.; Pelet, S.; Krueger, J.; Gratzel, M.; Bach, U., Quantum dot sensitization of organic-inorganic hybrid solar cells. *Journal of Physical Chemistry B* **2002,** *106* (31), 7578-7580.

156. Sun, W. T.; Yu, Y.; Pan, H. Y.; Gao, X. F.; Chen, Q.; Peng, L. M., CdS quantum dots sensitized TiO2 nanotube-array photoelectrodes. *Journal of the American Chemical Society* **2008,** *130* (4), 1124-+.

157. Kumar, S.; Jones, M.; Lo, S. S.; Scholes, G. D., Nanorod heterostructures showing photoinduced charge separation. *Small* **2007,** *3* (9), 1633-1639.

158. Scholes, G. D., Controlling the optical properties of inorganic nanoparticles. *Advanced Functional Materials* **2008,** *18* (8), 1157-1172.

159. Costi, R.; Saunders, A. E.; Elmalem, E.; Salant, A.; Banin, U., Visible light-induced charge retention and photocatalysis with hybrid CdSe-Au nanodumbbells. *Nano Lett.* **2008,** *8* (2), 637-641.

160. Yang, T. T.; Chen, W. T.; Hsu, Y. J.; Wei, K. H.; Lin, T. Y.; Lin, T. W., Interfacial Charge Carrier Dynamics in Core-Shell Au-CdS Nanocrystals. *Journal of Physical Chemistry C* **2010,** *114* (26), 11414-11420.

161. Pons, T.; Medintz, I. L.; Sapsford, K. E.; Higashiya, S.; Grimes, A. F.; English, D. S.; Mattoussi, H., On the quenching of semiconductor quantum dot photoluminescence by proximal gold nanoparticles. *Nano Lett.* **2007,** *7* (10), 3157-3164.

162. Giepmans, B. N. G.; Adams, S. R.; Ellisman, M. H.; Tsien, R. Y., Review - The fluorescent toolbox for assessing protein location and function. *Science* **2006,** *312* (5771), 217-224.

163. Clapp, A. R.; Medintz, I. L.; Mauro, J. M.; Fisher, B. R.; Bawendi, M. G.; Mattoussi, H., Fluorescence resonance energy transfer between quantum dot donors and dye-labeled protein acceptors. *Journal of the American Chemical Society* **2004,** *126* (1), 301-310.

164. Goldman, E. R.; Medintz, I. L.; Whitley, J. L.; Hayhurst, A.; Clapp, A. R.; Uyeda, H. T.; Deschamps, J. R.; Lassman, M. E.; Mattoussi, H., A hybrid quantum dot-antibody fragment fluorescence resonance energy transfer-based TNT sensor. *Journal of the American Chemical Society* **2005,** *127* (18), 6744-6751.

165. Medintz, I. L.; Clapp, A. R.; Mattoussi, H.; Goldman, E. R.; Fisher, B.; Mauro, J. M., Self-assembled nanoscale biosensors based on quantum dot FRET donors. *Nature Materials* **2003,** *2* (9), 630-638.

166. Willard, D. M.; Carillo, L. L.; Jung, J.; Van Orden, A., CdSe-ZnS quantum dots as resonance energy transfer donors in a model protein-protein binding assay. *Nano Lett.* **2001,** *1* (9), 469-474.

167. Kulakovich, O.; Strekal, N.; Yaroshevich, A.; Maskevich, S.; Gaponenko, S.; Nabiev, I.; Woggon, U.; Artemyev, M., Enhanced luminescence of CdSe quantum dots on gold colloids. *Nano Lett.* **2002,** *2* (12), 1449-1452.

168. Gueroui, Z.; Libchaber, A., Single-molecule measurements of gold-quenched quantum dots. *Phys. Rev. Lett.* **2004,** *93* (16).

169. Jin, Y. D.; Gao, X. H., Plasmonic fluorescent quantum dots. *Nat. Nanotechnol.* **2009,** *4* (9), 571-576.

170. Zhang, J.; Badugu, R.; Lakowicz, J. R., Fluorescence quenching of CdTe nanocrystals by bound gold nanoparticles in aqueous solution. *Plasmonics* **2008,** *3* (1), 3-11.

171. Chen, Y. C.; Munechika, K.; Jen-La Plante, I.; Munro, A. M.; Skrabalak, S. E.; Xia, Y. N.; Ginger, D. S., Excitation enhancement of CdSe quantum dots by single metal nanoparticles. *Applied Physics Letters* **2008,** *93* (5).

172. Henson, J.; Dimakis, E.; DiMaria, J.; Li, R.; Minissale, S.; Dal Negro, L.; Moustakas, T. D.; Paiella, R., Enhanced near-green light emission from InGaN quantum wells by use of tunable plasmonic resonances in silver nanoparticle arrays. *Optics Express* **2010,** *18* (20), 21322-21329.

173. Munechika, K.; Chen, Y.; Tillack, A. F.; Kulkarni, A. P.; Plante, I. J. L.; Munro, A. M.; Ginger, D. S., Spectral Control of Plasmonic Emission Enhancement from

Quantum Dots near Single Silver Nanoprisms. *Nano Lett.* **2010,** *10* (7), 2598-2603.

174. Langhuth, H.; Frederick, S.; Kaniber, M.; Finley, J. J.; Ruhrmair, U., Strong Photoluminescence Enhancement from Colloidal Quantum Dot Near Silver Nano-Island Films. *J. Fluoresc.* **2011,** *21* (2), 539-543.

175. Fu, Y.; Zhang, J.; Lakowicz, J. R., Silver-enhanced fluorescence emission of single quantum dot nanocomposites. *Chem. Commun.* **2009,** (3), 313-315.

176. Toyoda, T.; Tsugawa, S.; Shen, Q., Photoacoustic spectra of Au quantum dots adsorbed on nanostructured TiO2 electrodes together with the photoelectrochemical current characteristics. *Journal of Applied Physics* **2009,** *105* (3).

177. Reiss, P.; Protiere, M.; Li, L., Core/Shell Semiconductor Nanocrystals. *Small* **2009,** *5* (2), 154-168.

178. Knight, T. E.; Guo, D.; Claude, J. P.; McCusker, J. K., Energy transfer dynamics in Re-I-based polynuclear assemblies: A quantitative application of Forster theory. *Inorganic Chemistry* **2008,** *47* (16), 7249-7261.

179. Ma, X. D.; Tan, H.; Kipp, T.; Mews, A., Fluorescence Enhancement, Blinking Suppression, and Gray States of Individual Semiconductor Nanocrystals Close to Gold Nanoparticles. *Nano Lett.* **2010,** *10* (10), 4166-4174.

APPENDIX A: PREPARATION OF TiO_2 NANOPARTICLE SLIDES

The preparation of TiO_2 nanoparticle slides is a two step process. First the nanoparticles are synthesized, then they are deposited on glass slides for experimental use. The nanoparticles are synthesized following a sol-gel procedure.[107]

To a 250 mL round bottom flask were added, 100 mL of de-ionized water and 0.84 mL of concentrated (67-70%) nitric acid. The flask was placed under vigorous stirring. 20 mL of titanium isopropoxide were added dropwise to this flask using a pipette. After addition of all 20 mL of titanium isopropoxide, the flask was covered as well as possible with aluminum foil to keep light out. The flask was then attached to a condenser and refluxed at 75-90 °C for approximately 5 hours. This solution was then transferred to a 250 mL Erlenmeyer flask and heated for approximately 3 hours while the temperature was increased to 90-95 °C. Heating was continued until the volume of solution reached 45 mL. If additional heat was required, the temperature was increased, however the solution was not allowed to boil.

15 mL of this solution was transferred to an acid bomb and sealed. The acid bomb was placed in a furnace and heated at 200 °C for 8 hours. After heating the acid bomb was removed and allowed to cool to room temperature. Once cool, any water remaining was poured into a vial. The remaining solution was transferred into a small (25 or 50 mL) Erlenmeyer flask and vigorously stirred until consistent. If residual water remained, the solution was gently heated to thicken the solution. 0.3 g of polyethylene glycol was added to the solution and heated at 70 °C for 20-30 minutes.

This solution was allowed to cool while glass slides were cleaned and cut to shape. Six of these glass slides were placed side by side on a clean counter top and

sandwiched by 2 larger uncut slides. Via a pipette, the solution was placed in excess on the first larger slide. Using another pipette as a roller, the solution was evenly distributed over all of the slides. If more solution was needed, it was added to one of the end slides, which were to be discarded. Using this method we were able to achieve relatively uniform coverage over the 6 experimental slides. These solutions were then tented with aluminum foil to keep out of the light and allowed to air dry until clear.

Once dry (usually after a few hours) the slides were placed in a furnace and heated to 370 °C. The slides were carefully watched during this heating. As the polymer sets, the slides go from clear to yellow to brown and then back to clear. As soon as the slides returned to clear they were removed from the furnace and cooled.

This method allowed us to produce thin, transparent layers of ~10 nm anatase TiO_2 nanoparticle films deposited on glass slides. An SEM of these films is provided in Figure A.1.

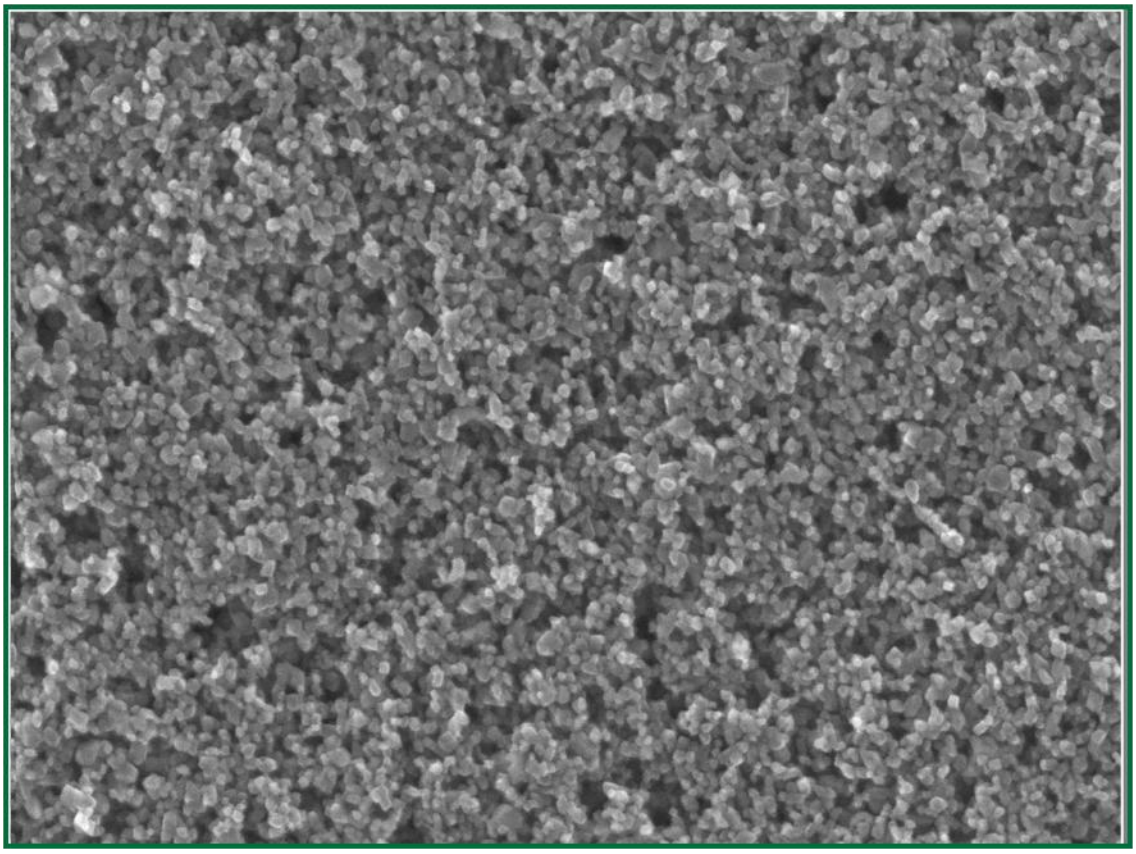

Figure A.1: SEM image of 10 nm anatase TiO_2 nanoparticles

APPENDIX B: SYNTHESIS OF CdSe QUANTUM DOTS

CdSe QDs were synthesized following an established wet-chemical procedure developed by Clapp *et. al.*[121] In a typical synthesis a 1 M stock solution of trioctylphosphine selenide (TOP:Se) was prepared by dissolving 7.9 g of Se in 100 mL of TOP. A 100 mL three-neck round bottom flask was fitted with a condenser, temperature sensor and vacuum inlet adapter. To this flask were added trioctylphosphine oxide (TOPO) (20 g), hexadecylamine (10 g) and TOP (5 mL), which was heated to 120 °C under vacuum to dissolve. The flask was then switched to nitrogen atmosphere and the temperature raised to 340 °C.

Meanwhile a precursor solution of $Cd(acac)_2$ (0.63 g), hexadecanediol (1.5 g), and TOP (10 mL) was prepared and heated to 140 °C before adding 2.5 mL of the prepared TOP:Se solution. This solution was cooled to 80 °C. Once the solvent solution reached 340 °C, the precursor solution was injected into the solvent flask. The solution was then allowed to grow from 0 to 60 minutes before rapid cooling of the flask in an ice bath depending on the desired size of the QDs. The particles were washed with methanol and centrifuged from solution before re-dispersing in clean toluene or hexanes.

APPENDIX C: ACQUIRING SIMULTANEOUS LIFETIMES ON JOBIN YVON FLUOROLOG

The Jobin Yvon Fluorolog is not specifically designed for automated collection of multiple, simultaneous lifetimes. However it is possible for the collection of consecutive lifetimes (with a few instrumentation adjustments), such that changes in fluorescence dynamics of a sample over time can be observed.

The first step is to determine the proper settings to collect a lifetime on the sample to be studied. This should be done precisely as normal. Once the emission monochromator wavelength and bandpass are set to the desired position, the metal housing containing the emission monochromator should be unscrewed and carefully opened. The monochromator (serial cable with a blue end) should be unplugged. This disables the monochromator from scanning.

Next a new TAS experiment is started. To be able to collect multiple decays, the experiment must be run for a set of wavelengths with certain increments. For instance, the samples collected in this dissertation were typically set to run from x-100 to x nm (where x is the wavelength of the QDs, where the bandpass is set to) at 2 nm intervals. This collected 50 consecutive scans. However, the amount of scans collected can be set to whatever is desired by simply either changing the scan range or the interval. It is recommended that the final scan is set to be collected with the monochromator set at the wavelength being used. This allows for the user to re-plug the emission monochromator in after data collection and having it set at the proper wavelength. If it is necessary to stop a scan before it has reached completion, it is advisable to set the emission

monochromator to the examined wavelength (where it should be residing) before plugging it back in to prevent it from becoming improperly calibrated.

No matter how the experiment is run, it is wise to re-check the calibration of the emission monochromator after running these types of experiments. To do so, the steady-state PL software should be used. The first check is to run a water raman spectra. This is explained in the Fluorolog manual. Simply run an emission spectra of de-ionized water in a cuvette. An excitation wavelength of 350 nm is used and the emission monochromator is scanned from 365 – 450 nm. The Raman emission peak should be at 397 nm. If the Raman peak is found at a different wavelength, real-time controls should be initialized and the emission monochromator should be moved to the wavelength at which the Raman peak appears. The monochromator should then be set to 397 nm. Using this process, one can get the emission monochromator relatively close to calibrated. If the monochromator was found to quite out of calibration (or for more precise calibration) a Newport Hg pencil lamp should be used for calibration in a similar fashion. Since the peaks of the pencil lamp are very sharp, a more accurate calibration can be obtained.

APPENDIX D: IGOR PROCEDURE CODE FOR ACQUIRING PL LIFETIME COLLECTION TIMES FROM THE JOBIN YVON FLUOROLOG

```
#pragma rtGlobals=1		// Use modern global access method.

Function GetCollectionTimes(prefix,start,num)
	String prefix
	Variable start,num

	Variable n
	String wvName,noteStr,timeStr

	Make/O/D/N=(num) $("root:"+prefix+"_CollectionTimes")
	WAVE CollWV=$("root:"+prefix+"_CollectionTimes")

	for (n=0;n<num;n+=1)
		wvName=prefix+num2istr(n+1)
		WAVE WV=$wvName

		noteStr=note(WV)
		timeStr=StringByKey("Elapsed real time",noteStr)

		CollWV[n]=str2num(timeStr)
	endfor

End
```

APPENDIX E: IGOR PROCEDURE CODE FOR DETERMINING THE PROBABILITY DISTRIBUTION OF AVAILABLE SITES FOR A QD SAMPLE

```
#pragma rtGlobals=1		// Use modern global access method.

Function QDConc(n,NSites,T0,TA,K0)
//	NSites - total number of ligand binding sites on a QD
//	T0 - Native TOPO concentration
//	TA - TOPO Added (Concentration)
//	K0 - Equilibrium constant for a single binding site.

	Variable NSites,T0,TA,K0,n
	Variable j,sumQDT, relTConc

	Make/O/D/N=(NSites) QDT=0
	SetScale/P x 1,1,"", QDT //QDT is the probability curve of a QD with n traps

	relTConc=(T0/10+TA)/3E-7 //3E-7 is the QD Concentration

	QDT[0]=1
	for (j=1;j<NSites;j+=1)
		QDT[j]=(((nSites+1-j)/j)*K0/10*relTConc*QDT[j-1])
		if (QDT[j]>1)
			QDT[]/=QDT[j]
		endif
	endfor
	sumQDT=sum(QDT)
	QDT[]/=sumQDT

	return QDT[n]
End
```